Title
Environmental Effects on the Solid-State Reaction Dynamics of Anthracene Derivatives

Permalink
https://escholarship.org/uc/item/07v7f9tw

Author
Tong, Fei

Publication Date
2017

Peer reviewed|Thesis/dissertation

UNIVERSITY OF CALIFORNIA
RIVERSIDE

Environmental Effects on the Solid-State Reaction Dynamics of Anthracene Derivatives

A Dissertation submitted in partial satisfaction
of the requirements for the degree of

Doctor of Philosophy

in

Chemistry

by

Fei Tong

December 2017

Dissertation Committee:
    Dr. Christopher. J. Bardeen, Chairperson
    Dr. Yadong Yin
    Dr. Ludwig Bartels

The Dissertation of Fei Tong is approved:

Committee Chairperson

University of California, Riverside

Acknowledgement

Time flies. I did not realize more than five years has passed already until I was told to graduate and obtain my PhD degree by the end of this year. Doctor of philosophy, the highest degree that one can achieve during the study process, will be going along with me in my future life. Thousands of words that I want to speak out of my mind, thousands of feelings that I want to express from my heart, and thousands of days and nights that I have spent, carved in the milestone of my life already, and recorded this memorable experience and duration.

By all means, I am always feeling lucky to have Dr. Christopher J. Bardeen, a true scientist and a brave pioneer in academic realm, as my graduate research adviser. All the time, I will be grateful that I have spent five years together with Dr. Bardeen, a reliable and patient educator, in exploring various research fields. It is my honor that I have ever worked with Dr. Bardeen, a senior with full kindness and a person with wide wisdom. I am deeply impressed by his profound knowledge in the world of chemistry, physics, and optics; it seems that every piece of leaf in the tree of quantum mechanics can be picked by him at any time without hesitation. I marvel at his excellent skills in mathematics; it looks like that every step and equation can be illuminated and pulled out of his brain immediately. Dr. Bardeen is the most industrious person that I have ever seen in my life even though his high reputation does not require such hard work anymore. When I arrived at office with my sleepy eyes in the morning, he has already finish tons of work; When I crawled into bed with my exhausting body at night, he must be still working. He

never drinks coffee or any energetic drinks, but he is always having a clear mind. Dr. Bardeen is the kindest principal investigator that I have ever worked for in my life since he never forces people to do things they may not want to. With no stubborn minds, he is always willing to take any advice and suggestions and praises these good ideas no matter whose brains they are coming from as long as these thoughts can benefit research. There is an old Chinese saying: *be strict with oneself, be a broad mind to others.* I can see it exactly from Dr. Bardeen.

I would have never conquered some tough problems without the help of Dr. Bardeen, and I would have never overcome my weakness without the encouragement of Dr. Bardeen. I can still recall the first question that Dr. Bardeen asked me when we firstly met five years ago. “Fei, What are you going to do after your graduation?” I could not give out a certain answer at that time. Not only was I confused about my future life but also I was too overwhelmed to consider such question because I have never expected that one day I would like to dedicate my life in scientific research field. But now, if you ask me the same question, I will answer without any hesitation, “a postdoctoral researcher and then find an academic position in China.” The person that leads me to the road of research is my graduate adviser Dr. Bardeen. He was always teaching me untiringly and ready to answer any scientific questions brought out by me no matter how stupid they were sometimes. He was always humble to listen to my talks which usually sounded ridiculous, giving out constructive suggestions and encouraging me to try those hypotheses in a rational way. I was then encouraged a lot and progressed to ponder issues with more carefulness and also toward a scientific direction in the same time. There is another old Chinese saying which was raised by Han Yu, an ancient Chinese philosopher, over 1200 years ago, to define the concept of teacher: *teacher, the person to impart, preach and demystify.* I can see a real teacher from Dr. Bardeen.

Second, I would like to thank my parents who are always supporting me whenever and whatever decision I have made. I am the first person who is doing science work in my big family; however, they are standing on my side all the time. When I told them that I decided to go to the United States, where is over 7000 miles away from my hometown, for my further study, they helped me to pack my luggage and bought airplane ticket for me without saying any blaming words. They are always proud of their son although they were told by their friends and relatives that research work might not bring much money in the future. Even now, they are trying to be helpful when I told them that I was going to graduate and try to find some academic jobs. I would have no opportunities to be able to study abroad without them and I would never have such achievements without their supports.

I would like to thank Dr. Lingyan Zhu who helped me a lot in my research work and was always willing to help me when I confronted problems during my experiments. She taught me plenty of useful experimental skills and techniques and guided me toward the right way in how to address harsh issues in research. She was always optimistic and it seemed that she could resolve any problems and finish all tasks with high efficiency on time. It is she showed me how a person who has already got PhD degree should be and how a person with the title “Dr.” would work. In daily life, she was a kind person who could enlighten my minds sometimes when I got confused and often encouraged and comforted me when I felt depressed and upset. We collaborated in research and obtained enormous good results and we are also good friend after work.

I would like to thank Dr. Rabih Al-Kaysi for his highly energetic enthusiasm in scientific research. As Chris once said, Rabih is an scientific artist who can prepare stunning samples all the time, I am impressed by his magic fingers at making all types of amazing samples for us and I also admire his ideas and perspectives in illustrating research projects. I would like to thank Dr. Kerry Hanson, who has made me feel welcomed and at home because of her kindness when I was truly alone here and she also offered a lot of help to me during this period. I would like to thank Dr. Mervin Hanson, an insightful scientist with sophisticated computational skills at such elder age and he is scrupulous with all details when we collaborated in our research projects.

I would like to thank all members in my research group, either have graduated already or are struggling to get their own PhD degrees currently. I would like to thank Dr. Sebastian Jezowski, Dr. Eric Chronister and Chad Cruz, the collaborators in my first first-author paper, who have help to open a door of the real world of scientific research for me when I was wandering in the ocean of ignorance. I would like to thank the names listed below: Dr. Taehyung Kim, Dr. Sarah Zhou, Dr. Robert Dillon, Dr. Valerie Nichols, Dr. Geoffrey

Piland, Hossein Mostafavi, Connor Easley, Emily Moses, Xinning Dong, Nathan Tierce, Brandon Luis with my full appreciations.

I would like to thank Dr. Daichi Kitagawa, an outstanding researcher from Osaka City University in Japan. The three months that Dr. Kitagawa has been here is too short for me to fully understand a person but is enough for me to find some most brilliant spots from one. Dr. Kitagawa is a hardworking, frank, and wise person with strong responsibility in research work. He is too nice and happy to offer any help if it is necessary. He is so considerate and it is comfortable and lifelong benefit to work and talk with him as he could teach me a lot of knowledge and illustrate experimental project very well. I may have chance to work with him in the near future and I am really looking forward to it.

I also want to thank all my friends, specifically, Dr. Wanli You, Dr. Zhiyuan Huang, Dr. Xitong Chen, Dr. Wenjing Xu, Dr. Xin Li, and Mingyue Liu, with their help during my PhD duration in UC Riverside. I want to thank my previous roommate, Lin Wang, who has demonstrated to me nothing is impossible with his 60 pounds weight lost within 2 months if one is really dedicated. I want to thank my current roommate, Zhiwei Li, who accommodated me warmly when I was going to be homeless this summer. I want to thank my potential future wife whose name I do not know yet for now and she has never ever come into my life to distract me, leaving me enough time to be able to focus on my research work and fulfilment enough achievements when I graduate.

At last, I would like to thank myself who finished all the missions and tasks to obtain the doctoral degree and never gave up and was always trying to resolve any problems, and who worked, worked, and worked continuously to get things done on time. I am proud of myself and I should pride of myself. Even though with some pity, I will never regret for efforts in work that I have made. What I will regret, however, is the time I have wasted due to my laziness and indolence and the time I have squandered in the entertainments.

Dec, 2017, in Riverside, California, USA

ABSTRACT OF THE DISSERTATION

Environmental Effects on the Solid-State Reaction Dynamics of Anthracene Derivatives

by

Fei Tong

Doctor of Philosophy, Graduate Program in Chemistry
University of California, Riverside, December 2017
Dr. Christopher. J. Bardeen, Chairperson

Anthracene derivatives can undergo photochemical reactions under light irradiation, like a [4+4] photodimerization and a Dewar isomerization. When these molecules are made into micro- and nano-sized crystals, some of them exhibit interesting photomechanical motions and deformations like bending, twisting, curling, and expanding. Both the internal and external environmental effects were found to significantly influence the photomechanical behaviors and photochemical reactions of these molecules in the solid-state. One goal of this research is to better understand the relationship between dynamics of chemical reactions and crystal photomechanical behavior they produce, and to see if these reaction rates can be enhanced by internal or external factors.

9-tert-butylanthracene (9TBA) undergoes a Dewar isomerization in solution and in polymers, but produced no photomechanical response in the crystal, even though it generates a significant volume change and a highly strained molecular structure after

photoisomerization. But when this molecule is embedded in a polymer, a strong pressure dependence of the photoisomerization was observed in both forward and reverse reactions, providing us a possible way to engineer more pressure sensitive molecules in the future.

We investigated the photodimerization process of 9-methylanthracene (9MA) in polycrystalline thin films. It was found that both the photochemical reaction and nonradiative relaxation rates increase as more photoproduct is formed, which we denoted as an autocatalytic pathway. The local environment of a 9MA molecule changes as the surrounding molecules react. We derived rigorous equations and extended a current model (the Finke-Watzky Model) to describe the non-exponential reactant decay, and we were able to predict its time-dependent photoluminescence evolution over the course of the reaction, which showed agreement with the experimental results. The presence of autocatalytic reaction dynamics in a molecular crystal system may play a role in its photomechanical response. This new chemical reaction pathway is different from the single exponential process seen in photoresponsive soft polymer systems.

Besides internal factors, like intra- and intermolecular interactions, we also studied the external environmental effects on molecular crystals. Ionic surfactants like cetyltrimethylammonium bromide (CTAB) was discovered to dramatically promote both the photomechanical motion and the photochemical reaction rates of dimethyl-2-(3-anthracen-9-yl)allylidene)malonate (DMAAM) nanocrystals. These results may help illustrate how surface effects can enhance crystal reactivity. Future work will involve incorporating the photochemical processes with photomechanical behaviors and exploring more interesting mechanical motions with various shapes and sizes of molecular crystals.

Table of Contents

List of Figures

Chapter 1 Introduction

1.1 History and background of photomechanical materials

People always make efforts to take advantage of energy sources from nature to help them to do work. One example is the appearance of mills. People in ancient periods started to build windmills[1] and watermills[2] to mill cereals to replace animals such as donkeys or horses. Wind flow or water flow generated by differences of potential energy (pressure or gravity) can generate rotation to do mechanical work[3, 4]. Once proper constructions are built, such resources (wind and water) from nature can keep working continuously. As a result, they can accomplish more work in a certain duration compared to manpower or animals. The larger the difference in potential energy, the more work they can generate. The steam engine was invented when people realized that they could utilize different energy forms and convert them to do mechanical work[5]. The huge kinetic energy generated via the volume change of vapor from heating water can do extensive mechanical work in a short time. Various energy sources were explored in order to drive the development of society after this industrial evolution, such as electricity, heat, light and chemical energy[6-10].

As for light energy, the nature has already learned how to take advantage of this resource during the evolution of billions of years. Plants can convert light energy into chemical energy via photosynthesis[11, 12], accumulate it as they grow, and supply energy to other organism like insects and animals[13]. However, this enormous energy resource is not fully utilized by human beings. People started to make use of light and convert it into electricity via devices such as solar cells over the last 200 year. The first photovoltaic effect was experimentally demonstrated by a French physicist Edmond Becquerel in 1839[14] and Willoughby Smith first described the effect of light on selenium in 1873[15, 16].

The direct conversion of photons to mechanical motion is called "photomechanical effect". Photomechanical behavior is attracting more and more attention because it does not require direct contact with materials or by hard connections such as wires[17]. Light, as a clean and green resource, can achieve precise control in space, intensity, polarity and wavelength. The first application of photomechanical device could date from the late 1800s when Alexander Graham Bell tried to make a photophone that could enable communication without wires[18]. Initial research activities of photomechanical effects in polymeric materials were undertaken in the 1960s. In 1967, Lovrien proposed four strategies to convert light energy into mechanical energy using photochromic molecules such as azobenzenes in polymer chains[9]. The general approach of these initial studies remains largely unchanged today, focusing on incorporating photoresponsive moieties into polymeric or crystalline materials.

1.2 Photomechanical molecular crystals

Instead of embedding molecules inside host materials such as liquid crystal polymers, some single crystals can also show a photomechanical response under light. The first systematic study of the photochemistry of molecular crystals dates back to 1964, when Schmidt and Cohen studied the photodimerization of cinnamic acid derivatives. The “topochemistry” they postulated described how the spatial arrangement of reactant molecules can affect the photochemistry[19-21]. The prototypical reaction, much studied by Schmidt and others, is the [2 + 2] photodimerization of cinnamic acid, shown in Figure 1.1 (f). In the solid state, UV light irradiation produces the α-truxillic acid photodimer if the trans-cinnamic acid is crystallized in the α-polymorph, the β-truxinic acid dimer if the cinnamic acid crystalizes in the α-polymorph, and there is no photoreaction if the cinnamic acid crystallized in the γ-polymorph.[21-23] Recent work by MacGillivray et al. in expanding the scope and utility of the [2 + 2] dimerization is particularly noteworthy[24]

In 1966, Tatsuzaki et al. first reported a photomechanical response in an inorganic SbSI single crystal. This photomechanical behavior was attributed to the unique coexistence of photoconductivity and ferroelectricity in SbSI crystals. The length of a SbSI crystal changed when it was illuminated by visible light in the presence of an electric field[25]. The first example of photomechanical motion based on a photochemical reaction in an organic molecular crystal was reported in 1982 by Abakumov and Nevodchikov[26]. The crystals were composed of a semiquinone complex of platinum group metals that generated a free-radical complex when exposed to visible or near-infrared light.

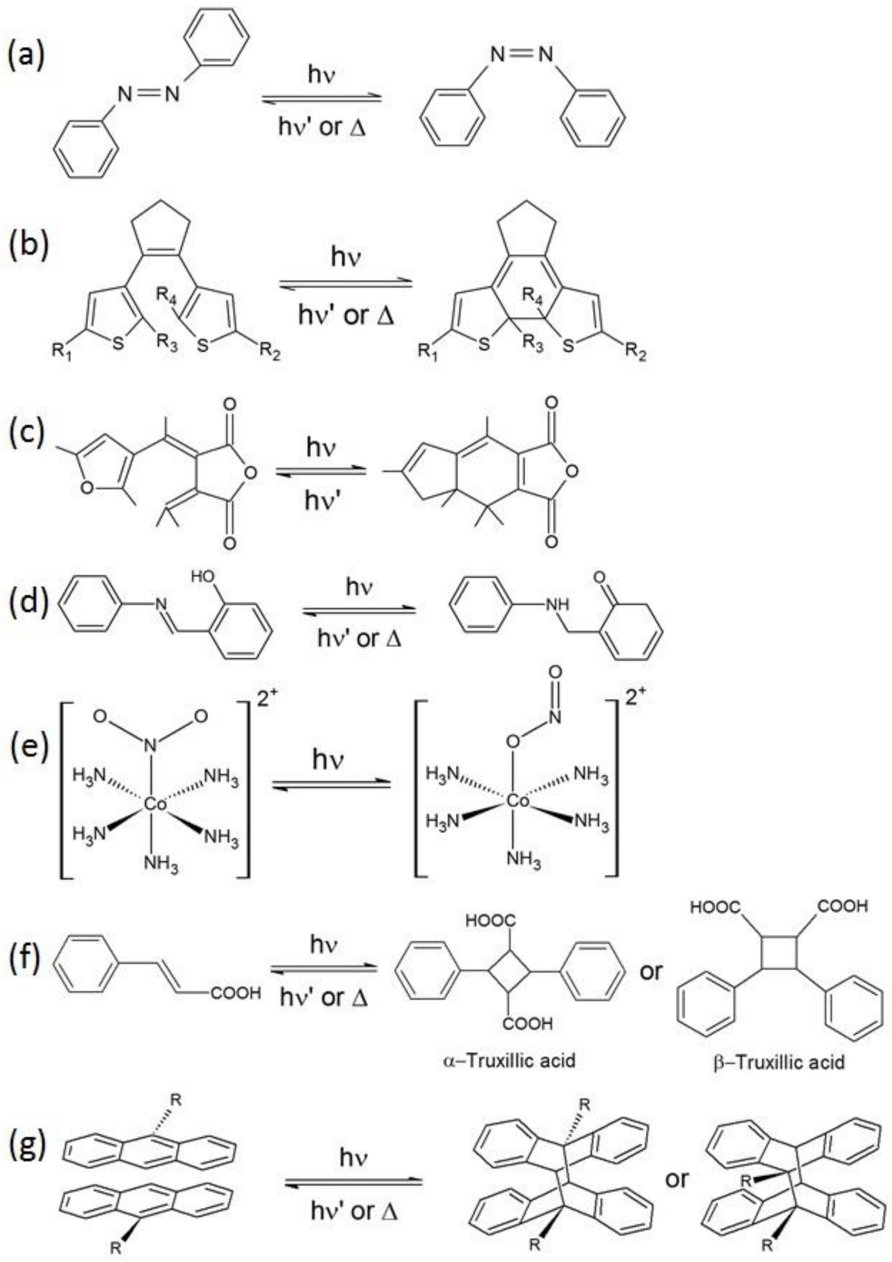

Figure 1.1. Examples of reversible photochromic reactions that have been used to drive photomechanical motion in crystals. (a) trans-cis isomerization of azobenzene; (b) ring formation and cleavage reaction of diarylethene derivatives; (c) ring formation and cleavage isomerization of furylfulgide; (d) intramolecular hydrogen transfer reaction of salicyldienoanilines; (e) intramolecular linkage isomerization of a nitropentaaminecobalt(III) complex; (f) [2+2] cycloaddition reaction of cinnamic acid; and (g) [4+4] cycloaddition reaction of anthracene derivatives. (Reproduced with the permission of Elsevier.)

The bending action in this complex was ascribed to the radical-mediated formation of dimerized Rh—Rh bonds between stacked complexes within the crystal. A decade later, in 1992, Abakumov and coworkers were involved in a study that clarified the chemistry of the rhodium semiquinone complexes but left the question of the bending mechanism unanswered.[27]

In 2002, Nakanishi and coworkers showed that while the photopolymerization of a diolefin derivative resulted in the disintegration of bulk crystals, the same photoreaction did not destroy nanocrystals[28]. In 2006, our group showed that although larger crystals composed of the anthracene derivative 9-tert-butylanthracene ester (**9TBAE**) shattered under light illumination, but crystalline nanorods composed of the same molecule could expand up to 15% when irradiated by 365 nm light.[29]This expansion was driven by a crystal-to-crystal [4 + 4] photodimerization reaction and did not fragment the nanorods (Figure 1.2). This result suggested that such crystals could generate large mechanical displacements, possibly useful for photomechanical applications. The MacGillivray and Garcia-Garibay groups have also reported that organic nano- and microcrystals can survive photochemical transformations with their morphology intact.[30, 31]

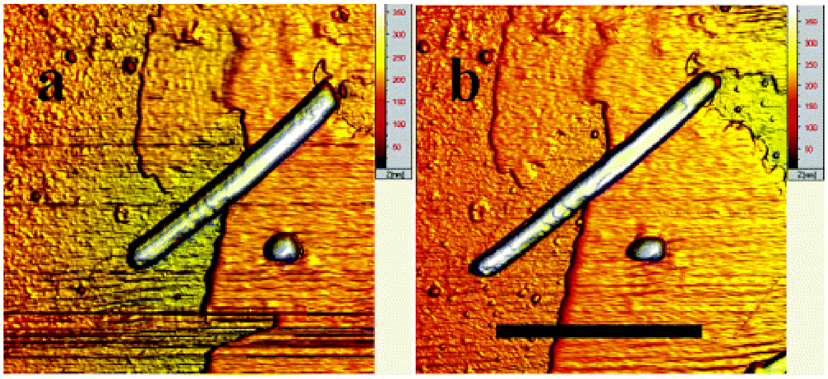

Figure 1.2 (a) AFM image of a single-crystal 9TBAE nanorod before illumination and (b) after illumination with 365 nm. Scale bar is 6 μm. Note that the diameter of the rod in the *xy*-plane appears greater than 200 nm due to its convolution with the broad AFM tip. (Reproduced with the permission of American Chemical Society.)

During this same period, work on solid-state photochromic materials proceeded, with notable progress in Irie's group on the photoinduced ring-opening/closing reaction of the diarylethene (DAE) family (Figure 1.1b).[32] Several derivatives that could undergo the ring-opening/closing reaction in crystalline form were found.[33] Experiments demonstrated that crystal surface features could be switched back and forth by exposure to UV followed by visible light.[34] In 2007, Irie's group also demonstrated that a molecular crystal composed of the DAE derivative shown in Figure 1.3 could undergo reversible deformations upon exposure to different wavelengths of light.[35] Although the magnitude of the shape changes was small (<1%), when vacuum evaporation was used to generate microcrystals on a surface, more dramatic deformations could be observed (Figure 1.3).

Irie and other workers have continued to explore the diarylethene ring-opening and closing reaction for possible applications[35, 36]. One example is the use of a 10 micro diameter molecular crystal rod and to push a metallic microparticle. Upon photoexcitation, the large force generated by flexing of the crystal rod will push a gold microsphere as far as 30 μm. (Figure 1.4)

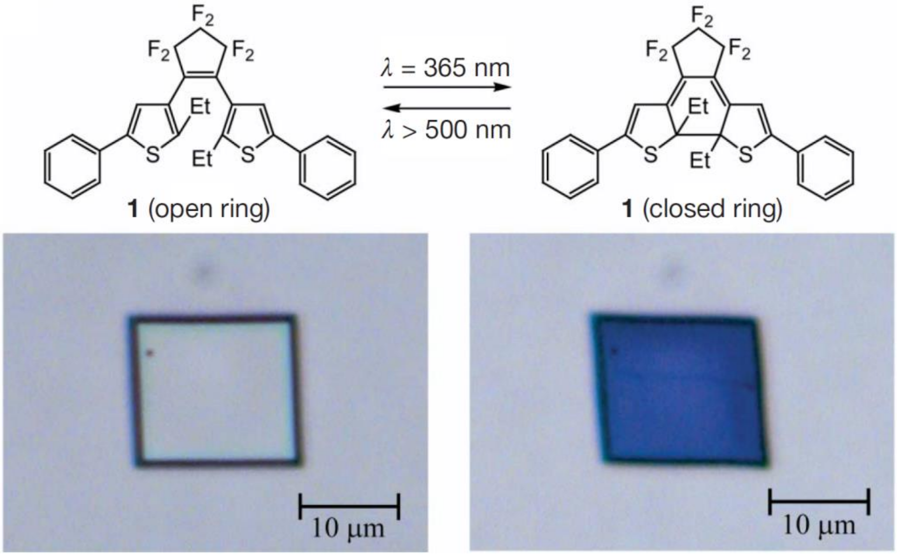

Figure 1.3 Open- and closed-ring chemical structures and reaction scheme for a diarylethene derivative, 1, 2-bis(2-ethyl-5-phenyl-3-thienyl)perfluorocyclopentene. The images illustrate the reversible deformation of a single crystal that can be switched back and forth using ultraviolet (365 nm) and visible (500 nm) light. A square single crystal of (1) with corner angles of 88◦ and 92◦ reversibly changes to a shape with corner angles of 82◦ and 98◦. The crystal thickness was 570 nm. (Reproduced with the permission of Nature Publishing Group.)

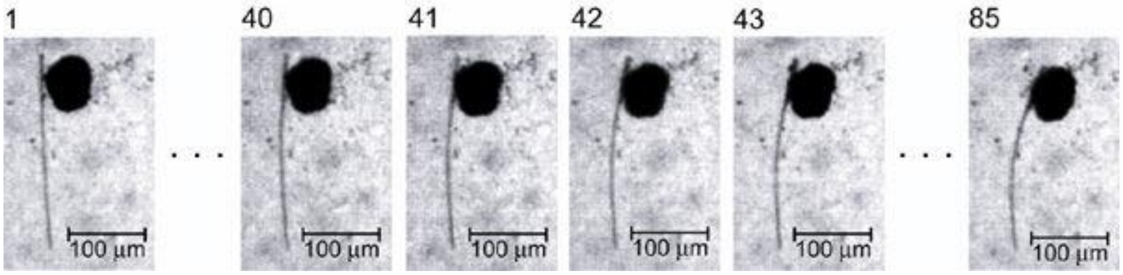

Figure 1.4 Movement of a gold microsphere by a rod-like diarylethene crystal after irradiation with UV (365 nm) light. The gold micro-particle is 90 times heavier than the rod-like crystal (250×5 ×5 mm) and appears in the images as a black spot. The ultraviolet light-induced bending of the crystal could push the gold micro-particle as far as 30 μm. The exposure time of each frame was 500 ms (2000 frames sec^{-1}) and the numbers above the images are frame numbers. (Reproduced with the permission of Nature Publishing Group.)

1.3. Advantages of molecular crystals

As hard materials, molecular crystals are usually regarded as fragile. However, there are a few examples that have shown that molecular crystals can have large deformation. For instance, some molecular crystals can be bent elastically over 180^o or even 360^o.[37-39] In 2015, Naumov et al demonstrated a superelastic single crystal that exhibited perpetually self-propelling behavior.[40] The good elasticity was attributed to the low-dimensional hydrogen-bonding network which can provide enough internal strain to do propulsion while also keeping the crystal intact.

One advantage of molecular crystals is that they can respond more rapidly than soft materials (polymer and liquid crystal elastomers) as they do not need a matrix to help them to amplify the deformation of molecules to the macroscopic level. Moreover, the energy transfer process (from light energy to mechanical energy) will be more efficient and faster as the heat dissipation of polymer chains has been avoided.[41] And also, even though the deformation or displacement of molecular crystal may be smaller, the local stress or force that produced is usually the same or even larger than soft elastomers.[42-44] Photomechanical molecular crystals can do much more work under light illumination. In 2010, Irie et al demonstrated that a rod-like diarylethene co-crystal can lift a metal ball which is at least 200 times heavier than the crystal itself under UV light illumination[45] (Figure 1.5). Another advantage of molecular crystals is their simplicity and ease of analysis. For example, X-ray diffraction techniques can easily get detailed information on crystal structure under varying temperature and pressure conditions.[46-48]

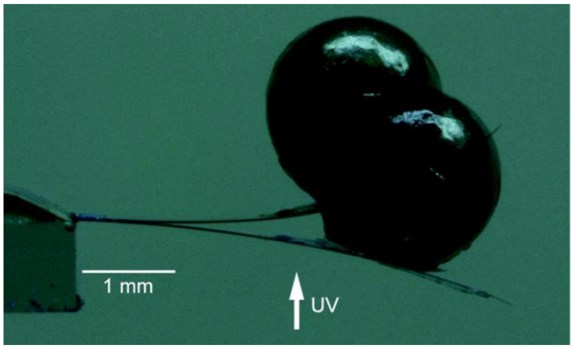

Figure 1.5 Superimposed photographs of a crystal cantilever lifting a lead ball with a mass 275 times larger than the crystal upon irradiation with UV light from the underside of the actuator. (Reproduced with the permission of American Chemical Society.)

1.4 Engineering molecular structure to get better photomechanical behavior

1.4.1 Photoisomerization – the intramolecular reaction

Even though the photomechanical effects are mostly shown in polymers and liquid crystals[49-51], azobenzene derivatives can also show photomechanical behavior when they are in single crystals. In 2009, Koshima et al firstly reported that crystals composed of amino-azobenzene derivatives could undergo up to 100 bending and unbending cycles under repeated UV light irradiation.[52] The crystal would bend away from light source after UV irradiation while revert back after about 30s due to the thermal effects. Barrett et al. have prepared numerous azobenzene derivatives and extensively characterized their crystal-to-crystal photoisomerizations and mechanical response.[46, 53, 54] One interesting example shown in Figure 1.6 is how the illumination conditions of light could control the photomechanical bending.[53] Their work has demonstrated that the use of halogen substitution allows this class of molecules to exhibit fast photomechanical motion with good cycling behavior and that derivatives that allow visible light to drive the photomechanical motion can be prepared. This work also proved that it is possible to engineer molecule structures to design promising photomechanical molecular crystals in the future.

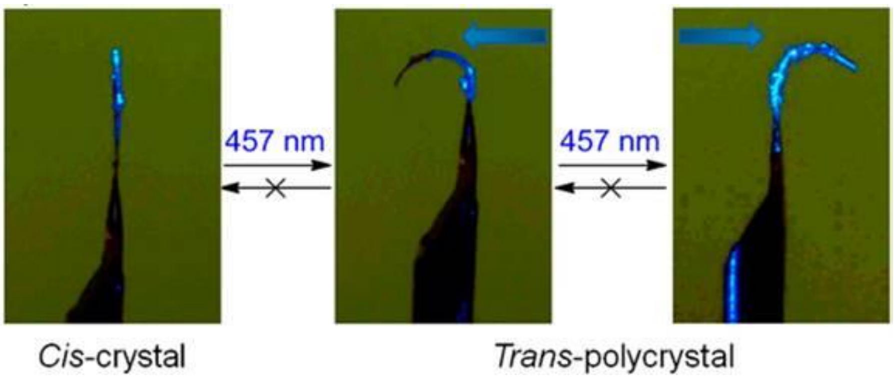

Figure 1.6 Irreversible bending of a thin crystal of cis-1 by 457 nm light, with the arrow at the top of the figures indicating the direction of irradiation. (Reproduced with the permission of American Chemical Society.)

1.4.2 Photodimerization – the intermolecular reaction

The photochemical reaction of azobenzene derivatives is based on its trans ↔ cis intramolecular isomerization, but very good photomechanical behavior can also be found in molecular crystals that undergo intermolecular reactions such as [2+2] and [4+4] cycloadditions.[24, 55, 56] Recently, in order to expand the photomechanical capabilities of molecular crystals, our group has systematically modified the 9-anthracene carboxylic acid (9AC) molecule by replace the H at the C-10 position, which is directly across from the COOH group, with CH_3, F, Cl, Br, and another COOH group[57-59]. But we had more success by placing substituents at other positions on the anthracene ring. One successful example is 4-fluoro-9-anthracene carboxylic acid (4F9AC), which can exhibit the most rapid photomechanical responses with at least an order of magnitude improvement in both mechanical recovery and photodimer dissociation rate (Figure 1.7).

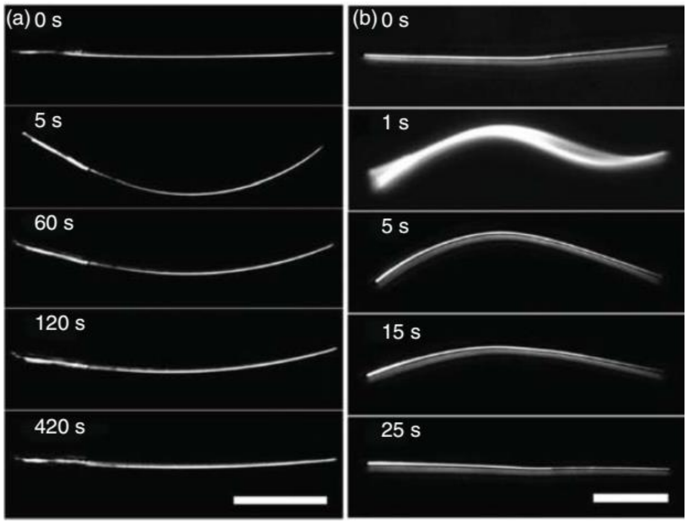

Figure 1.7 Series of optical microscopy images of (a) 9AC and (b) 4F-9AC microcrystalsafter a 1 s exposure to 405 nm light causes them to deform. The 4F-9AC crystal completely untwists in 25 s, while the 9AC crystal requires 420 s to unbend. Both scale bars are 50 μm. (Reproduced with the permission of American Chemical Society.)

1.4.3 T-type and P-type molecular crystals

Currently, various organic compounds can show photomechanical behaviors in their crystal forms. This includes diarylethene derivatives[32-36], furyl fulgide[60], azobenzene derivatives[52-54], salicylideneaniline[61], anthracene derivatives[29, 57-59], 4-chlorocinnamic acid[62], 1,2-bis(4-pyridyl)ethylene salt[63], and benzylidenedimethylimidazolinone[64]. And people are trying to prepare more organic compounds to obtain better molecules.

From a practical standpoint, the photomechanical response should be reversible so that the motion can be repeated for multiple cycles. This reversibility can be divided into two forms: T-type and P-Type.[65, 66] In T-type crystal, the photochemical reaction produces a metastable product that will thermally revert back to the reactant under ambient conditions. The advantage of such crystals is that only a single wavelength of light is needed to cause the photomechanical response, some anthracene derivatives is one of T-type crystals.[57-59] But the rate of reverse reactions cannot be controlled precisely since the crystal resets itself depending on ambient temperature. On the other hand, in P-type crystals, the forward and reverse reactions can be initiated by using light with different wavelengths. In this way, people can obtain either the reactant or photoproduct selectively. Most of azobenzene derivatives and diarylethene derivatives belong to P-type crystals.[32-36, 52-54]

However, one cannot claim arbitrarily which type of crystal is better than the other as both of them have own advantages and disadvantages. Moreover, molecular crystals provide a synthetically accessible way to prepare molecules with more diversity and variety and that is why people are still exploiting in this field and trying to make more interesting molecules.[32, 54, 58]

1.5 Mechanism of the photochemistry

1.5.1 The Warner Theory in polymer system

Making more useful molecules is one goal we have in the field photomechanical molecular crystals. The other one would be understanding mechanism – what is actually happening during the process photochemical reaction inside those molecular crystals? Currently, most researchers use Warner Theory[67] which assumed first-order reaction kinetics in reactions and is widely used in liquid crystal elastomers and polymer systems.

In Warner Theory, the propagation of light traveling through the materials is described by Beer-Lambert Law and the intensity of light will attenuate with a single-exponential decay [68]. The photoactive elastomer will then deform due to interfacial strain caused by bimorph structure of reactants and products (Figure 1.8).

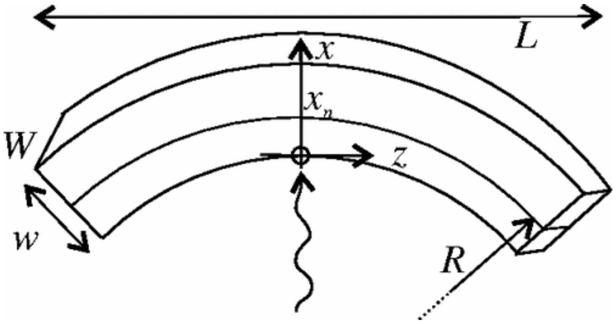

Figure 1.8 A beam of light, traveling in the x-direction is incident on the surface of film of a photoactive nematic elastomer, absorption leads to bend. (Reproduced with the permission of American Physical Society.)

It is obvious that the mechanism in molecular crystals would be different from the polymer system. Not only the photomechanical behavior of molecular crystals is different, but also the photochemical reaction process is different. There were already some research that suggested that the situation may be more complicated in molecular crystal systems. Previous work in our group of 9-methylanthracene (9MA) showed that here is a clear delay between the start of the reaction and the onset of bending when we measured the 9MA photomechanical response and fluorescence signal simultaneously (Figure 1.9a).[69] In 2014, Brillante et al showed that the photodimerization of solid-state 9-cyanoanthracene exhibited non-exponential kinetics. The data was measure by Raman spectroscopy and the analysis was based on the Finkey-Watzky model, which is different from Warner Theory that is widely used in polymer systems (Figure 1.9b).[70]

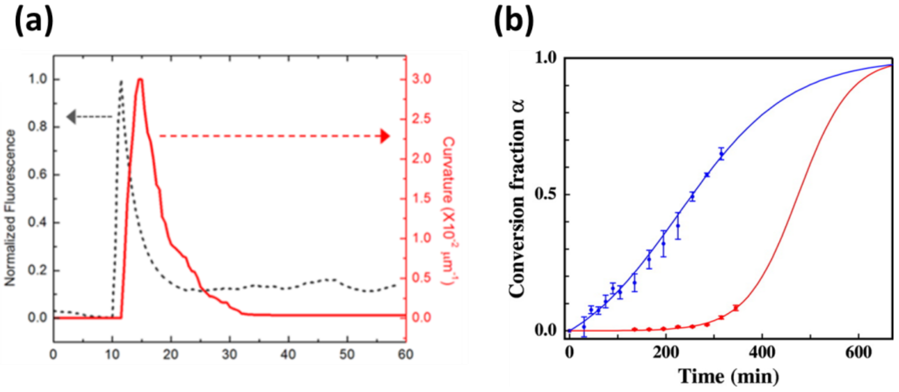

Figure 1.9 (a) Normalized time-dependent fluorescence and curvature data for individual 9MA microneedles. The data points are generated by measurement of the monomer fluorescence signal at 550 nm and analysis of fluorescence microscopy images, both collected simultaneously. (b) Conversion fraction of solid-state 9-cyanoanthracene as a function of time as obtained from the band intensities of micro-Raman spectra. (Reproduced with the permission of American Chemical Society.)

1.5.2 The JAMK Model in molecular crystals system

McBride and Eckhardt have done extensive work on measuring such effects and developing theoretical models to understand them[71-73]. The cooperative nature of photochemistry in crystals can lead to complicated kinetic behavior, and the Johnson–Mehl–Avrami–Kolmogorov (JMAK) model of nucleation is often invoked to analyze reaction rates.[74, 75]

The JMAK model, also known as the JMAK equation was first derived by Kolmogorov in 1937 and popularized by Melvin Avrami in a series of papers published in the Journal of Chemical Physics from 1939 to 1941.[76-78]Basically, it can be summed up through a simple equation:

$$V(t) = 1 - e^{-V_e(t)}$$

where V is the fraction of the transformed phase and V_e is the so-called extended volume of the transformed phase, that is the volume the transformed phase would acquire if the overlap among the growing nuclei was disregarded.

The kinetics of the JMAK model usually predicts a sigmoidal shape or S-shape, where the transformation rates of crystal nucleation are low at the beginning and the end of the transformation but rapid in between. The initial slow rate can be attributed to the time required for a significant number of nuclei of the new phase to form and begin growing. During the intermediate period the reaction rate speeds up as the nuclei grow into particles and consume the old phase while nuclei continue to form in the remaining parent phase. Once the transformation approaches completion the rate will slow as there is little untransformed material for further nucleation.[79]

The JMAK model has been widely used due to its simplicity research areas. However, it has some drawbacks which prevent it from describing the chemical reactions at molecular level. For example, the JMAK model assumes nucleation always occurs randomly and homogeneously over the entire untransformed portion of the material, which is usually not true in reality due to the defects and edges of materials. And also it claims that the crystal growth occurs at the same rate in all directions during the chemical reaction, which excludes the intrinsic effects of materials like self-catalyzed processes due to the accumulation of products in many biological systems and metallic nanoparticles systems.

1.5.3 The Finke -Watzky Model in molecular crystal system

In 1997， Dr. Watzky and Finke successfully developed a model to describe the continuous nucleation and autocatalytic growth of Ir nanoclusters. This model consists of a slow, continuous nucleation (A→B, rate constant k_1) followed by a fast, autocatalytic growth (A+B→2B, rate constant k_2). The model has become known as the Finke-Watzky (F-W) two-step model and has been applied to a variety of phenomena involving nucleation and growth, including catalyst formation,[80] protein aggregation,[81-84] and solid-state reactions.[85] The F-W two-step kinetic model uses the concept of pseudo-elementary steps and allows for the quantitative determination of average rate constants for nucleation and autocatalytic growth, which provides both a physical model and a mathematical solution[2]. When it is applied to solid-state reaction processes, its balanced reactions and associated rate constants enable transparent physical interpretations and easy connection to experimental observables.

We applied the F-W two-step model to the 9MA system and showed that it could be used to analyze both the time-dependent decrease in reactant concentration and the speed-up in the fluorescence decay. The details of this research project can be found in Chapter 4. The ability to quantitatively model the kinetics will be necessary to quantitatively model the crystal photomechanical response, which we plan to do in our future work.[86]

1.6 Models coupling with photomechanical behavior

In addition to explaining the photochemistry in solid-state photomechanical molecular crystals, how photomechanical behavior arises from photochemical kinetics also attracts chemists' attention. For example, if the distribution of photoproducts follows an exponential distribution according the first-order kinetics, the same as responsive polymers, the interface strain caused by weak gradient of displacement between reactant and photoproduct molecules will be relatively small.[67] On the other hand, photomechanical bending may be enhanced if the distribution of photoproducts follows a non-exponential profile, especially in microscopic-sized materials like nanowires (Figure 1.110).

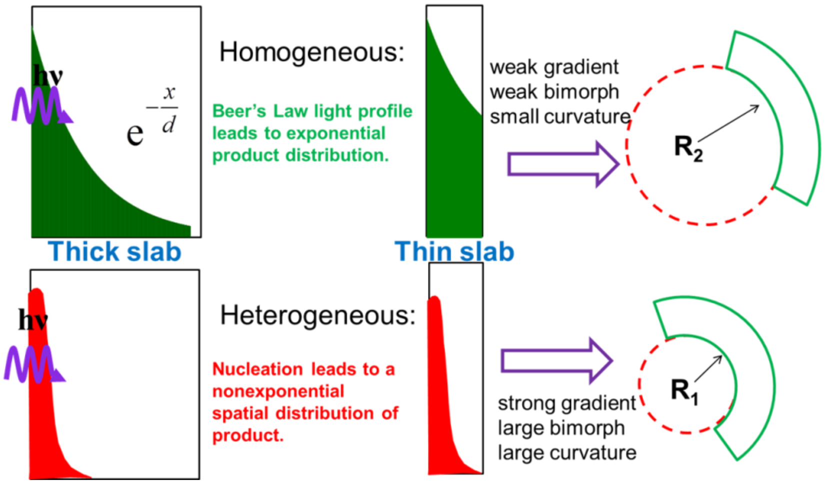

Figure 1.10 Two different types of kinetics models lead to different photomechanical behaviors.

1.6.1 Basic ideal of deformation – bimorph structure

As with the photomechanical responsive polymers, the most common mechanical deformation observed in molecular crystals is bending. Basically, the bending occurs when the photoproducts form preferentially on the illuminated side of an optically thick crystal, generating a bimorph structure.[87] Therefore, bending is the result of the strain gradient that arises at the interface between two different chemical phases containing the reactant and photoproduct molecules (Figure 1.11). This type of motion usually depends on the shape of the crystal, and a long flat crystal may want to seek to alleviate internal strain by twisting. Examples of twisting crystals can be found in diarylethene[88] and anthracene derivatives[57].

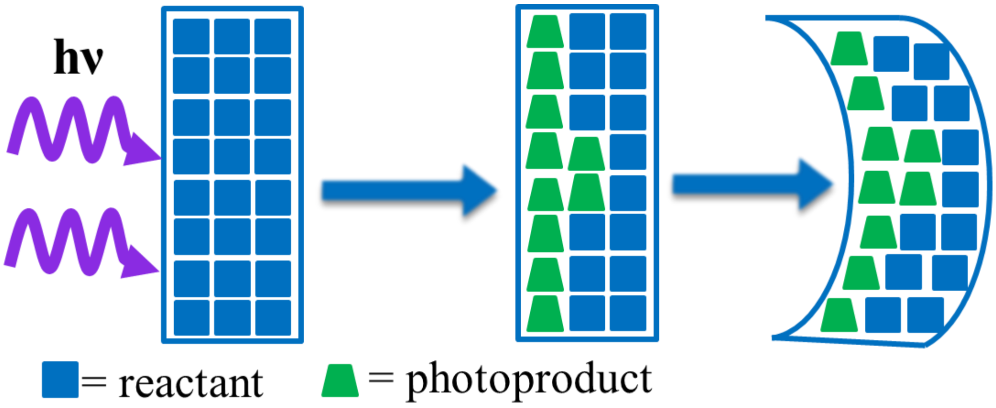

Figure 1.11 Attenuation of exciting light leads to a gradient of reacted and unreacted molecules. This forms a bimorph-type structure where the motion is driven by strain between the different phases.

1.6.2 The Bimetal Model

The bimorph structure idea provides people a basic idea of how to generate photomechanical bending of crystals via tuning illumination conditions such direction, intensity and duration. Based on this, in 2015, Kitagawa et al proposed an simple model which originated from Timoshenko's bimetal model to describe the bending of diarylethene crystals.[89] The Timoshenko bimetal model was first reported in 1925 and was used to explain the thermal behavior of a strip thermostat under various temperatures.[90] The bending curvature of the crystals can be described in the following equation and figure 1.11:

$$curvature = \frac{1}{R} = (\frac{\alpha_1 - \alpha_2}{h_2})\frac{6mn(1+m)}{1+4mn+6m^2n+4m^3n+m^4n^2}$$

where R is the curvature radius, a_i(i = 1, 2) are the actuation strains, h_i (i = 1, 2) are the layer thickness, m = h_1/h_2, n = E_1/E_2, and E_i (i = 1, 2) are the Young's moduli.

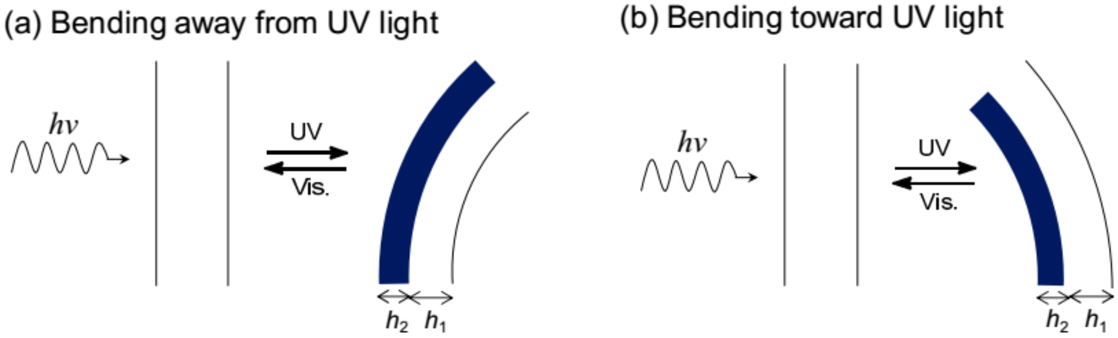

Figure 1.12 Illustration of Timoshenko's bimetal model in the case of (a) bending away from UV light and (b) bending toward UV light. (Reproduced with the permission of MDPI.)

In this model, the needle-shaped crystal is basically divided into two layers: one is photoreacted and the other is non-photoreacted. In the non-photoreacted layer, the value of actuation strain α_1 is assumed to be zero because the layer cannot expand or contract. In bending away from UV light, the value of α_2 is the coefficient of expansion. In contrast, it is the coefficient of contraction when the crystal bends toward UV light. The equation can be simplified further if the two Young's modulus values E_1 and E_2 are assumed to be the same because only a few percent of the molecules are reacted form due to the assumption. Then the equation can be rewritten as follows:

$$Curvature = \frac{\alpha_2}{h} \frac{6m(1+m)}{1+4m+6m^2+4m^3+m^4}$$

One advantage of the bimetal model is that it is easy to handle and understand, and can help people to collect useful information about how the bending speeds depend on thickness of rod-like crystals. But it ignores the both gradient change of excitation light and the distribution of photoproducts. It is not clear how to apply the model when it is applied to no needle-shaped crystals[91] or crystals showing twisting[57] or coiling motion[92].

1.6.3 External environmental effects

In addition to exploring the intrinsic effects of crystals, people are also trying to exploit effects of external environment that can produce photomechanical phenomena. Molecules in molecular crystals can communicate with external environment directly, which raises the possibility to have side reactions like oxidation but also provides more opportunities to optimize their properties by changing external environmental conditions. One way to get rid of side reactions is to add a protective layer outside the molecular crystal. In 2008, Bardeen et al used a sol-gel method to coat silica onto the surface of 9AC nanorods, and adjusting them from hydrophobic into hydrophilic (Figure 1.14).[93]The reversible photomechanical bending behavior of 9AC nanorods was preserved but with a much reduced rate. The hard template or shell consisting of silica was proposed to inhibit the bending during the light irradiation, A softer surfactant – sodium dodecyl sulfate (SDS) was used to coat the crystals instead.[94] As a result, the SDS-treated nanorods showed much more consistent bending behavior than the uncoated rods. These results demonstrated that it is possible to optimize the external environment to tune the photomechanical properties of molecular crystals.

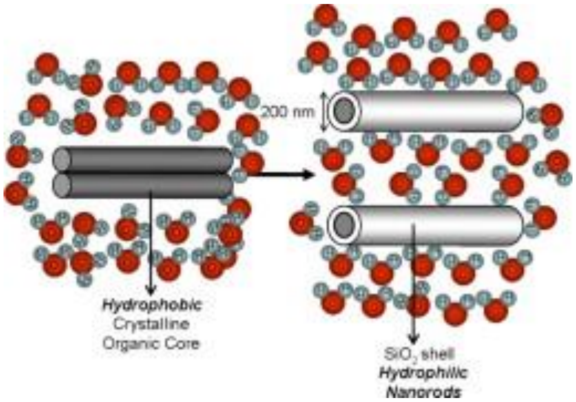

Figure 1.13 The scheme of preparing SiO_2 coated 9AC nanorods. (Reproduced with the permission of Elsevier.)

1.7 Different shapes of molecular crystals

In addition to finding better molecular structures and understanding the mechanism of photomechanical molecular crystals, people also make efforts to prepare different shapes that can show various motions under light. People can grow crystals into numerous shapes by using methods such as solvent-annealing[95, 96], vapor evaporation[97], template method[98], slow reprecipitation growth[99, 100], and even laser induced methods[101]. One question is how to take advantages of those shapes and harness crystals to do useful mechanical work.

1.7.1 Needle-shaped bending and twisting

Currently, organic crystals that are prepared in rod-like or needle shapes are most studied photomechanical molecular crystals. They show bending or twisting upon excitation light. The bending motion is easy to observe and characterize, and it is easy also to fabricate kinetic models based on bending of slender crystals. For now, the organic crystals that can show bending or twisting can mainly be divided into three parts (Figure 1.15) according to their photochemical reactions: (i) [2+2] and [4+4] cycloadditions[24, 55, 56]; (ii) trans ↔ cis photoisomerization[102]; (iii) ring open and ring close photoreaction[32].

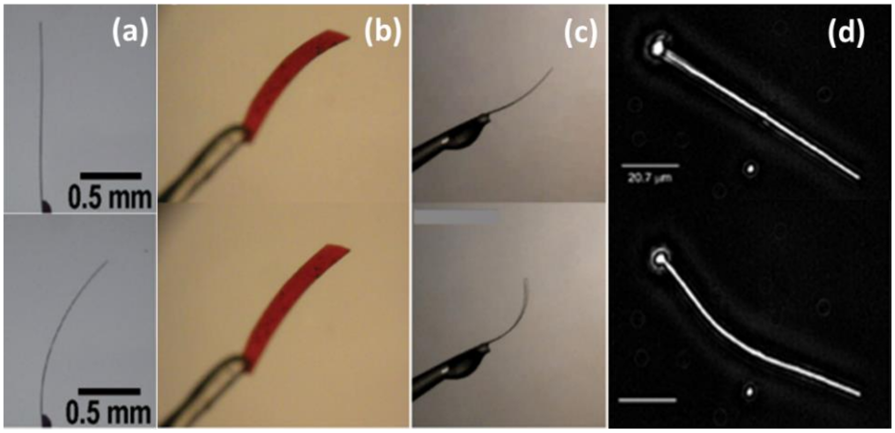

Figure 1.14 (a) 1000th bending of diarylethene crystals based on ring open and close photoreactions. (b) Bending of azobenzene crystal based on cis ↔ trans photoisomerization. (c) and (d) Photomechanical bending of molecular crystals based on [2+2] and [4+4] photodimerization. (Reproduced with the permission of American Chemical Society.)

The bend angle of slender crystal bending can reach as large as 90 ° and some of them have high reversibility[64]. Irie et al has demonstrated one rod-like diarylethene crystal that can show at least 1000 reversible bending motions under alternative UV and visible light illumination.[36]Besides, people have narrowed down crystal size to achieve smaller materials that may have potential applications in cells or even inside human bodies. Bardeen et al has demonstrated that nanowires with 35 nm in diameter could show reversible photomechanical bending via two-photon excitation.[94]

1.7.2 Plate or sheet like photomechanical crystals

Although the majority of photomechanical molecular crystals are rod-like or needle shaped, the crystals with other shapes like plates and sheets are not rare. For example, the first photomechanical behavior of a diarylethene crystal was observed in a rhomboid crystal (Figure 1.3). In 2009， Koshima et al reported a plate-like microcrystal of azobenzene exhibited reversible rolling up under irradiation with UV light.[52]The bending deflection angle was as large as a semicircle of ~ 180° along the short axis, and the rolled up crystal could revert back in darkness after a few seconds (Figure1.16).

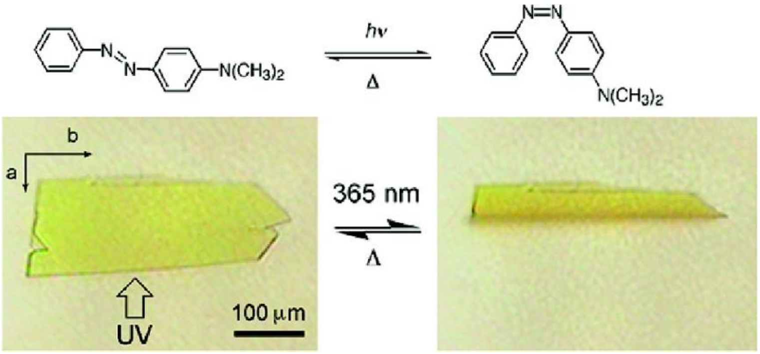

Figure 1.15 The plate-like azobenzene crystal shows reversible large angle bending under light and resets itself when in darkness. (Reproduced with the permission of American Chemical Society.)

The crystal could be switched more than 100 times despite with a very low quantum yield of isomerization, estimated as ~1%. Such microplate crystals can also be prepared using other organic molecules. In 2011, Koshima et al extended their work to a furylfulgide crystal.[60, 103]

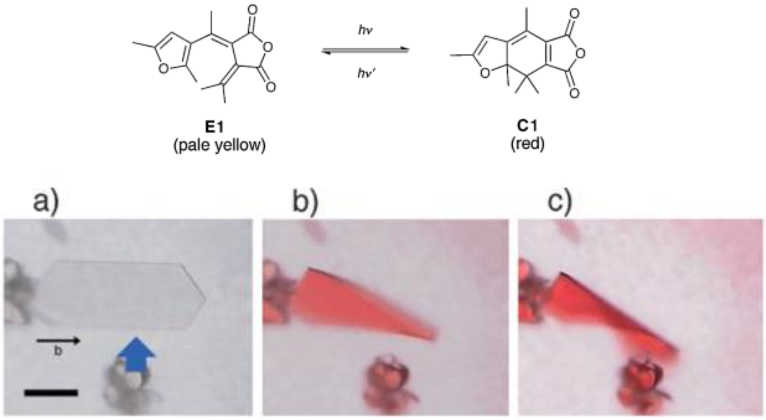

Figure 1.16 The furylfulgide molecule that was used to make plate-like crystal (up) The plate-like furylfulgide crystal before (a) and after UV irradiation (b) 1 and 2s (down). The scale bar: 50μm (Reproduced with the permission of American Chemical Society.)

The microplates they obtained from furylfulgide could exhibit 200 reversible bending motions under alternative light exposures, and significant photochromic changes were observed before and after light irradiation (Figure 1.17). Their work demonstrated that it is possible to change the shape of a crystal but still retain the photomechanical response.

1.7.3 Photomechanical molecular crystals with branched structures

One challenge for the field of photomechanical molecular crystals is to find ways to turn these different crystal motions with various shapes into useful work. Previously, several groups have constructed devices in which crystal bending in harnessed to turn gears or clamp objects[104], and also demonstrated a single crystal can lead to translational motion[91, 40]. However, these motions are usually based on asymmetric environments or situations constructed artificially. An alternate approach is to prepare a crystal shape that rotates or translates in a specific direction under repeated illuminations, analogous to a photon-powered ratchet. Bardeen et al recently used a pH-drop method to grow 4F9AC crystals with 2-10 arms branching out from a central point. These branched microcrystals exhibited a ratchet-like, unidirectional rotational motion under repeated light exposures, suggesting that more complex crystal shapes can lead to more interesting behavior (Figure 1.18)[100]. This approach can be extended to highly branched crystals which have hundreds of arms and function as microscopic brooms.[99]

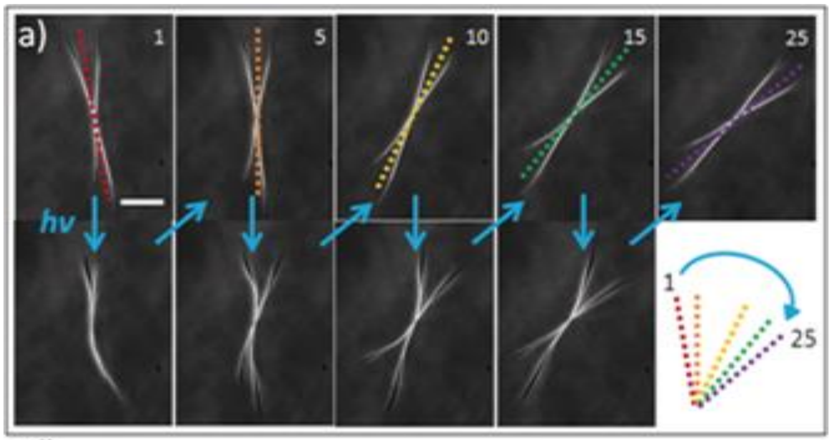

Figure 1.17 Optical microscopy images of an X-shaped crystal that rotates clockwise after each irradiation period. The cycle was repeated for 25 times. 5 cycles of the X-shaped crystal before and after irradiation are illustrated. Scale bar: 20µm. (Reproduced with the permission of John Wiley and Sons.)

1.7.4 Photosalient effects of photomechanical molecular crystals

In order to mimic the natural motions of animals such as jumping and hopping, the photosalient effects have been studied. Naumov et al. have characterized these “photosalient” crystals, showing that the buildup of strain during a photochemical reaction could be released in a sudden, violent shape change that could propel the crystal over considerable distances (cm).[105-107] Often, this jumping behavior was accompanied by crystal fragmentation, and controlling this effect depends on controlling the crystal shape and irradiation conditions. The different mechanical response modes of differently shaped crystals are illustrated in Figure 1.19.

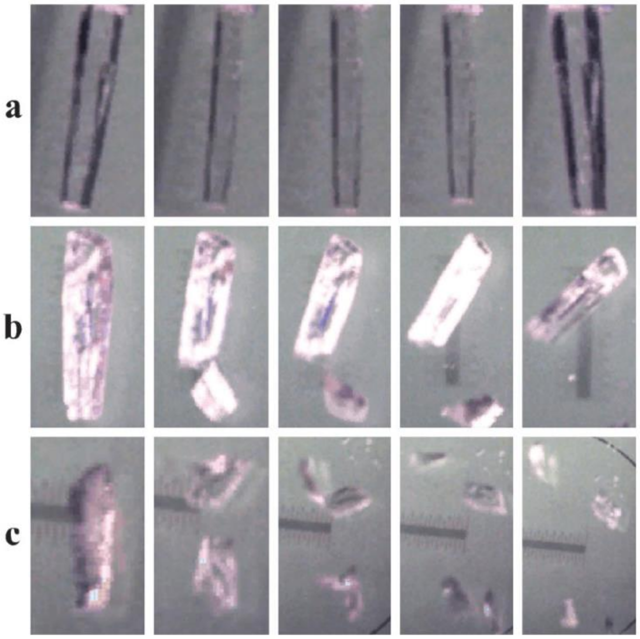

Figure 1.18 Various kinematic effects observed after UV irradiation of coordination metal complex crystals. (a) Rolling or flipping; (b) separation of a small fraction of the crystal, which propels the remaining portion of the crystal; (c) explosion or splitting of a crystal. (Reproduced with the permission of John Wiley and Sons.)

Such photosalient phenomena can also be observed in diarylethene crystals.[108-110] Continuously UV-irradiated crystals initially underwent a photochromic change, but when the energy reached ∼10 μJ they typically jumped 1−2 mm nearly perpendicular to the long molecular axis. However, larger crystals did not jump and merely cracked under the accumulated strain. The photosalient effect in photomechanical crystals represents a direct and visually impressive demonstration of the conversion of light into mechanical motion through a photochemical reaction on a macroscopic scale. It sets the platform for the design of actuating materials that can mimic animal motions. The degree to which solid-state reactions affect crystal mechanical properties and how these properties affect fracture and photosalient behavior is just beginning to be explored.

1.8 Summary

In conclusion, there are mainly three challenges in the field of photomechanical molecular crystals to be addressed currently. First of all, how can we make more new photomechanical molecules that show more interesting motions? Secondly, what is mechanism of photochemistry inside molecular crystals and how do the photochemical reactions lead to their photomechanical behaviors? The last one will be what is the best crystal shape for specific motions or mechanical work?

This thesis is trying to do deal with the three questions above by using solid-state molecular crystals based on anthracene derivatives. First, we tried to investigate the pressure dependence of the photoisomerization of 9-tert-butylanthracene (9TBA) molecule[111]. We utilized optical spectroscopy methods to probe this process and we found that its molecular structure could play a vital role in its sensitivity to external mechanical stimulus. We want to find out how we can design mechanochemical and pressure sensitive molecules by doing this project, which will be discussed in detail in Chapter 3. Second, as for mechanism of photomechanical molecular crystals, we implemented the Finke-Watzky (F-W) model and took advantage of 9-methylanthrace

(9MA) as a sample to investigate the photochemical reaction kinetics of photodimerization in this molecular crystal.[86] We have extended F-W model and derived rigorous equations to describe kinetics and predict the photoluminescence changes during the photochemical reaction process. Third, we studied how texternal environmental factors can influence both photochemical reaction rate and photomechanical behavior using an ionic surfactant, cetyl trimethylammonium bromide (CTAB).[112]The details will be discussed in Chapter 4 and Chapter 5, respectively. Last, we are currently synthesizing different types of molecular crystal with different shapes, sizes, and compositions, with the aim of getting more interesting and useful photomechanical motions. We have already prepared highly branched crystals and work on ultra-long microribbons and hexagonal plates are on. Some work will be discussed in Chapter 6. Finally, we hope the context in this thesis can make some contribution to the field of solid-state photomechanical molecular crystals and help drive developments in photochemistry.

1.9 Reference

(1) Lucas A. Wind, Water, Work: Ancient and Medieval Milling Technology. *Brill.*, **2006**.
(2) Reynolds TS. Stronger than a hundred men: a history of the vertical water wheel. *JHU Press.*, **2002**.
(3). Hills RL. Power from wind: a history of windmill technology. *Cambridge University Press.*, **1996**.
(4). Ritti T, Grewe K, Kessener P. A relief of a water-powered stone saw mill on a sarcophagus at Hierapolis and its implications. *J. Roman. Archaeology.*, **2007**.
(5). Rosen W. The most powerful idea in the world: A story of steam, industry, and invention. *Random House.*, **2010**.
(6). Baigrie BS. Electricity and magnetism: a historical perspective. *Greenwood Publishing Group.*, **2007**.
(7). Jevons HS. The second industrial revolution. *Eco. J.*, **1931**, 41, 161, 1-8.
(8). Leland Jr TW, Mansoori GA. Basic Principles of Classical and Statistical Thermodynamics. *University of Illinois, Chicago.*, **2001**.
(9). Lovrien, R., The Photoviscosity Effect. *Proc. Nat. Acad. Sci.*, **1967**, 57, 236–242.
(10). Dabelstein W, Reglitzky A, Schütze A, Reders K. Automotive fuels. *Ullmann's Encyclopedia of Industrial Chemistry.*, **2007**.
(11). Blankenship RE. Molecular mechanisms of photosynthesis. *John Wiley & Sons.*, **2013**.
(12). Beatty JT, Gest H, Allen JF, editors. Discoveries in photosynthesis. *Springer Science & Business Media.*, **2006**.
(13). Ciais P, Sabine C, Bala G, Bopp L, Brovkin V, Canadell J, Chhabra A, DeFries R, Galloway J, Heimann M, Jones C. Carbon and other biogeochemical cycles. *InClimate change.*, **2013**.
(14). Becquerel AE. Mémoire sur les effets électriques produits sous l'influence des rayons solaires. Comptes Rendus 9: 561–567. *Originalarbeit zur Einwirkung von Licht auf Elektroden.*, **1839**.
(15). Williams R. Becquerel photovoltaic effect in binary compounds. *J. Chem. Phys.*, **1960**, 32, 1505-1514.
(16). Smith W. Effect of light on selenium during the passage of an electric current. *SPIE MILESTONE SERIES MS.*, **1992**, 56, 3.
(17). White TJ. Photomechanical Materials, Composites, and Systems: Wireless Transduction of Light into Work. *John Wiley & Sons.*, **2017**.
(18). Vacca, J.R., Optical Networking Best Practices Handbook, *John Wiley & Sons, Inc., Hoboken.*, **2006**.
(19). Schmidt GM. Photodimerization in the solid state. *Pure Appl. Chem.*, **1971**, 1, 27, 647-678.
(20). Schmidt, G.M.J., Cohen, M.D., Donitz, J.D., and Hammond, C.S. Solid-State Photochemistry, *Verlag Chemie, Weinheim.*, **1976**
(21). Schmidt GM, Cohen MD, Sonntag FI. The photochemistry of trans-cinnamic acids. *J. Chem. Soc.*, **1964**, 384, 2000-2013.

(22). Durr, H. and Bouas-Laurent, H. Photochromism: Molecules and Systems, *Elsevier*, *New York*. **1990**
(23). Bregman J, Osaki K, Schmidt GM, Sonntag FI. Topochemistry. Part IV. The crystal chemistry of some cis-cinnamic acids. *J. Chem. Soc.*, **1964**, 386, 2021-2030.
(24). MacGillivray LR, Papaefstathiou GS, Friščić T, Hamilton TD, Bučar DK, Chu Q, Varshney DB, Georgiev IG. Supramolecular control of reactivity in the solid state: from templates to ladderanes to metal− organic frameworks. *Acc. Chem. Res.*, **2008**, 19, 41,280-291.
(25). Tatsuzaki I, Itoh K, Ueda S, Shindo Y. Strain along c axis of SbSI caused by illumination in dc electric field. *Phys. Rev. Lett.*, **1966**, 17, 198.
(26). Abakumov, G.A. and Nevodchikov, V.I. Termo and photomechanical effects on crystals of a free-radical complex. *Doklady Akademii Nauk SSSR.*, **1983**, 266, 1407–1410.
(27). Lange, C.W., Foldeaki, M., Nevodchikov, V.I., Cherkasov, K., Abakumov, G.A. and Pierpont, C.G., Photomechanical properties of rhodium (I)-semiquinone complexes. The structure, spectroscopy, and magnetism of (3, 6-di-tert-butyl-1, 2-semiquinonato) dicarbonylrhodium (I). *J. Am. Chem. Soc.*, **1992**, 114, 4220-4222.
(28). Takahashi, S., Miura, H., Kasai, H. et al., Single-crystal-to-single-crystal ransformation of diolefin derivatives in nanocrystals. *J. Am. Chem. Soc.*, **2002**,124, 10944–10945.
(29). Al-Kaysi, R.O., Muller, A.M., and Bardeen, C.J. Photochemically driven shape changes of crystalline organic nanorods. *J. Am. Chem. Soc.*, **2006**, 128, 15938–15939.
(30). Bucar, D.K. and MacGillivray, L.R. Preparation and reactivity of nanocrystalline cocrystals formed via sonocrystallization. *J. Am. Chem. Soc.*, **2007**, 129, 32–33.
(31). Kuzmanich, G., Gard, M.N., and Garcia-Garibay, M.A. Photonic amplification by a singlet-state quantum chain reaction in the photodecarbonylation of crystalline diarycyclopropenones. *J. Am. Chem. Soc.*, **2009**, 131, 11606–11614.
(32). Irie, M. Diarylethenes for memories and switches. *Chem. Rev.*, **2000**, 100, 1685–1716.
(33).Shibata, K., Muto, K., Kobatake, S., and Irie, M. Photocyclization/cycloreversion quantum yields of diarylethenes in single crystals. *J. Phys. Chem. A.*, **2002**, 106, 209–214.
(34). Irie, M., Kobatake, S., and Horichi, M. Reversible surface morphology changes of a photochromic diarylethene single crystal by photoirradiation. *Science.*, **2001**, 291, 1769–1772.
(35). Kobatake, S., Takami, S., Muto, H. et al. Rapid and reversible shape changes of molecular crystals on photoirradiation. *Nature.*, **2007**, 446, 778–781.
(36). Terao F, Morimoto M, Irie M. Light ‐ Driven Molecular ‐ Crystal Actuators: Rapid and Reversible Bending of Rodlike Mixed Crystals of Diarylethene Derivatives. *Angew. Chem. Int. Ed.*, **2012**, 23, 124, 925-928.
(37). Jiang, L.; Hu, W.; Wei, Z.; Xu, W.; Meng, H. High-Performance Organic Single-Crystal Transistors and Digital Inverters of an Anthracene Derivative. *Adv. Mater.*, **2009**, 21, 3649−3653.
(38). Panda, M. K.; Ghosh, S.; Yasuda, N.; Moriwaki, T.; Dev Mukherjee, G.; Reddy, M. C.; Naumov, P. Spatially Resolved Analysis of Short-Range Structure Perturbations in a Plastically Bent Molecular Crystal. *Nat. Chem.*, **2015**, 7, 65−72.

(39). Ghosh, S.; Reddy, C. M. Elastic and Bendable Caffeine Cocrystals: Implications for the Design of Flexible Organic Materials. *Angew. Chem., Int. Ed.*, **2012**, 51, 10319−10323.

(40). Panda, M. K.; Runcevski, T.; Husain, A.; Dinnebier, R. E.; Naumov, P. Perpetually Self-Propelling Chiral Single Crystals. *J. Am. Chem. Soc.*, **2015**, 137, 1895−1902.

(41). Naumov P, Chizhik S, Panda MK, Nath NK, Boldyreva E. Mechanically responsive molecular crystals. *Chem. Rev.*, **2015**, 4, 115, 12440-12490.

(42). Boldyrev, V. V. Topochemistry of the Thermal Decomposition of Solid Substances. Russ. *Chem. Rev.*, **1973**, 42, 515−528.

(43). Chupakhin, A. P.; Sidel'nikov, A. A.; Boldyrev, V. V. Control of the Reactivity of Solids by Changing Their Mechanical Properties. *React. Solids.*, **1987**, 3, 1−19.

(44). McBride, J. M.; Segmuller, B. E.; Hollingsworth, M. D.; Mills, D. E.; Weber, B. A. Mechanical Stress and Reactivity in Organic Solids. *Science.*, **1986**, 234, 830−835.

(45). Morimoto M, Irie M. A diarylethene cocrystal that converts light into mechanical work. *J. Am. Chem. Soc.*, **2010**, 132, 14172-14178.

(46). Bushuyev, O. S.; Corkery, T. C.; Barrett, C. J.; Frisčic, T. Photo-mechanical azobenzene cocrystals and in situ X-ray diffraction monitoring of their optically-induced crystal-to-crystal isomerization. *Chem. Sci.*, **2014**, 5, 3158−3164.

(47). Hoshino, M.; Uchida, E.; Norikane, Y.; Azumi, R.; Nozawa, S.; Tomita, A.; Sato, T.; Adachi, S.; Koshihara, S. Crystal Melting by Light: X-ray Crystal Structure Analysis of an Azo Crystal Showing Photoinduced Crystal-Melt Transition. *J. Am. Chem. Soc.*, **2014**, 136, 9158−9164.

(48). Steiner, T.; Hinrichs, W.; Saenger, W.; Gigg, R. 'Jumping Crystals': X-ray Structures of the Three Crystalline Phases of (±)-3,4-Di-O-acetyl-1,2,5,6-tetra-O-benzyl-myo-inositol. *Acta Crystallogr., Sect. B: Struct. Sci.*, **1993**, B49, 708−718.

(49). Hosono N, Kajitani T, Fukushima T, Ito K, Sasaki S, Takata M, Aida T. Large-area three-dimensional molecular ordering of a polymer brush by one-step processing. *Science.*, **2010**, 330, 6005, 808-811.

(50). Yu Y, Nakano M, Ikeda T. Photomechanics: directed bending of a polymer film by light. *Nature.*, **200**3, 425, 6954, 145.

(51). Yamada M, Kondo M, Mamiya JI, Yu Y, Kinoshita M, Barrett CJ, Ikeda T. Photomobile polymer materials: towards light‐driven plastic motors. *Angew. Chem. Int. Ed.*, **2008**, 47, 23, 4986-4988.

(52). Koshima, H.; Ojima, N.; Uchimoto, H. Mechanical Motion of Azobenzene Crystals upon Photoirradiation. *J. Am. Chem. Soc.*, **2009**, 131, 6890−6891.

(53). Bushuyev OS, Tomberg A, Friščić T, Barrett CJ. Shaping crystals with light: crystal-to-crystal isomerization and photomechanical effect in fluorinated azobenzenes. *J. Am. Chem. Soc.*, **2013**, 135, 34, 12556-12559.

(54). Bushuyev OS, Singleton TA, Barrett CJ. Fast, reversible, and general photomechanical motion in single crystals of various azo compounds using visible light. *Adv. Mater.*, **2013**, 25,12, 1796-1800.

(55). Sun, J.-K.; Li, W.; Chen, C.; Ren, C.-X.; Pan, D.-M.; Zhang, J. Photoinduced Bending of a Large Single Crystal of a 1,2-Bis(4-pyridyl)ethylene-Based Pyridinium Salt Powered by a [2+2] Cycloaddition. *Angew. Chem., Int. Ed.*, 2013, 52, 6653−6657.

(56). Kim T, Zhu L, Al‐Kaysi RO, Bardeen CJ. Organic photomechanical materials. *ChemPhysChem.*, **2014**, 15, 3, 400-414.
(57). Zhu, L., Al-Kaysi, R.O. and Bardeen, C.J., Reversible photoinduced twisting of molecular crystal microribbons. *J. Am. Chem. Soc.*, **2011**, 133, 12569-12575.
(58). Zhu, L., Al-Kaysi, R.O., Dillon, R.J. et al. Crystal structures and photophysical properties of 9-anthracene carboxylic acid derivatives for photomechanical applications. *Cryst. Growth Des.*, **2011**, 11, 4975–4983.
(59). Zhu, L., Tong, F., Salinas, C. et al. Improved solid-state photomechanical materials by fluorine substitution of 9-anthracene carboxylic acid. *Chem. Mater.*, **2014**, 26, 6007–6015.
(60). Koshima H, Nakaya H, Uchimoto H, Ojima N. Photomechanical motion of furylfulgide crystals. *Chem. Lett.*, **2011**, 41, 107-109.
(61). Koshima H, Matsuo R, Matsudomi M, Uemura Y, Shiro M. Light-driven bending crystals of salicylidenephenylethylamines in enantiomeric and racemate forms. *Cryst. Growth Des.*, **2013**, 13, 10, 4330-4337.
(62). Kim T, Zhu L, Mueller LJ, Bardeen CJ. Dependence of the solid-state photomechanical response of 4-chlorocinnamic acid on crystal shape and size. *CrystEngComm.*, **2012**, 14, 22, 7792-7799.
(63). Sun JK, Li W, Chen C, Ren CX, Pan DM, Zhang J. Photoinduced Bending of a Large Single Crystal of a 1, 2‐Bis (4‐pyridyl) ethylene‐Based Pyridinium Salt Powered by a [2+ 2] Cycloaddition. *Angew. Chem. Int. Ed.*, **2013**, 52, 26, 6653-6657.
(64). Naumov P, Kowalik J, Solntsev KM, Baldridge A, Moon JS, Kranz C, Tolbert LM. Topochemistry and photomechanical effects in crystals of green fluorescent protein-like chromophores: effects of hydrogen bonding and crystal packing. *J. Am. Chem. Soc.*, **2010**. 132. 16. 5845-5857.
(65). H. Durr and H. Bouas-Laurent, Photochromism: Molecules and Systems, *Elsevier, New York.*, **1990**.
(66). S. Kobatake and Y. Terakawa, Acid-Induced Photochromic System Switching of Diarylethene Derivatives between P- and T-Types, *Chem. Commun.*, **2007**, 1698–1700.
(67). M. Warner, Photoinduced Deformations of Beams, Plates, and Films, *Phys. Rev. Lett.*, **2004**, 92, 134302.
(68). Lambert JH. Photometria sive de mensura et gradibus luminis, colorum et umbrae. *Klett.*, **1760**.
(69). T. Kim, L. Zhu, L. J. Mueller and C. J. Bardeen, Mechanism of Photo-Induced Bending and Twisting in Crystalline Microneedles and Microribbons Composed of 9-Methylanthracene, *J. Am. Chem. Soc.*, **2014**, 136, 6617–6625.
(70). Salzillo T, Zaccheroni S, Della Valle RG, Venuti E, Brillante A. Micro Raman Investigation of the Photodimerization Reaction of 9-Cyanoanthracene in the Solid State. *J. Phys. Chem. C.*, **2014**, 118, 18, 9628-9635.
(71). McBride, J.M., Segmuller, B.E., Hollingsworth, M.D. et al. Mechanical stress and reactivity in organic solids. *Science.*, **1986**, 234, 830–835.
(72). Luty, T. and Eckhardt, C.J. General theoretical concepts for solid state reactions: quantitative formulation of the reaction cavity, steric compression, and reaction-induced

stress using an elastic multipole representation of chemical pressure. *J. Am. Chem. Soc.*, **1995**, 117, 2441–2452.

(73). Peachey, N.M. and Eckhardt, C.J. (1993) Energetics of organic solid-state reactions: lattice dynamics in the 2, 5-distyrlpyrazine photoreaction. *J. Phys. Chem.*, **1993,** 97, 10849–10856.

(74). Bertmer, M., Nieuwendaal, R.C., Barnes, A.B., and Hayes, S.E. Solid-state photodimerization kinetics of a-trans-cinnamic acid to a-truxillic acid studied via solid-state NMR. *J. Phys. Chem. B.*, **2006**, 110, 6270–6273.

(75). More, R., Busse, G., Hallmann, J. et al. Photodimerization of crystalline 9-anthracenecarboxylic acid: a nontopotactic autocatalytic transformation. *J. Phys. Chem. C.*, **2010**, 114, 4142–4148.

(76). Avrami, M. Kinetics of Phase Change. I. General Theory. *J. Chem. Phys.*, **1939**, 7, 1103–1112.

(77). Avrami, M. Kinetics of Phase Change. II. Transformation-Time Relations for Random Distribution of Nuclei. *J. Chem. Phys.*, **1940**, 8, 212–224.

(78). Avrami, M. Kinetics of Phase Change. III. Granulation, Phase Change, and Microstructure. *J. Chem. Phys.*, **1941**, 9, 177–184.

(79). Fanfoni, M. and Tomellini, M., The johnson-mehl-avrami-kohnogorov model: a brief review. *Il Nuovo Cimento D.*, **1998**, 20, 1171-1182.

(80). J. F. Sonnenberg and R. H. Morris, Distinguishing Homogeneous from Nanoparticle Asymmetric Iron Catalysis., *Catal. Sci. Technol.*, **2014**, 4, 3426–3438.

(81). M. B. Borgia, A. A. Nickson, J. Clarke and M. J. Hounslow, A Mechanistic Model for Amorphous Protein Aggregation of Immunoglobulin-like Domains, *J. Am. Chem. Soc.*, **2013**, 135, 6456–6464.

(82). A. M. Morris, M. A. Watzky and R. G. Finke, Protein Aggregation Kinetics, Mechanism, and Curve-Fitting: A Review of the Literature, *Biochim. Biophys. Acta.*, **2009**, 1794, 375–397.

(83). A. M. Morris, M. A. Watzky, J. N. Agar and R. G. Finke, Fitting Neurological Protein Aggregation Kinetic Data via a 2-Step, Minimal/‘‘Ockham’s Razor’’ Model: The Finke–Watzky Mechanism of Nucleation Followed by Autocatalytic Surface Growth, *Biochemistry.*, **2008**, 47, 2413–2427.

(84). S. A. Sievers, J. Karanicolas, H. W. Chang, A. Zhao, L. Jiang, O. Zirafi, J. T. Stevens, J. Munch, D. Baker and D. Eisenberg, Structure-Based Design of Non-Natural Amino-Acid Inhibitors of Amyloid Fibril Formation, *Nature.*, **2011**, 475, 96–100.

(85). E. E. Finney and R. G. Finke, Is There a Minimal Chemical Mechanism Underlying Classical Avrami-Erofe’ev Treatments of Phase-Transformation Kinetic Data? *Chem. Mater.*, **2009**, 21, 4692–4705.

(86). Tong, F., Hanson, M.P. and Bardeen, C.J., Analysis of reaction kinetics in the photomechanical molecular crystal 9-methylanthracene using an extended Finke–Watzky model. *Phys. Chem. Chem. Phys.*, **2016**, 18, 31936-31945.

(87). Kitagawa D, Tanaka R, Kobatake S. Dependence of photoinduced bending behavior of diarylethene crystals on irradiation wavelength of ultraviolet light. *Phys. Chem. Chem. Phys.*, **2015**, 17, 41, 27300-27305.

(88). Kitagawa D, Nishi H, Kobatake S. Photoinduced twisting of a photochromic diarylethene crystal. *Angew. Chem. Int. Ed.*, **2013**, 52, 35, 9320-9322.
(89). Kitagawa D, Iwaihara C, Nishi H, Kobatake S. Quantitative Evaluation of Photoinduced Bending Speed of Diarylethene Crystals. *Crystals.*, **2015**, 5, 4, 551-561.
(90). Timoshenko S. Analysis of bi-metal thermostats. *JOSA*. **1925**, 11, 3, 233-255.
(91). Uchida E, Azumi R, Norikane Y. Light-induced crawling of crystals on a glass surface. *Nat. Comm.*, **2015**, 18, 6.
(92). Kim T, Al‐Muhanna MK, Al‐Suwaidan SD, Al‐Kaysi RO, Bardeen CJ. Photoinduced curling of organic molecular crystal nanowires. *Angew. Chem. Int. Ed.*, **2013**, 52, 27, 6889-6893.
(93). Al-Kaysi RO, Dillon RJ, Zhu L, Bardeen CJ. Template assisted synthesis of silica-coated molecular crystal nanorods: from hydrophobic to hydrophilic nanorods. Journal of colloid and interface science., **2008**, 327, 1, 102-107.
(94). Good JT, Burdett JJ, Bardeen CJ. Using Two‐Photon Excitation to Control Bending Motions in Molecular‐Crystal Nanorods. *Small.*, **2009**, 18, 5, 24, 2902-2909.
(95). Dong Q, Fang Y, Shao Y, Mulligan P, Qiu J, Cao L, Huang J. Electron-hole diffusion lengths>175 μm in solution-grown CH3NH3PbI3 single crystals. *Science.*, **2015**, 347, 6225, 967-970.
(96). Campione M, Ruggerone R, Tavazzi S, Moret M. Growth and characterisation of centimetre-sized single crystals of molecular organic materials. *J. Mater. Chem.*, **2005**, 15, 25, 2437-2443.
(97). Chen S, Ji H, Chou H, Li Q, Li H, Suk JW, Piner R, Liao L, Cai W, Ruoff RS. Millimeter‐size single‐crystal graphene by suppressing evaporative loss of Cu during low pressure chemical vapor deposition. *Adv. Mater.*, **2013**, 25, 14, 2062-2065.
(98). Al-Kaysi RO, Bardeen CJ. General method for the synthesis of crystalline organic nanorods using porous alumina templates. *Chem. Comm.*, **2006**, 11, 1224-1226.
(99). Al-Kaysi, R.O., Tong, F., Al-Haidar, M., Zhu, L. and Bardeen, C.J., 2017. Highly branched photomechanical crystals. *Chem.Comm.*, **2017**, 53, 2622-2625.
(100). Zhu, L., Al‐Kaysi, R.O. and Bardeen, C.J., Photoinduced Ratchet‐Like Rotational Motion of Branched Molecular Crystals. *Angew. Chem. Int. Ed.*, **2016**, 55, 7073-7076.
(101). Adachi H, Takano K, Hosokawa Y, Inoue T, Mori Y, Matsumura H, Yoshimura M, Tsunaka Y, Morikawa M, Kanaya S, Masuhara H. Laser irradiated growth of protein crystal. *Jpn. J. Appl. Phys.*, **2003**, 42, 798-800.
(102). Abendroth JM, Bushuyev OS, Weiss PS, Barrett CJ. Controlling motion at the nanoscale: rise of the molecular machines. *ACS nano.*, **2015**, 9, 7746-7768.
(103). Koshima H, Takechi K, Uchimoto H, Shiro M, Hashizume D. Photomechanical bending of salicylideneaniline crystals. *Chem. Comm.*, **2011**, 47, 41, 11423-11425.
(104). Lee J, Oh S, Pyo J, Kim JM, Je JH. A light-driven supramolecular nanowire actuator. *Nanoscale.*, **2015**, 7, 15, 6457-6461.
(105). Naumov P, Sahoo SC, Zakharov BA, Boldyreva EV. Dynamic single crystals: kinematic analysis of photoinduced crystal jumping (the photosalient effect). *Angew. Chem. Int. Ed.*, **2013**, 52, 38, 9990-9995.

(106). Commins, P.; Natarajan, A.; Tsai, C.-K.; Khan, S. I.; Nath, N. K.; Naumov, P.; Garcia-Garibay, M. A. Structure−Reactivity Correlations and Mechanistic Understanding of the Photorearrange ment and Photosalient Effect of α-Santonin and Its Derivatives in Solutions, Crystals, and Nanocrystalline Suspensions. *Cryst. Growth Des.*, **2015**, 15, 1983−1990.

(107). Medishetty, R.; Husain, A.; Bai, Z.; Runcevski, T.; Dinnebier, R. E.; Naumov, P.; Vittal, J. J. Single Crystals Popping Under UV Light: The First Example of a Photosalient Effect Triggered by a [2+2] Cycloaddition Reaction. *Angew. Chem., Int. Ed.*, **2014**, 53, 5907−5911.

(108). Kitagawa D, Okuyama T, Tanaka R, Kobatake S. Photoinduced Rapid and Explosive Fragmentation of Diarylethene Crystals Having Urethane Bonding. *Chem. Mater.*, **2016**, 28, 14, 4889-4892.

(109). Colombier, I.; Spagnoli, S.; Corval, A.; Baldeck, P. L.; Giraud, M.; Leaustic, A.; Yu, P.; Irie, M. Diarylethene Microcrystals Make Directional Jumps Upon Ultraviolet Irradiation. *J. Chem. Phys.*, **2007**, 126, 011101.

(110) Colombier, I.; Spagnoli, S.; Corval, A.; Baldeck, P. L.; Giraud, M.; Leaustic, A.; Yu, P. Strong Photomechanical Effects in Photo-chromic Organic Microcrystals. *Mol. Cryst. Liq. Cryst.*, **2005**, 431, 495−499.

(111) Tong, F., Cruz, C.D., Jezowski, S.R., Zhou, X., Zhu, L., Al-Kaysi, R.O., Chronister, E.L. and Bardeen, C.J., Pressure dependence of the forward and backward rates of 9-tert-butylanthracene dewar isomerization. *J. Phys. Chem. A.*, **2014**, 118, pp.5349-5354.

(112) Tong, F., Liu, M., Al-Kaysi R.O. Bardeen C. J., Surfactant-enhanced photoisomerization and photomechanical response in molecular crystal nanowires. *Langmuir.*, **2017**, (submited)

Chapter 2 Experimental details

2.1 Solid-state organic nanowires preparation by AAO template method

2.1.1 Introduction of AAO template method

The synthesis of such organic nanostructures with good control over both size and morphology is challenging because the cohesive forces between units (molecules) are relatively weak compared to the covalent bonds found in inorganic materials. A more promising route is the use of uniformly sized templates which force the organics to assemble within a well-defined space.[1,2] The commercial availability of high porosity Al_2O_3 filters has made them the most commonly used template for the fabrication of organic nanotubes and nanowires. Because of the surface energy gained by interaction of the organics with the walls of the Al_2O_3 channels, the most common outcome of exposing such membranes to organics is the formation of tubes.[3]

2.1.2 Bell jar vails setups for nanowires preparation

In our lab, we usually take advantage of anodic aluminum oxide (AAO) templates to growth nanosized rod-like organic compounds. Figure 2.1 shows the setup that we use to prepare organic nanowires. Usually, several milligrams of solid compound will dissolve into 50~100 microliters of organic solvents to form a homogenous solution. The solution will be dropped cast onto a blank AAO template which is sitting on a flat Teflon stage. The Teflon stage with the AAO template will be then put into a glass bell jar for solvent annealing. It usually takes a few days for all solvent to evaporate and allow organic compound to grow into crystallize inside the AAO template channels. The temperature setting will depend on the compound and solvent. Basically, solvents with low viscosity will need more time and higher temperature to evaporate, but the temperature will never go over 100 ^{o}C.

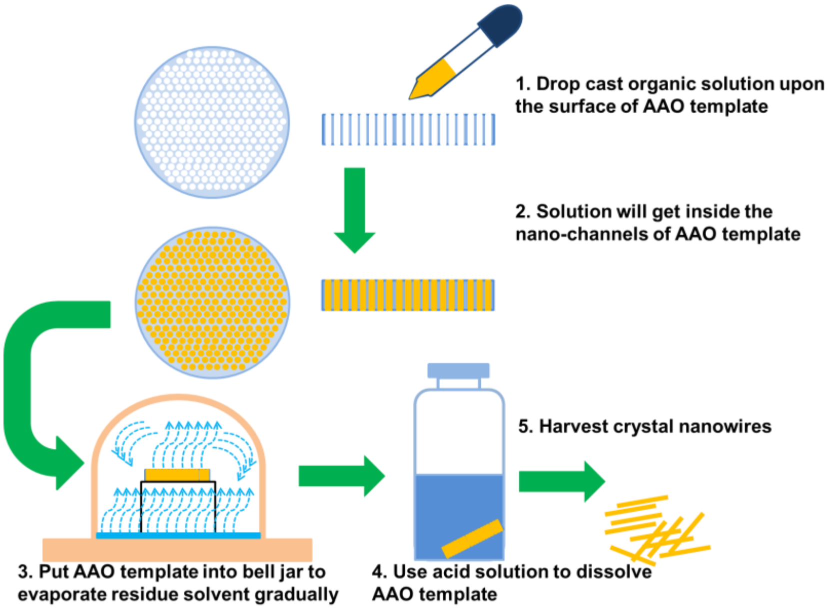

Figure 2.1 The general procedures of preparing organic compounds by using AAO template method.

2.1.3 Sample polishing and separation

We take out the AAO template after the solvent inside the AAO template fully evaporates. Sandpaper (2000 grit, main material: SiC) will be used to polish the AAO template in order to get rid of the residual compound left on the template surface. The AAO template is first placed onto a Teflon stage with several small holes and then the whole stage will be put onto a filtering flask. During the polishing process, a small vacuum will be applied in order to fix the AAO template during the polish. It is necessary to polish both faces of template so that they become shiny.

After polishing, the whole template will be put in an aqueous solution consisting of 20~50% wt phosphoric acid and 0.2 % wt sodium dodecyl sulfate (SDS). Individual nanowires will be obtained after a few days of dissolving the AAO template and Figure 2.2 is the Scanning Electron Microscopy (SEM) image of diarylethene nanowires harvested after dissolving AAO template.

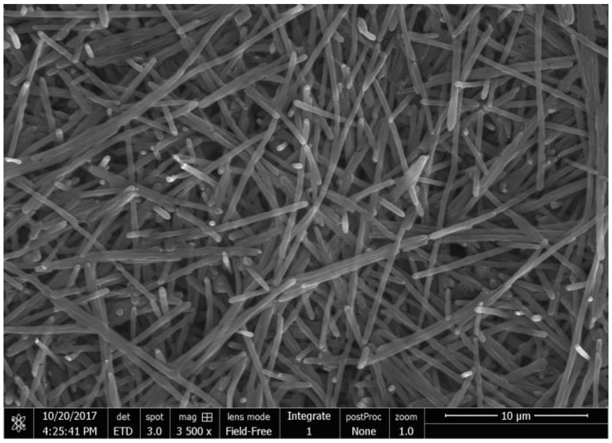

Figure 2.2 SEM images of diarylethene nanowires prepared by AAO template method.

2.2 Solid-state organic microcrystals preparation by floating drop method

2.2.1 Introduction of floating drop method

It is very important to make high quality single crystal of organic compounds with large size for characterization techniques, such as optical characterization and reflection measurements[4]. Some reliable methods have been proposed for single crystal growth in organic compounds, such as vapor-phase crystal growth[5, 6]. However, the phase transitions during the heating process may limit or even prevent crystallization in certain materials. Moreover, it is easy to damage crystals when they are removed from the growth vessel, as most of the resulting crystals are thin and brittle.

One alternative way is to grow crystals from solution when a suitable solvent can be found. Also one can place the solution upon the surface of a denser, immiscible, and non-wettable liquid, which is called the floating drop (FD) method[7]. This method was used to grow single crystal of proteins from aqueous solution and then extended to the growth of anthracene and pyrene single crystals.

When a drop of solvent is added upon the surface another liquid in which it cannot be dissolved, we can expect two different behaviors:

(i) The drop spreads over the liquid surface until it covers the whole surface.

(ii) The drop forms a compact lens.

These two different behaviors can be described in terms of the spreading coefficient $S=\gamma_1-\gamma_2-\gamma_{12}$, where$\gamma_1$, γ_2 andγ_{12} are the surface tensions of the liquid substrate, solvent, and liquid substrate/solvent interfaces, respectively. The physics of the liquid on the surface of liquid substrate has been studied extensively by Langmuir[8]. The thickness of compact lens in case (ii) can be also described in the following equation:

$$t_\infty^2 = \frac{-2S\rho_1}{g\rho_2(\rho_1-\rho_2)}$$

where ρ_1 and ρ_2 are the density of the liquid substrate and the solvent respectively, and the g is the gravity acceleration. Figure 2.3 shows the two-liquid system at equilibrium in case (ii) by Langmuir. During the floating-drop process, the drop of the solvent that contains the dissolved compound is deposited onto the liquid substrate surface and it is allowed to dry slowly to obtain good crystal eventually.

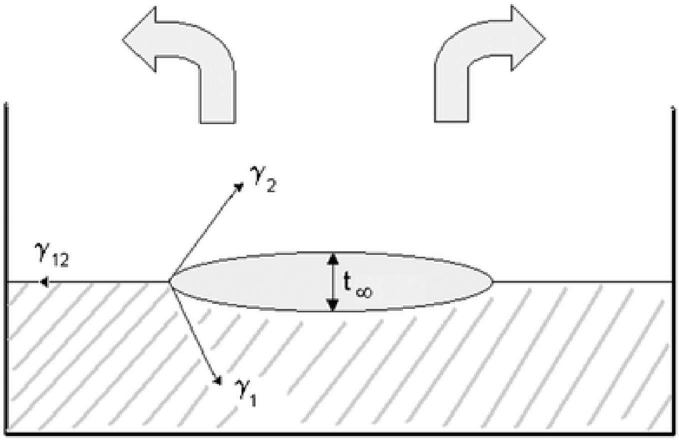

Figure 2.3 Lens floating on the surface of a liquid bath. The surface tensions of the liquid substrate, solvent, and substrate/solvent interface are marked γ_1, γ_2, and γ_{12}, respectively; t_∞ is the equilibrium thickness of the lens. (Reproduced with the permission of Royal Society of Chemistry.)

2.2.2 Setups description and sample preparation

In our group, we use the floating drop method to grow microcrystals of anthracene derivatives. Figure 2.4 shows the typical scheme of the experiment.

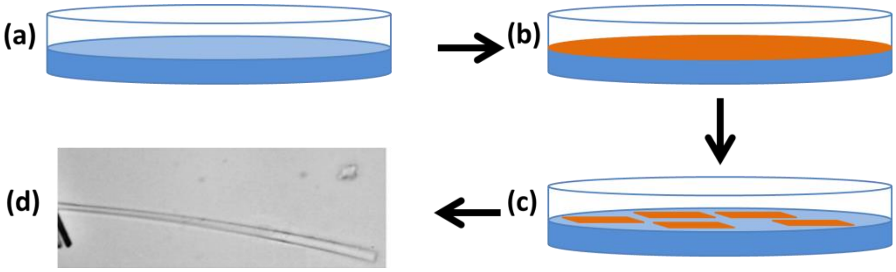

Figure 2.4 The typical procedure of floating drop method to make microcrystals of anthracene derivatives. (a) Several milliliters of water have been added into a petri dish. (b) The solvent consisting of organic compound is deposited onto water surface. (c) Microcrystals form after slowing evaporation of solvent. (d) Optical microscope image of a single 9AC microribbon obtained by using floating drop method.

Usually several milliliters of H_2O will be added into a Petri dish to form a flat surface as the liquid substrate. Then the several microliters of solvent which contains organic compound will be deposited upon the H_2O surface using a pipette. The Petri dish will be covered to slow down the evaporation of organic solvent in order to grow good crystals.

It usually takes a few days for the solvent evaporate entirely and eventually get the micro sized crystals.

As we mentioned above, the duration of the solvent evaporation depends on the solvent. Slower evaporation of solvent will generate better crystals. Usually solvents with high boiling points need to more time to evaporate than others with low boiling points. For example, it usually it takes a week for xylenes to reach full evaporation while it only takes one day for the same amount of hexane to achieve full evaporation. Another effect that may affect the evaporation rate is the concentration of compounds. As for choice of solvent, it must not dissolve in water, and also its density should be less than the density of H_2O. Ethyl acetate is a good candidate for the floating-drop method as its boiling point (77^oC) is between xylenes ($\sim 140^oC$) and hexane (68^oC), so it will evaporate neither too slowly nor too fast. Moreover, ethyl acetate can dissolve most organic compounds with its medium polarity and viscosity. Figure 2.5 shows a 4F9AC microcrystal prepared by using ethyl acetate.[9]

In summary, the floating-drop method is an alternative way to prepare high quality crystals with large size. Moreover, this method does not require high temperature heating and the set-up for sample preparation is quite simple. In some cases, the crystal shape can be optimized by using different solvents and tuning the concentration.

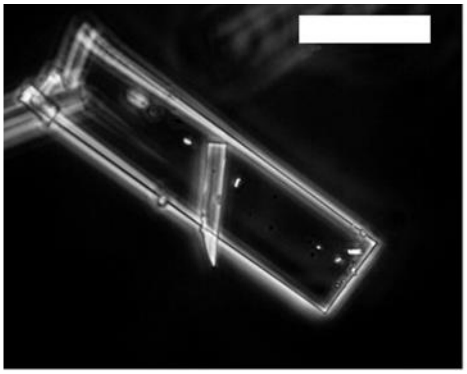

Figure 2.5 Optical microscopy images 4F-9AC crystals via floating drop method with ethyl acetate as solvent, scale bars: 50μm.

2.3 Other methods to prepare microcrystals

2.3.1 Seed-growth method to prepare microcrystals

The crystal size and shape play a key role in the photomechanical properties. Nano-sized crystals made by AAO template method allows us to make rod-like nanowires and the floating-drop method allows us to obtain ribbon like shape crystals. However, such simple one or two-dimensional shapes are limited in the type of mechanical motions they can generate, such as bending and twisting.

We continued to explore if we would grow more interesting shapes with interesting photomechanical properties. By optimizing the growth conditions we successfully made some highly branched microcrystals with hundreds of arm from the center point. These highly branched microcrystals showed reversible bending towards the center part under light irradiation. Therefore, the entire structure can act as a microscopic broom, sweeping silica microspheres across a surface.[10]

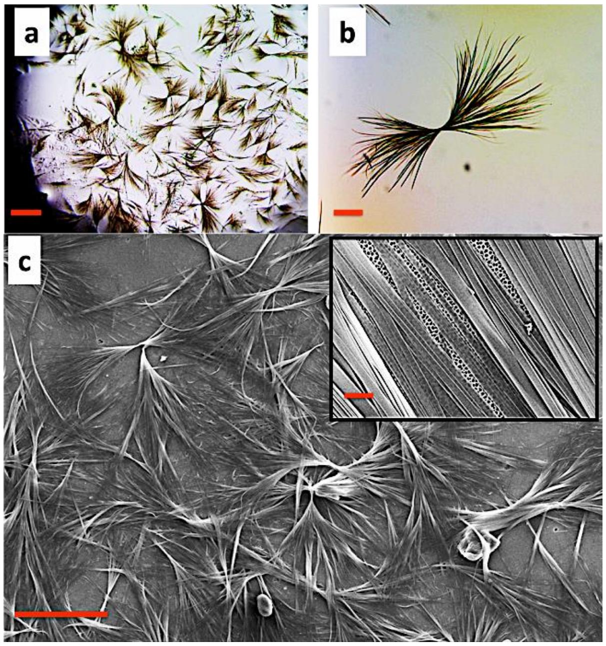

Figure 2.6 (a) Optical microscope image of a cluster of branched microcrystals grown under the optimal conditions. Scale bar = 400 µm. (b) A single symmetrical branched crystal. Scale bar = 50 µm. (c) SEM image of branched microcrystals filtered over an anodisc. Scale bar = 100 µm. Inset: Magnified image of the branches showing their ribbon like morphology. Scale bar = 2 µm. (Reproduced with the permission of Royal Society of Chemistry)

Here is how we prepare these highly branched microcrystals. A solution of *tert*-butyl-4F9AC in acetonitrile (50 mM) was used to deposit ~ 1.0 mg of the *tert*-butyl ester in a 20 mL reaction vial. The acetonitrile was evaporated under argon gas, leaving behind a thin polycrystalline film. A 10 mL aqueous solution of H_3PO_4 (3.5 M), sodium dodecyl sulfate (SDS, 10 mM) and 1-dodecanol (1 mM) was added to the vial, resulting in a *tert*-butyl-4F9AC concentration of ~0.3 mM. The resulting mixture was sonicated for a minute to disperse the ester film. The vial was fixed perpendicular to the rotational axis of a benchtop rotary laboratory mixer set at 8 rpm inside a large convection oven t at 35°C. Mixing for 3 days resulted in a cloudy suspension of highly branched 4F9AC microcrystals. Figure 2.6 shows the optical microscope and SEM images of highly branched microcrystals.

2.3.2 9MA microplates preparation

9MA hexagonal microplates can be prepared by using the seed-growth method as well and the preparation procedures were described as follows:

Preparation of 9MA seeds: 9MA (Sigma Aldrich, 99% +) powder was dissolved in N, N-DMF (ACS, 99% +) to form a solution (0.2 M). 10 mL of an aqueous solution (0.025 M)of sodium dodecyl sulfate (SDS, Sigma Aldrich, 99% +) was added into a 20 mL glass vial. Then the glass vial was placed into a water bath with the temperature at 37^{o}C. When the temperature stabilized, 50 μL of the 9MA solution was rapidly injected into the SDS solution and a magnetic stir bar (1/2 × 1/8 inch) was used (400 rpm) to stir the solution. Small 9MA crystals could be observed after about 15 min stirring. These 9MA seeds usually are 30~60 μm in length and 20~30 μm in width (Figure 2.7a).

Preparation of large 9MA microplates: 10 mL SDS/ 1-dodecanol (Alfa Aesar, 98% +) aqueous solution (SDS: 0.02 M, 1-dodecanol: 0.0022 M) was added into a 20 mL glass vial. The glass vial was placed in a water bath set at 37^{o}C. When the temperature stabilized, 50μL of the 9MA solution was quickly injected and the vial was given a gentle swirl. When the solution was clear, the vial was put back to the water bath and a 50μL suspension of the 9MA seeds was gently pipetted inside the metastable 9MA/SDS/1-

dodecanol solution. The mixture was left at 37°C without stirring and large microplates, usually in several hundred of micrometers in length, could be seen in the solution after two hours (Figure 2.7b).

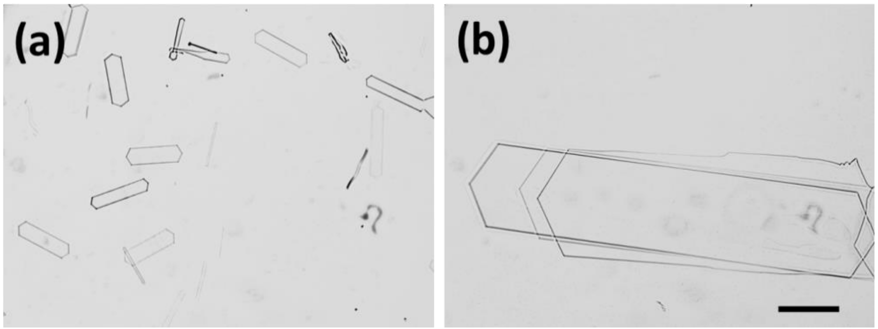

Figure2.7 (a) Seeds of 9MA hexagon microplates. (b) 9MA hexagon microplates after 2 hours incubation in oven. Scale bar: 50 µm

2.4 Solid-state film preparation

2.4.1 9TBA in polymeric film and diamond anvil cell setups

Sometimes people need to probe chemical processes of organic compounds in organic solvents. However, people have to be careful when they measure samples under some specific conditions. For example, most organic solvents tend to evaporate when the ambient temperature increases, and also some of them like chloroform contain O_2, which may lead to side reactions. Some properties like the fluorescence lifetime and molecular orientation will be quite different between solid-state and liquid phase.

One way to avoid evaporation is to make solid-state polymer films for measurements. People can choose different polymers according to various experimental requirements. We have used Zeonex polymer as a matrix to contain 9TBA molecules to measure the pressure dependence of photochemical reactions. Zeonex is a cyclolefin resin polymer which offers excellent optical properties and it used in cameras, laser printers and other optical measurements. In order to drive the photochemical reaction of 9TBA, which undergoes photoisomerization to its Dewar isomer under 365 nm UV light irradiation, we need to monitor its main absorption band near 263 nm, the UV- transparent Zeonex was chosen as the polymer host. Both 9TBA and Zeonex were dissolved into cyclohexane. Then, the mixture was ultrasonicated in the dark for about 1 h. The mixture can also be heated up at 60^{o}C in order to speed up the dissolution process. After all solids dissolved in the cyclohexane, the solution was then drop cast into a glass cylinder holder which is sitting on a clean glass side (Figure 2.8) to allow cyclohexane to evaporate in darkness.

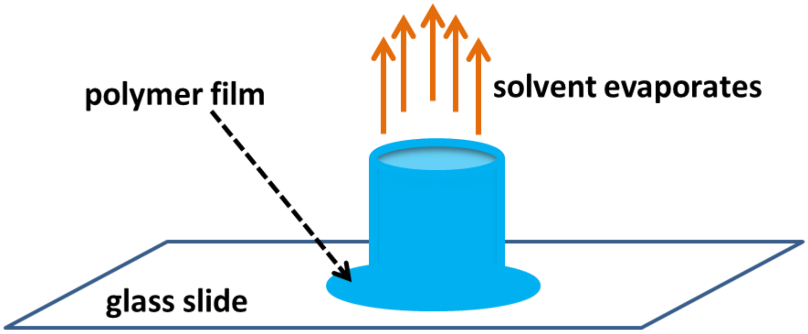

Figure 2.8 The setup and process of preparation 9TBA-Zeonex film. Cyclohexane will evaporate through the channel of the cylinder glass holder.

It usually takes 2~3 days to evaporate the solvent, leaving a transparent solid-state polymer film. The thickness of the film can be adjusted by adding more solution during the evaporation process, and the average thickness of polymer film is around 0.5~1 mm. The polymer film usually contains O_2 since the cyclohexane evaporates in the air. It is necessary to use a cryostat connected to a vacuum pump to get rid of O_2 since it will affect the photoreaction.

For pressure dependent measurements, we used a diamond anvil cell (DAC) to host the polymer film and applied external high pressure during the experiments (Figure 2.9). Usually a 2 mm × 2mm of square polymer film will be cut and put into the DAC for measurements. More details about this can be found in Chapter 3 as well.

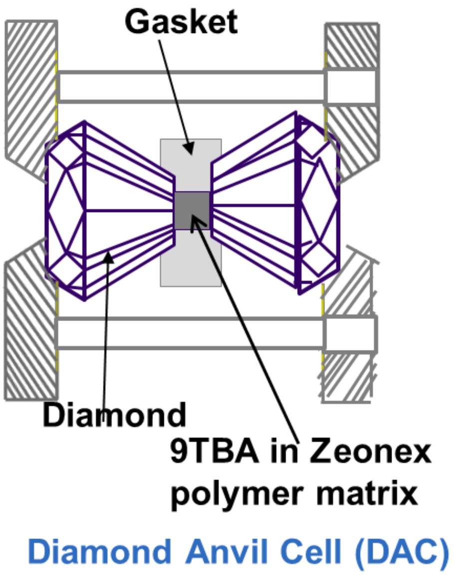

Figure 2.9 The image of diamond anvil cell that was used in pressure dependent experiments.

2.4.2 9MA polycrystalline film preparation

Unlike 9TBA undergoing an intramolecular photoisomerization, 9MA reacts via an intermolecular photodimerization upon UV light irradiation. This requires a monomer pair to be in a specific orientation. Therefore, the random distribution inside a polymer film will inhibit the 9MA photodimerization to occur. In addition, it is usually difficult to obtain large 9MA single crystals, and photodimerization in a large single crystal will result in disintegration. An alternative way is to prepare a 9MA polycrystalline film by drop casting.

Usually, several milligrams of 9MA powder will be dissolved in several milliliters of an organic solvent like chloroform or methylene chloride to form a homogenous solution. A calibrated pipet will be used for drop casting the solution onto a clean glass slide and a light yellow thin polycrystalline film of 9MA will form after all solvent evaporates. The thickness of the film can be tuned by adjusting the concentration and the numbers of drops dropped onto the glass slide. The process of preparing of polycrystalline thin film is shown in Figure 2.10.

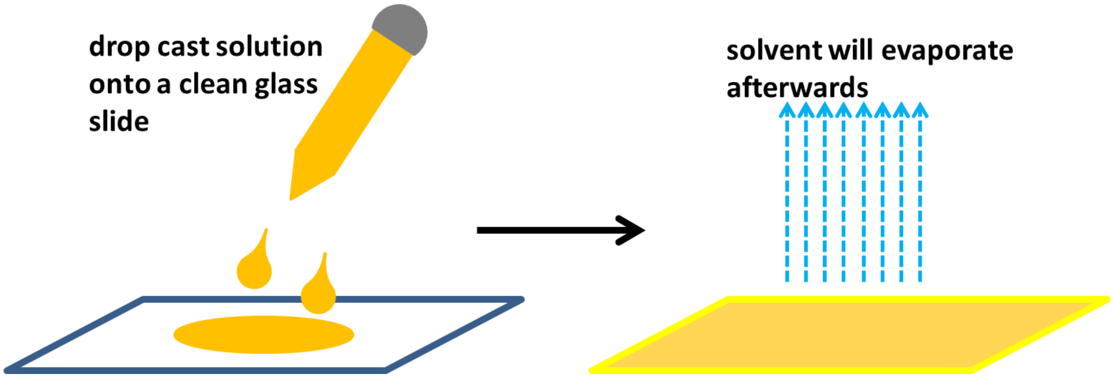

Figure 2.10 The process of preparing of polycrystalline thin film of 9MA via using drop casting method.

The thin polycrystalline film can also contain some amount of O_2, and O_2 can interfere with the photodimerization of 9MA. Therefore, it is necessary to eliminate O_2 before UV light irradiation. The cryostat vacuumed was used to remove O_2 in our experiment, and more details can be found in Chapter 4.

2.5 Characterization methods

2.5.1 Optical microscopy

Optical microscopes are commonly used in our lab to monitor the photomechanical behavior of molecular crystals. Usually both Olympus inverted microscope and upright microscope will be used for the measurements and video recording. Different objectives are chosen according to various requirements. Polarizers will be used in monitor the crystalline samples if it is necessary. Plenty of details can be found in the following chapters of this thesis as well as in publications of our group.

One thing to be mentioned is the method to prevent water from evaporating during the microscopy measurements. We usually add some amount of phosphoric acid (20% in wt) to the aqueous solution, and also we put a cover slide to on top of the sample slide to slow down the evaporation.

2.5.2 UV-Vis absorption spectroscopy

As most of our compounds are highly conjugated anthracene derivatives, they can absorb in the UV and visible regions. UV-Vis absorption spectroscopy is a method which we always use to probe the excited status of our samples. In the Chemistry Department of University of California, Riverside, we use CARY 50 and CARY 500 spectrophotometers for experimental measurements and the standard operations of these instruments can be found in their manuals.

One thing to be mentioned is that the UV-Vis absorption spectra of solid-state samples are different from those in liquid phases. Shown in the Figure 2.11, the UV-Vis absorption spectra of 9-divinylanthracene malonitrile (9DVAM) in the solid state and in liquid solution are showing significantly different. The absorption band in solid state is broader than that in the liquid phase and shows a red shift.[11]

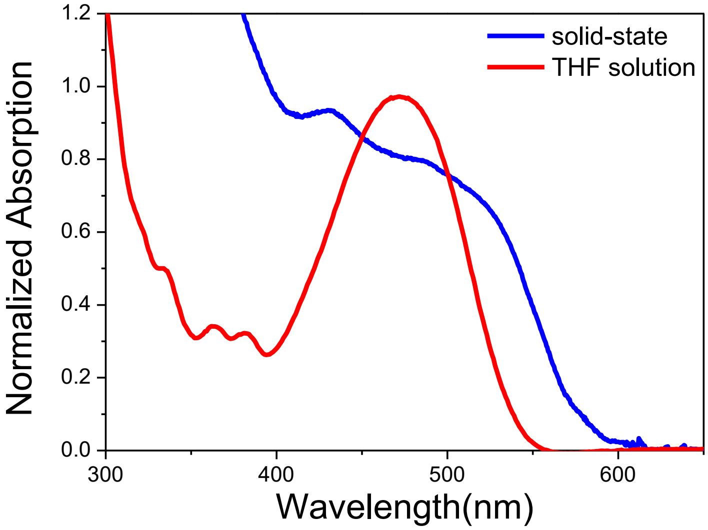

Figure 2.11 UV-Vis absorption spectra of 9DVAM as a solid-state crystalline thin film and in solution with THF as the solvent. 1.5 mg solid of (E)-9DVAM was dissolved in 300μL methylene chloride, then evaporated on a glass slide. During the evaporation period of solvent, 200μL more methylene chloride was deposited onto the glass slide to get high quality solid-state thin film for UV-Vis absorption spectrum.

One reason is because the molecules inside solid-state crystalline film are closely packed together which lowers the energy and extends the absorption to longer wavelength region. On the other hand, the molecules in solution are separated from each other. People can measure the intensity of the absorption peaks and use the absorption coefficient to obtain parameters like kinetic rates and quantum yields from the time-dependent evolution of sample UV-Vis spectra. The relationship of quantum yields and kinetic rates is shown below.

$$k = \sigma I \Phi$$

In this equation, the σ is the cross section of sample which usually indicates the area of absorbed photons and σ can be determined by measuring the absorption coefficient. I is the intensity of excitation light at specific wavelength. Φ is quantum yield and k is the kinetic rate of chemical reaction.

2.5.3 Fluorescence spectroscopy

Fluorescence spectroscopy method is used to complement UV-Vis absorption spectroscopy as a probe of excited electronic and vibrational states of our compounds. The spectra tend to be in solid-state samples as compared to the liquid phase. The time-resolved fluorescence spectroscopy can be used to probe the fluorescence life times of our samples. A Jablonski diagram[12] (Figure 2.12) is necessary to analyze fluorescence data and the relationship of the rate parameters is shown below.

$$k_{fl} = k_f + k_{ic} + k_{isc} + k_{ET} + \ldots = k_{rad} + k_{nr}$$

k_{rad} is the radiative rate of fluorescence, k_{ic} is the rate of internal conversion and vibrational relaxation, k_{isc} is the rate of intersystem crossing, k_{ET} is the rate of intermolecular energy transfer and k_{nr} is the sum of rates non-radiation pathways. Therefore, the overall fluorescence lifetime will be determined by the following equation:

$$\tau_{fl} = k_{fl}^{-1} = (k_{rad} + k_{nr})^{-1}$$

The fluorescence quantum yield can be obtained by

$$QY = \frac{k_{rad}}{k_{rad} + k_{nr}}$$

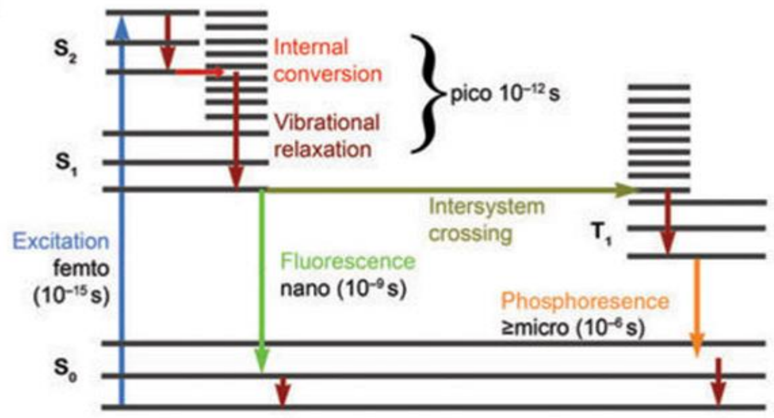

Figure 2.12 The general Jablonski diagram. (Reproduced with the permission of Nature Publishing Group.)

2.5.4 Powder X-Ray diffraction

Powder X-ray diffraction (PXRD) is a technique that we use for identification of a crystalline material, and it also can provide information on unit cell dimensions. The operation of this instrument goes beyond this thesis, and details can be found in the relative manuals. Usually, the samples for PXRD measurements should be fully ground and dry. However, as we found some crystals like 9MA microplates prepared by seed-growth method (Figure 2.13) will become amorphous after grinding.

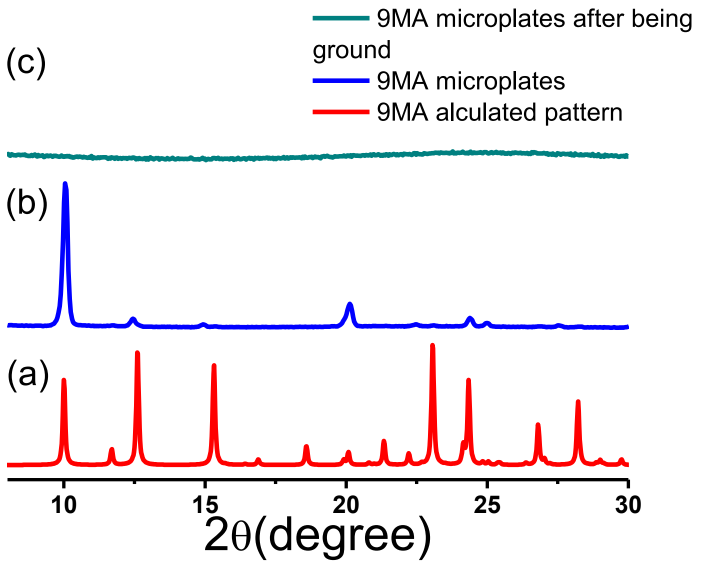

Figure 2.13 The powder X-ray diffraction data of (a) calculated pattern of 9MA compound, (b) 9MA microplates before light exposure and being ground and (c) 9MA microplates after being ground.

2.5.5 SEM

The scanning electron microscope (SEM) is a type of electron microscope that can image surface morphology of a sample by scanning a focused beam of electrons across it. It is usually used when we need to obtain information about small sized materials such as nanocrystals. One issue for organic compounds is that they tend to decompose or sublime under high vacuum in a SEM chamber. One way to avoid this is to sputter coat a metallic thin film upon the surface to protect the sample. Many examples can be found in our previous publications.

2.6 Conclusion

In this chapter we have introduced three general methods we usually use in our lab to make different types of molecular crystals. (1) The AAO template method for nanowires and nanorods. (2) The floating drop method for microcrystal growth. (3) The seed growth method to grow various shapes of crystals. We also discussed some typical characterization methods. Both sample preparation methods and characterization methods are not limited to the descriptions above and can vary according to different experimental requirements. We hope that our work can benefit people who are going to explore this research field, and we also hope that more methods will be established for improved characterization.

2.7 Reference

(1). Martin CR. Nanomaterials: a membrane-based synthetic approach. *Science.*, **1994**, 23, 1961-1966.
(2). Zhi L, Wu J, Li J, Kolb U, Müllen K. Carbonization of Disclike Molecules in Porous Alumina Membranes: Toward Carbon Nanotubes with Controlled Graphene-Layer Orientation. *Angew. Chem. Int. Ed.*, **2005**, 44, 14, 2120-2123.
(3). Al-Kaysi RO, Bardeen CJ. General method for the synthesis of crystalline organic nanorods using porous alumina templates. *Chem. Comm.*, **2006**, 11, 1224-1226.
(4). Siegrist T, Kloc C, Laudise RA, Katz HE, Haddon RC. Crystal Growth, Structure, and Electronic Band Structure of α-4T Polymorphs. *Adv. Mater.*, **1998**, 10, 5, 379-382.
(5). Kloc C, Simpkins PG, Siegrist T, Laudise RA. Physical vapor growth of centimeter-sized crystals of α-hexathiophene. J. *Cryst. Growth.*, **1997**, 182, 3, 416-427.
(6). Laudise RA, Kloc C, Simpkins PG, Siegrist T. Physical vapor growth of organic semiconductors. J. *Cryst. Growth.*, **1998**, 15, 187, 449-454.
(7). Campione M, Ruggerone R, Tavazzi S, Moret M. Growth and characterisation of centimetre-sized single crystals of molecular organic materials. *J. Mater. Chem*., **2005**, 15, 25, 2437-2443.
(8). Langmuir I. Oil lenses on water and the nature of monomolecular expanded films. *J. Chem. Phys.*, **1933**, 11, 756-776.
(9). Zhu L, Tong F, Salinas C, Al-Muhanna MK, Tham FS, Kisailus D, Al-Kaysi RO, Bardeen CJ. Improved solid-state photomechanical materials by fluorine substitution of 9-anthracene carboxylic acid. *Chem. Mater.*, **2014**, 26, 20, 6007-6015.
(10). Al-Kaysi RO, Tong F, Al-Haidar M, Zhu L, Bardeen CJ. Highly branched photomechanical crystals. *Chem. Comm.*, **2017**, 53, 17, 2622-2625.
(11). Zhu L, Tong F, Zaghloul N, Baz O, Bardeen CJ, Al-Kaysi RO. Characterization of a P-type photomechanical molecular crystal based on the E→ Z photoisomerization of 9-divinylanthracene malonitrile. *J. Mater. Chem. C.*, **2016**, 4, 35, 8245-8252.
(12). Lichtman JW, Conchello JA. Fluorescence microscopy. *Nature methods.*, **2005**, 2, 12, 910-919.

Chapter 3 Pressure dependence of the forward and backward rates of 9-tert-butylanthracene Dewar isomerization

3.1 Introduction

Mechanochemistry is a rapidly growing area of research in which mechanical force is used to initiate chemical changes.[1−3] Chemical groups designed to be activated by mechanical force include four-membered rings generated by both chemical and photochemical means,[4,5] as well as six-membered rings that are susceptible to Diels−Alder[6] and retro-Diels−Alder reactions.[7−9] To break chemical bonds, it is generally accepted that some sort of anisotropic shear force must be generated at the molecular level.[10] Examples of such shear forces include pulling on a molecule using a scanning probe microscope tip,[11−13] stretching polymer films,[14] mechanical grinding,[1,3,15−17] and using cavitating bubbles in a sonicated sample.[1,18,19] We have recently investigated the ability of isotropic hydrostatic pressure, as opposed to shear, to generate chemical changes in highly strained photoisomers with different three-dimensional structures.[20] By tethering two anthracene chromophores together using ethyl linkers, we made a cyclophane molecule, bi(anthracene-9,10-dimethylene) (BA), that could undergo intramolecular photodimerization to form a high energy isomer that we denoted PI, as shown in Figure 3.1a.We found that the dissociation of PI in a polymer matrix could be greatly accelerated by the application of relatively low pressures on the order of 1.0 GPa. Pressure-dependent rate measurements indicated that this reaction has a negative activation volume, and this was recently confirmed by ab initio calculations. [21] This pressure sensitivity was not observed in the untethered analogue An_2 (Figure 3.1b). The dramatic acceleration of the PI photodimer dissociation demonstrated that isotropic pressure, as opposed to anisotropic shear, could be used to break chemical bonds.

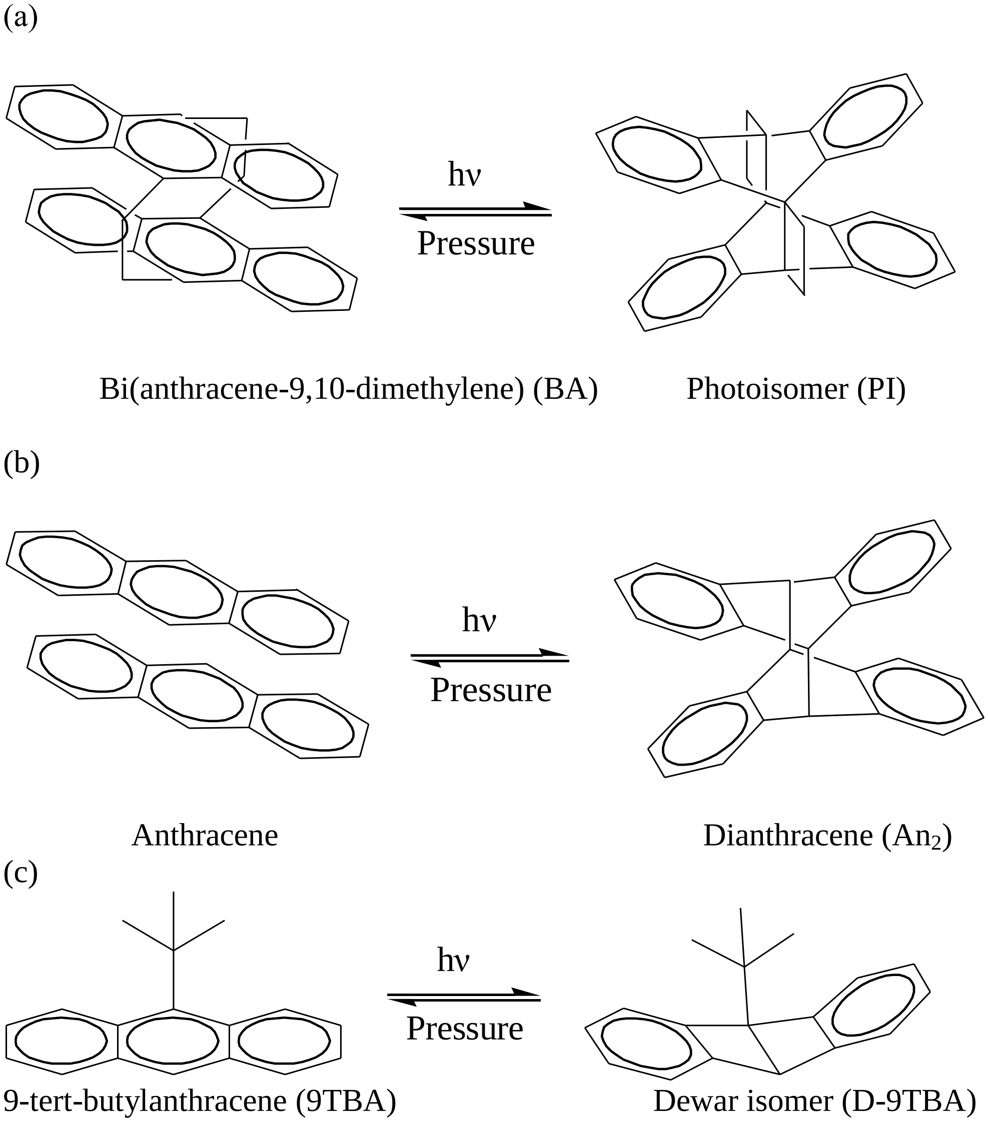

Figure 3.1 (a) [4 + 4] Cyloaddition of bi(anthracene-9,10-dimethylene) (BA) to its high energy photoisomer (PI). (b) [4 + 4] Cyloaddition of anthracene to dianthracene. (c) Photoisomerization of 9-tert-butyylanthracene (9TBA) to its Dewar isomer (D-9TBA). All three reactions are reversible, but only the reverse reactions of (a) and (c) are catalyzed by pressure.

Motivated by our results on BA, we decided to search for other pressure-sensitive reactions. Since the dissociation of the untethered anthracene dimer An_2 was not sensitive to pressure, it seemed clear that the presence of internal six-membered 1,4-cyclohexadiene rings of the [4 + 4] photodimer was not sufficient to induce pressure sensitivity. We decided to examine whether the presence of a pair of internal four-membered rings could lead to increased pressure sensitivity. The Dewar photoisomerization of aromatic molecules is an example of a reaction that produces a pair of strained four-membered rings.[22] Therefore, we used 9-tert-butylanthracene (9TBA), a molecule that photoisomerizes to its 9,10 Dewar form (D-9TBA) in liquid solution[23–25] (Figure 3.1c) to test this hypothesis. The Dewar form is somewhat stable in room temperature solution, with a lifetime of several hours in hexane. By dissolving 9TBA in a polymer matrix and placing it in a diamond anvil cell (DAC), we could test the effect of pressure on the rate of the D-9TBA → 9TBA reaction, which is analogous to the PI → BA conversion. We find that this reaction is also sensitive to pressure, speeding up by almost a factor of 3 as we go from ambient pressure to 1.43 GPa. As expected, we obtain a negative activation volume (-2.3 Å^3) for this reaction. This rate acceleration is about 100× smaller than we observed for the PI→ BA reaction. Taken together, our results on An_2 and D-9TBA suggest that the presence of strained four-membered rings can lead to pressure sensitivity, but not to the degree seen in our earlier work on the PI → BA reaction. Our results suggest that the geometrical arrangement of the molecular elements is of crucial importance to attaining the high pressure sensitivity seen in the PI → BA reaction. The results of this work comprise an important step in understanding what makes PI so pressure-sensitive. Eventually, these insights will enable the design of molecules that can act as pressure sensors or as components of self-healing materials.

3.2 Experimental part

3.2.1 Sample preparation

9-tert-Butylanthracene (9TBA) was synthesized in the dark following the procedure described in ref 26. The tert-butyl group was attached to anthrone using a Grignard reaction, followed by dehydration with P_2O_5 leading to aromatization and then purification recrystallization from methanol. The purity was greater than 98% as confirmed by NMR, GC−MS, and melting point determination.

Spectroscopic investigations of 9TBA and D-9TBA were performed in both liquid solution and polymer films. A polymer matrix provided a hydrostatic pressure medium under the pressure range of this study. Intramolecular chemistry and photophysics tend to be insensitive to different particular polymer systems.[27] The UV-transparent (>237 nm) polycycloolefin resin (Zeonex Z480, Tg = 138−140 °C, Zeon Chemicals L.P.) was used as the polymer host. Zeonex was chosen for its UV transparency, which is needed to resolve the major 9TBA absorption band near 263 nm. 9TBA and colorless pellets of Zeonex polymer were dissolved in a few milliliters of cyclohexane (EMD ACS grade). The mixture was ultrasonicated in the dark for about 1 h, after which the solvent was allowed to evaporate in the air at room temperature and in the dark. Transparent films of 9TBA-doped Zeonex films were obtained ($\sim 1 \times 10^{-3}$ M) and stored in a vacuum cryostat under vacuum (10^{-4} Torr) for 48 h to remove residual O_2 before exposing the sample to light.

3.2.2 Photophysical measurements at variable pressure

All experiments were performed at room temperature, 298 ± 1.5 K. Pressure-dependent measurements were performed by placing the 9TBA sample film in a diamond anvil cell (DAC). The DAC utilized type II diamonds (1.0 mm culet diameter) with an Inconel gasket, and a typical sample size was ~500 μm in diameter and ~100 μm thick. Ruby microcrystal emission was used to determine the pressure of the sample with an accuracy of ±0.05 GPa. The 9TBA absorption band near 260 nm showed a red shift of 5 nm/GPa under pressure, which provided a sensitive internal pressure standard. Pressure broadening in the 9TBA absorption band was not observed below 2 GPa, indicating that the underlying pressure inhomogeneity was small relative to the pressure. We sometimes observed a change in absorbance intensity after we applied pressure to the DAC, which we attribute to a change in sample cross-sectional area due to changes in the gasket aperture in the DAC. No pressure broadening was observed in the ruby emission spectrum. UV−vis absorption spectra were obtained using a Varian CARY 500 spectrometer (0.5 nm/step with 0.2 s integration time). Two 38 mm focal length lenses (SI-UV grade) were utilized to focus the transmitted light through the ~500 μm diameter DAC sample aperture. The spectral background due to the absorption of the Zeonex film was determined by measuring a Zeonex sample loaded in the same DAC at 1 atm pressure and room temperature. The spectrometer excitation intensity was orders of magnitude weaker than the photolysis source, and control experiments confirmed that negligible photochemistry was induced during the spectrometer scans. The photoconversion and reversion reactions were quantified by the changes in the area of the major 9TBA absorption band peaked at 263 nm and integrated over the range 240−280 nm. The absorption red shift associated with increased pressure was taken into account in the spectral analysis.

To initiate the 9TBA → D-9TBA photochemical reaction, a mercury lamp was used as the source of 365 nm light. The light intensity at the sample in the cryostat was ~2.7 mW/cm$^{2.}$ To measure the kinetics of the D-9TBA → 9TBA reaction, a photoconverted polymer sample was placed into a DAC, and the three connecting bolts were tightened to generate a pressure "jump" within 30 s. The ensuing absorption scans of the UV region of the Dewar absorption spectrum required ~30 s as well. The resulting DAC pressure was measured after the experiment by the ruby emission shift.

3.3 Results and discussion

The 9TBA → D-9TBA transformation can be monitored using absorption spectroscopy. As shown in Figure 3.2, the anthracene chromophore in 9TBA has two distinct absorption features that diminish when D-9TBA is formed: the characteristic anthracene $S_0 \rightarrow S_1$ absorption in the 350−450 nm range and the $S_0 \rightarrow S_2$ feature peaked at 263 nm.[28] Since the $S_0 \rightarrow S_2$ absorption coefficient is approximately 10× larger than that of the visible $S_0 \rightarrow S_1$ transition, we integrate the area under this peak to assess the concentration of 9TBA present in the sample. One complication in these experiments is that the presence of O_2 can lead to peroxidation of the anthracene ring, 29 providing a competing reaction channel. Side reactions with O_2 are a much bigger concern for 9TBA than for BA due to its lower isomerization quantum yield (~1% versus >50% for BA). The O_2 photoproduct does not revert to 9TBA at room temperature, unlike D-9TBA, and this lack of reversibility provides a measure of the relative importance of this reaction channel. We found that exposing the polymer sample to a vacuum of 10^{-4} Torr for approximately 48 h was required to sufficiently remove O_2, consistent with previous results on 9TBA in polystyrene.[30] If a thoroughly degassed 9TBA/Zeonex sample is photolyzed and then left in the dark for >24 h, we found complete recovery of the absorption spectrum.

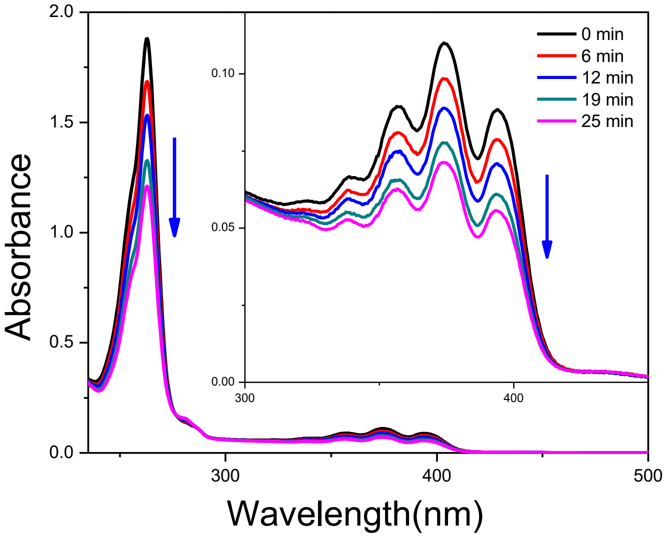

Figure 3.2 Time-dependent spectral evolution of 9TBA/Zeonex sample under vacuum by 365 nm irradiation at ambient pressure. The black trace is the absorption spectrum of 9TBA without any irradiation. When the light is removed, the spectra evolution is reversed. High pressure samples exhibit identical changes, except for slight shifts in the absorption peak positions.

In cyclohexane solution at room temperature, we measured both forward and reverse Dewar reaction dynamics. The forward reaction (9TBA → D-9TBA) quantum yield was found to be 6% for 365 nm irradiation, while the reverse reaction rate was measured to be 4.0×10^{-5} s^{-1}, both in good agreement with values previously reported in the literature for similar solvents.[23–25] We found the forward rate for the 9TBA → D-9TBA reaction to be 1.5×10^{-4} s^{-1} under 2.7 mW/cm^2 365 nm irradiation in a Zeonex matrix under vacuum. From this data, we were able to estimate a photochemical reaction yield of 0.6 ± 0.3%, using 9TBA's absorption cross section of $5.8 \times 10^{-18} cm^2$ at 365 nm. This quantum yield value is similar to what has been observed in polystyrene[30] but about an order of magnitude smaller than what is seen in solution. The reverse reaction rate was measured to be 4.5×10^{-5} s^{-1} in Zeonex, similar to the values obtained both in liquid solution and in polystyrene.[30] The different forward rates in solid polymers versus liquid solutions are understandable considering the large geometry changes required for the Dewar isomerization, which is presumably inhibited by the solid polymer matrix. Since the reverse reaction occurs in a cavity that is already expanded to accommodate the Dewar form, steric constraints likely play less of a role, as previously observed for Dewar benzene.[31] We also measured the rate of 9TBA reaction for a Zeonex sample that had not been placed under vacuum. The rate of the forward reaction was measured to be 3.1×10^{-4} s^{-1} under the same illumination conditions. If we assume that this rate is the sum of the Dewar isomerization and peroxidation rates, then the two rates must be almost equal at ambient pressure and temperature.

The rate of the 9TBA → D-9TBA photoreaction is very pressure-dependent. Since we were not able to completely exclude O_2 from the DAC during the pressure-loading process, we cannot separate the pressure dependence of the Dewar isomerization and peroxidation rates.

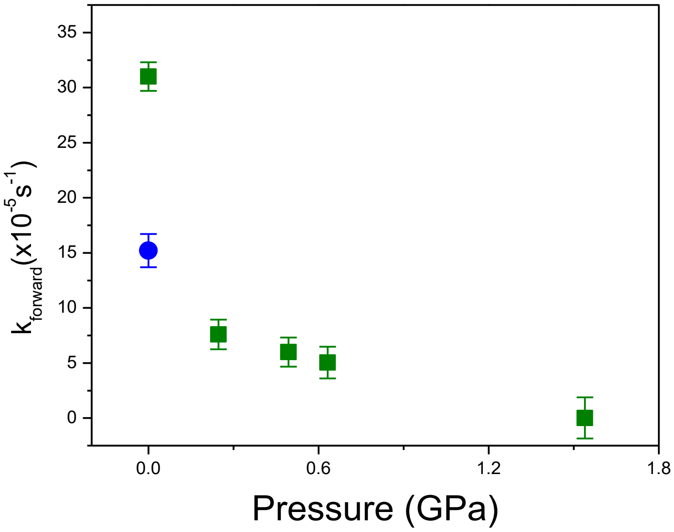

Figure 3.3 The rate of the 9TBA photo reaction in air-exposed samples for pressures up to 1.5 GPa (green squares). At ambient pressure, the rate of the photoreaction without O_2 is also shown as a blue circle. At ambient pressure, photoperoxidation and Dewar isomerization contribute make approximately equal contributions to the disappearance of 9TBA. Both rates slow by at least 100× at higher pressures. The error bars reflect the uncertainty range obtained by exponential fits to the absorption decays.

As shown in Figure 3.3, the total rate at ambient pressure (3.1×10^{-4} s^{-1}) slowed down considerably at 1.55 GPa (1.5×10^{-7} s^{-1}). Both the isomerization and the photoperoxidation rates must be pressure-dependent, since if only one of these rates decreased with pressure, the total rate would never drop below the ambient value of $\sim 1.5 \times 10^{-4}$ s^{-1} for either reaction. The Dewar isomerization is expected to be pressure-dependent because it requires a large geometry change that will become more difficult in a denser medium. It has also been shown that the photoperoxidation reaction is sensitive to the free volume in the polymer host, [32] presumably because it requires O_2 diffusion.

Increased pressure reduces the available volume for O_2 diffusion, which should slow the peroxidation reaction as well.

The presence of O_2 should not affect the back-reaction of D-9TBA to 9TBA, which is of primary interest in this work. In order to measure the pressure dependence of the D-9TBA → 9TBA back reaction, we first photolyzed the 9TBA/Zeonex sample under vacuum. The sample was then transferred and loaded into the DAC within 5 min to minimize O_2 exposure. The absorption of the DAC sample was then monitored over the course of hours as the D-9TBA → 9TBA back-reaction proceeded. Typical recovery curves are shown in Figure 3.4 for ambient, 0.68 and 1.43 GPa pressures. The recovery becomes more rapid at higher pressures, roughly by a factor of 3. Also shown for comparison are the pressure-dependent components of the PI → BA recovery at ambient and high pressures. This component of the PI → BA reaction is clearly much slower at ambient pressure but much faster at high pressures, bracketing the D-9TBA → 9TBA data. To model the recovery, we assume that the D-9TBA → 9TBA back-reaction is a simple first-order process and the concentration of 9TBA, N9TBA, is given by

$$N_{9TBA} = N_{9TBA}^{0}\left(1 - f_{conv}e^{-k_{back}t}\right) \qquad (1)$$

where N9TBA 0 is the original 9TBA concentration before photolysis, fconv is the fraction reacted by 365 nm ($f_{conv} < 0.4$ in all our experiments), and kback is the back-reaction rate. Fits to the data using eq 1 are overlaid with the data in Figure 3.4. The k_{back} values obtained from the fits are given in Table 3.1 In Figure 3.5, we plot the natural log of k_{back} versus pressure P, using the relation

$$\ln(k_{back}) = \frac{-\Delta V^{\neq}}{RT} P + const. \qquad (2)$$

where R is the ideal gas constant, T is the temperature, and $\Delta V^{\ddagger}$ is the activation volume.33 A linear fit to the data yields $\Delta V^{\ddagger} = -2.3 \pm 0.2\ \text{Å}^3$. The activation volume can be associated with the volume change of the transition state, which in our case must be smaller than that of the reactant D-9TBA. Higher pressure favors the smaller transition state and thus accelerates the reaction. While this $\Delta V^{\ddagger}$ value is significant, it is almost an order of magnitude smaller than the $\Delta V^{\ddagger} = -16\ \text{Å}^3$ we obtained for the PI → BA reaction.

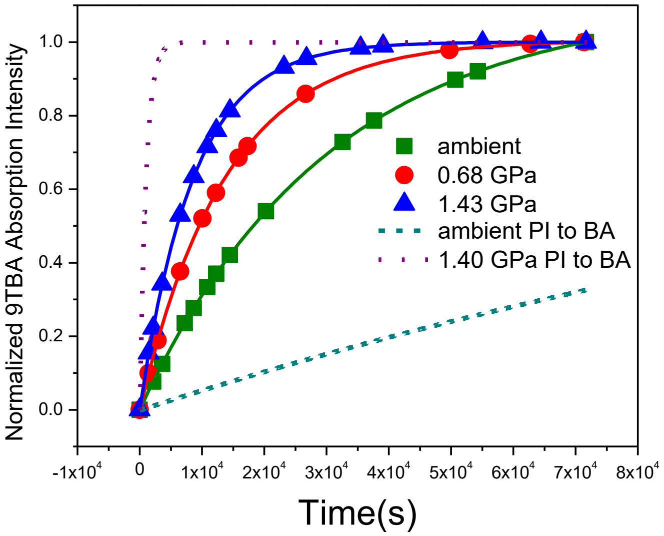

Figure 3.4 Pressure-enhanced D-9TBA →9TBA kinetics at room temperature. The rate of formation of 9TBA is enhanced by the application of mechanical compression. The solid curves are exponential fits to equation (1). The pressure-dependence kinetic rate constants, k_{back} are listed in Table 1. Also shown for comparison are the calculated recovery curves from reference 14 for the PI→BA reaction, which exhibit a much more dramatic pressure-dependence.

Table 3.1 Rate constants k_{back} for D-9TBA→9TBA reaction obtained by fitting the time-dependent change in absorption (e.g., Figure 3.3) to Equation (1).

Pressure (GPa)	k_{back} ($\times 10^{-5} s^{-1}$)
0	4.5 ±0.3
0.1	6.4 ±0.5
0.42	7.7 ±0.9
0.68	7.4 ±0.4
1.1	9.5 ±0.3
1.43	11.5 ±1.3

The recovery rate of 9TBA increases by almost a factor of 3, from 4.5×10^{-5} to $11.5 \times 10^{-5}\ s^{-1}$ as the pressure is increased. The PI → BA recovery was modeled as a biexponential process due to the presence of different conformers. One of these rates appeared to be insensitive to pressure, while the other increased from $5 \times 10^{-6}\ s^{-1}$ to $1 \times 10^{-3}\ s^{-1}$ over the same pressure range. We can then ask why are the pressure-dependent reaction dynamics of D-9TBA and PI so different. Both are metastable, high energy photoisomers. Our DFT calculations place D-9TBA 184 kJ/mol above 9TBA, close to the experimental ΔH_0 = 172 kJ/mol.[34, 35] PI is calculated to be only 87 kJ/mol above BA, again comparable to experimental values.[20] The higher energy of D-9TBA is likely due to the formation of two adjacent cylcobutene rings with higher strain than the two separate cyclobutane rings in PI. Despite their enthalpic differences, the PI → BA and D-9TBA → 9TBA reactions have very similar activation energies of 93−96 kJ/mol at room temperature and pressure.[20,24,25] Thus, from an energetic standpoint, there is no reason to suspect that PI would become so reactive at high pressure relative to D-9TBA. A second point of comparison involves the product and reactant molecular volumes obtained from the crystal structures. Although estimating molecular size from crystal structures is inexact due to packing considerations, these numbers provide a well-defined reference point for comparing similar molecules.[36] In many organic isomerization reactions, the activation volume is close to the reaction volume,[37,38] i.e., the difference between equilibrium product and reactant molecular volumes. Thus, destabilization of a higher volume reactant at higher pressures is typically expected to lead to more rapid reaction kinetics.

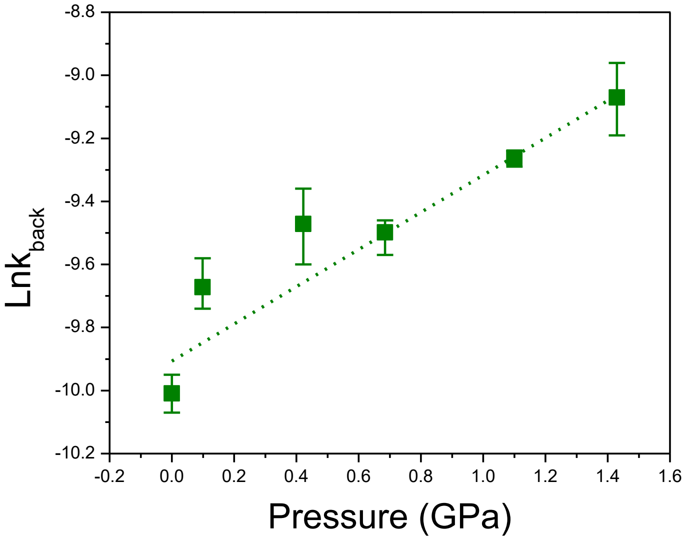

Figure 3.5 Dependence of the natural log of the rate constant versus pressure up to 1.43 GPa. A linear least squares fit to the data yields an estimate of the activation volume $\Delta V^{\neq}=-2.3\pm0.2$ Å^3 for the D-9TBA→9TBA reaction. The error bars reflect the uncertainty range obtained by exponential fits to the absorption recoveries shown in Figure3.4.

9TBA has a volume of 325 Å^3, while D-9TBA occupies a larger volume of 334 Å^3.[39] The negative reaction volume (−9 Å^3) calculated from the crystal structures predicts a negative activation volume for the D-9TBA → 9TBA reaction, as observed. PI, on the other hand, occupies a slightly smaller volume than BA, as estimated from their crystal structures, and thus a positive activation volume would be predicted for the PI → BA reaction, with a concomitant slowing of the reaction at higher pressures. This is the opposite of what is observed experimentally. To summarize, if we consider energy differences and volume changes, we would expect the high-energy, high-volume D-9TBA to be more sensitive to pressure than PI.

Theoretical work by Slepetz and Kertesz suggests that the tethering of the two anthracenes in PI leads to an asymmetric diradicaloid transition state whose volume is significantly smaller than that of the reactant or product.[21] The idea is that this asynchronous transition state avoids transient crowding by nonbonded carbons. If this is true, then we would expect a large negative $\Delta V^{‡}$ only for the cyclophane PI, as observed. Neither An_2 nor D-9TBA has the same degree of crowding, and neither shows the same pressure sensitivity as PI. From these results, we can begin to form some ideas about what is important for making a pressure-sensitive mechanophore. For example, in PI, we hypothesized that the symmetric three-dimensional structure could exclude most of the pressurized medium (i.e., the polymer) from its interior and permit the generation of local shear forces on the top and bottom anthracene rings. If correct, this idea suggests that boxlike molecular structures should exhibit greater pressure sensitivity than planar structures. However, the absence of a pressure effect in An_2 shows that such a box-like structure by itself is not sufficient. Now our results on D-9TBA, a twodimensional molecule, show that the presence of strained fourmembered rings is also not sufficient to generate very high pressure sensitivity (although it is more pressure-sensitive than An_2). Taken together, our results on the three molecules in Figure 3.1 are consistent with the idea that a crowded threedimensional carbon environment provides constraints on the transition state that lead to a highly negative $\Delta V^{\ddagger}$. Although much work needs to be done, both experiment and theory imply that there may exist general principles for designing molecules whose reactivity can be modulated by pressure.

3.4 Conclusion

The pressure dependence of the back-reaction rate of the Dewar isomer of 9TBA has been measured. This rate increases by a factor of ~3 at high pressure (1.43 GPa). Despite being a highly strained isomer, this reaction rate is at least 100× less sensitive to pressure than the PI → BA back-reaction studied previously. These results suggest that the pressure sensitivity of the PI → BA reaction arises from the unique molecular geometry of PI, as opposed to the presence of a single structural motif. Further experiments will be necessary to understand the precise molecular origins of PI's pressure sensitivity and eventually guide the development of other strained molecules that are sensitive to pressure.

3.5 References

(1) Beyer, M. K.; Clausen-Schaumann, H., Mechanochemistry: The Mechanical Activation of Covalent Bonds. *Chem. Rev.*, **2005**, 105, 2921-2948.

(2) Kaupp, G., Mechanochemistry: The Varied Applications of Mechanical Bond-Breaking. *CrystEngComm.*, **2009**, 11, 388-403.

(3) Todres, Z. V., Organic Mechanochemistry and Its Practical Applications. *CRC Press: Boca Raton, FL*, **2006**.

(4) Kean, Z. S.; Niu, Z.; Hewage, G. B.; Rheingold, A. L.; Craig, S. L., Stress-Responsive Polymers Containing Cyclobutane Core Mechanophores: Reactivity and Mechanistic Insights. *J. Am. Chem. Soc.*, **2013**, 135, 13598-13604.

(5) Kean, Z. S.; Ramirez, A. L. B.; Yan, Y.; Craig, S. L., Bicyclo[3.2.0]heptane Mechanophores for the Non-scissile and Photochemically Reversible Generation of Reactive Bis-enones. *J. Am. Chem. Soc.*, **2012**, 134, 12939-12942.

(6) Bian, S.; Scott, A. M.; Cao, Y.; Liang, Y.; Osuna, S.; Houk, K. N.; Braunschweig, A. B., Covalently Patterned Graphene Surfaces by a Force-Accelerated Diels-Alder Reaction. *J. Am. Chem. Soc.*, **2013**, 135, 9240-9243.

(7) Wiggins, K. M.; Syrett, J. A.; Haddleton, D. M.; Bielawski, C. W., Mechanically Facilitated Retro [4+2] Cycloadditions. *J. Am. Chem. Soc.*, 2011, 133, 7180-7189.

(8) Larsen, M. B.; Boydston, A. J., "Flex-Activated" Mechanophores: Using Polymer Mechanochemistry To Direct Bond Bending Activation. *J. Am. Chem. Soc.*, **2013**, 135, 8189-8192.

(9) Larsen, M. B.; Boydston, A. J., Successive Mechanochemical Activation and Small Molecule Release in an Elastomeric Material. *J. Am. Chem. Soc.* **2014**, 136, 1276-1279.

(10) Gilman, J. J., Mechanochemistry. *Science.*, **1996**, 274, 65.

(11) Davis, D. A., et al., Force-Induced Activation of Covalent Bonds in Mechanoresponsive Polymeric Materials. *Nature.*, **2009**, 459, 68-72.

(12) Lenhardt, J. M.; Ong, M. T.; Choe, R.; Evenhuis, C. R.; Martinez, T. J.; Craig, S. L., Trapping a Diradical Transition State by Mechanochemical Polymer Extension. *Science.*, **2010**, 329, 1057-1060.

(13) Wu, D.; Lenhardt, J. M.; Black, A. L.; Akhremitchev, B. B.; Craig, S. L., Molecular Stress Relief through a Force-Induced Irreversible Extension in Polymer Contour Length. *J. Am. Chem. Soc.*, **2010**, 132, 15936-15938.

(14) Caruso, M. M.; Davis, D. A.; Shen, Q.; Odom, S. A.; Sottos, N. R.; White, S. R.; Moore, J. S., Mechanically-Induced Chemical Changes in Polymeric Materials. *Chem. Rev.*, **2009**, 109, 5755-5798.

(15) Sheth, A. R.; Lubach, J. W.; Munson, E. J.; Muller, F. X.; Grant, D. J. W., Mechanochromism of Piroxicam Accompanied by Intermolecular Proton Transfer Probed by Spectroscopic Methods and Solid-Phase Changes. *J. Am. Chem. Soc.*, **2005**, 127, 6641-6651.

(16) Ito, H., et al., Reversible Mechanochromic Luminescence of [($C_6F_5Au)_2$(m-1,4-diisocyanobenzene)]. *J. Am. Chem. Soc.*, **2008**, 130, 10044-10045.

(17) Zhang, G.; Lu, J.; Sabat, M.; Fraser, C. L., Polymorphism and Reversible Mechanochromic Luminescence for Solid-State Difluoroboron Avobenzone. *J. Am. Chem. Soc.*, **2010**, 132, 2160-2162.

(18) Hickenboth, C. R.; Moore, J. S.; White, S. R.; Sottos, N. R.; Baudry, J.; Wilson, S. R., Biasing Reaction Pathways with Mechanical Force. *Nature.*, **2007**, 446, 423-427.

(19) Klukovich, H. M.; Kean, Z. S.; Iacono, S. T.; Craig, S. L., Mechanically Induced Scission and Subsequent Thermal Remending of Perfluorocyclobutane Polymers. *J. Am. Chem. Soc.*, **2011**, 133, 17882-17888.

(20) Jezowski, S. R.; Zhu, L.; Wang, Y.; Rice, A. P.; Scott, G. W.; Bardeen, C. J.; Chronister, E. L., Pressure Catalyzed Bond Dissociation in an Anthracene Cyclophane Photodimer. *J. Am. Chem. Soc.*, **2012**, 134, 7459-7466.

(21) Slepetz, B.; Kertesz, M., Volume Change during Thermal [4+4] Cycloaddition of [2.2](9,10)Anthacenophane. *J. Am. Chem. Soc.*, **2013**, 135, 13720-13727.

(22) Tamelen, E. E. v., Valence Bond Isomers of Aromatic Systems. Acc. Chem. Res., **1972**, 5, 186-192.

(23) Gusten, H.; Mintas, M.; Klasinc, L., Deactivation of the Fluorescent State of 9-tert-Butylanthracene. 9-tert-Butyl-9,10-(dewaranthracene). *J. Am. Chem. Soc.*, **1980**, 102, 7936-7937.

(24) Dreeskamp, H.; Jahn, B.; Pabst, J., Thermoreversible Photo Valence Isomerization of 9-t-Butylanthracene to Its 9,10-Dewar-isomer. *Z. Naturforsch.*, **1981**, 36, 665-668.

(25) Kraljic, I.; Mintas, M.; Klasinc, L.; Ranogajec, F.; Gusten, H., Thermo- and Photochemical Aspects of the Valence Isomerization of 9-tert-Butylanthracene. *Nouv. J. Chim.*, **1983**, 7, 239-243.

(26) Parish, R. C.; Stock, L. M., 9-t-Butylanthracene. *J. Org. Chem.* **1966**, 31, 4265-4267.

(27) Zhu, A.; Wang, B.; White, J. O.; Drickamer, H. G., The Effect of High Pressure on the Twisted Intramolecular Charge Transfer of 2-(4-Dimethylaminonaphthalen-1-ylmethylene) Malononitrile. *J. Phys. Chem. A.*, **2003**, 107, 6932-6935.

(28) Birks, J. B., *Photophysics of Aromatic Molecules. Wiley-Interscience:* **1970**.

(29) Stevens, B.; Perez, S. R.; Ors, J. A., Photoperoxidation of Unsaturated Organic Molecules. XIV. O_2 1Dg Acceptor Properties and Reactivity. *J. Am. Chem. Soc.*, **1974**, 96, 6846-6850.

(30) Minaylov, V. V.; Gurman, V. S.; Vorobiev, A. K., Photoisomerization of 9-tert-butylanthracene in Polystyrene Films under Photoselection Conditions. Consideration of Molecular Thermal Rotation. *J. Photochem. Photobiol.*, **1995**, 87, 67-73.

(31) Ferrar, L.; Mis, M.; Robello, D. R., Thermal Isomerization of Dewarbenzene Derivatives. *Tet. Lett.*, **2008**, 49, 4130-4133.

(32) Sheats, J. R., Media Effects on the Kinetics of Anthracene Photo-Oxidation in Polymers. *J. Photochem. Photobiol. A.*, **1994**, 80, 377-380.

(33) Jenner, G., High-Pressure Mechanistic Delineation Based on Activation Volumes. *J. Phys. Org. Chem.*, **2002**, 15, 1-13.

(34) Jahn, B.; Dreeskamp, H., The Valence Isomerization of 9,10 Dewar Isomers of 9-tert-Butylanthracene. *Z. Naturforsch.*, **1982**, 37, 376-379.

(35) Grimme, S.; Peyerimhoff, S. D., Theoretical Study of the Valence Isomerization of Anthracene and 9-tert-Butylanthracene to Their Dewar Forms in Ground and Excited States. *J. Phys. Chem.*, **1994**, 98, 12927-12932.
(36) Edward, J. T., Molecular Volumes and the Parachor. *Chem. & Ind.* **1956**, 774-777.
(37) Tanaka, T.; Sueishi, Y.; Yamamoto, S.; Nishimura, N., Pressure Dependence of the Photostationary trans/cis Concentration Ratio of 4-Dimethylamino-4'-nitroazobenzene. A New Method of Evaluating the Reaction Volume. *Chem. Lett.*, **1985**, 1203-1204.
(38) Noble, W. J. L., *Organic High Pressure Chemistry.* Elsevier: Amsterdam, 1988.
(39) Angermund, K.; Claus, K. H.; Goddard, R.; Kruger, C., High-Resolution X-ray Crystallography -- An Experimental Method for the Description of Chemical Bonds. *Angew. Chem. Int. Ed.*, **1985**, 24, 237-247.

Chapter 4 Analysis of reaction kinetics in the photomechanical molecular crystal 9-methylanthracene using an extended Finke–Watzky model

4.1 Introduction

Photochemical reactions in molecular crystals are a subject of both fundamental and practical importance. The ability of crystal packing to modify reactivity and steer reaction outcomes was recognized early on by Schmidt and coworkers as they developed the principles of topochemistry.[1,2] Researchers in the field continue to exploit these principles to control solid-state chemical reactions and synthesize new molecules.[3–5] But while we now have a good understanding of how crystal packing predicts the endpoint of a photochemical reaction, our understanding of how this final stage is reached is still lacking.

Empirically, it is often the case that photochemical reaction kinetics in molecular crystals do not obey simple first-order kinetics, in contrast to reactions that take place in homogeneous liquid solutions. The presence of different local environments can lead to a distribution of reaction rates and nonexponential kinetics.

The presence of multiple reaction rates in a single system is sometimes referred to as “heterogeneous kinetics”, but the experimentally observed nonexponential change in reactant concentration can have different origins. In one limit, heterogeneity in the form of structural defects can give rise to a distribution of reaction rates. But researchers have also shown that the densely ordered environment of a crystal can transmit the effect of product formation at one site to other sites in the lattice.[6–8] This causes the environment seen by a reactant molecule to evolve over time as more and more product is formed, leading to dynamic changes in the reaction rate. Note that nonexponential kinetics that arises from structural defects can be eliminated by improved sample preparation (at least in principle), while the environment changes that allow photoproduct molecules to catalyze or inhibit their own formation is an unavoidable consequence of the photochemical reaction itself. The potential role of autocatalysis or auto-inhibition adds a fundamentally new feature to the study of reaction dynamics in crystalline systems.

The study of solid-state photochemical reaction kinetics has taken on a new urgency with the realization that reactive molecular crystals can have applications in green chemistry[9,10] and as mechanical actuators.[11,12] In order to engineer new photomechanical materials, a quantitative model for the temporal response of a crystalline microneedle under light exposure is required. Up to now, most workers have assumed first-order reaction kinetics,[13,14] but the discussion in the preceding paragraph suggests that the situation may be more complicated in molecular crystals. Some hints that this is indeed the case were found when the photomechanical properties of microneedles and microribbons composed of crystalline 9-methylanthracene (9MA) were studied in a previous paper.[15] In that work, we assumed first-order reaction kinetics were operative, despite previous work that suggested nucleation may also play a role.[16,17] Although the photoinduced bending could be qualitatively described in the context of the homogeneous kinetic model, there were indications that it was not completely adequate. For example, there was a clear delay between the start of the reaction and the onset of bending, suggesting that there was some sort of induction time before sufficient photodimer could be formed to initiate the bending. Such a delay in photoproduct formation signals a departure from homogeneous kinetics. Figure 4.1 illustrates the difference between normal first-order versus autocatalytic reaction dynamics in this crystal, in which monomer pair reactants (A) form photodimer products (B).[18]

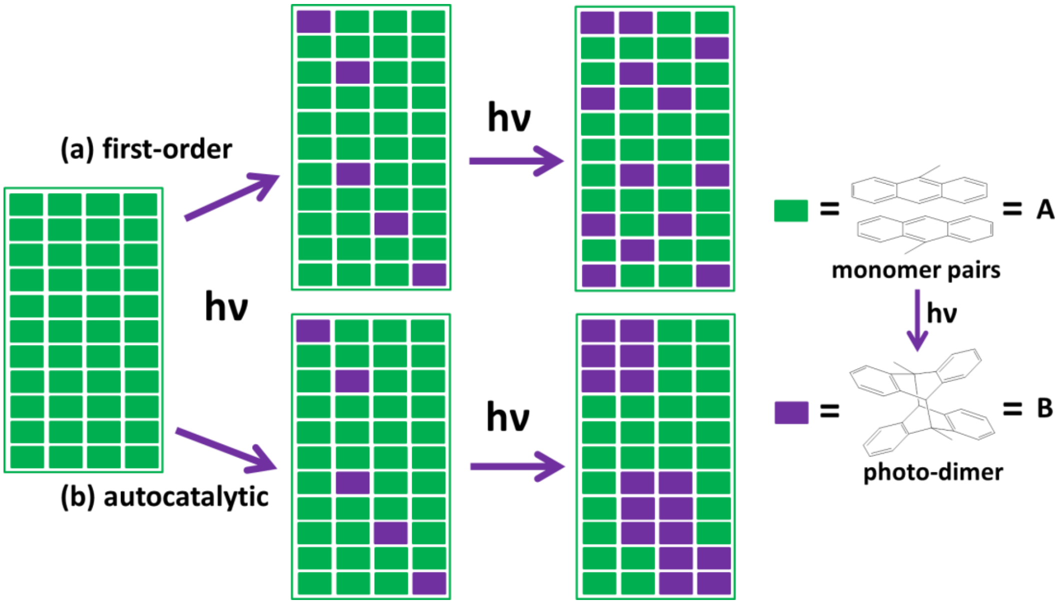

Figure 4.1 Two possible paths in the [4 + 4] photodimerization of monomeric 9-methylanthracene (9MA) pairs (green, A) to form photodimers (purple, B). (a) Simple first-order kinetics, in which the presence of initially formed photoproduct does not affect the reaction rate of neighboring molecules, leaving photoproduct evenly distributed within the crystal, and (b) autocatalytic reaction kinetic in which the initially formed photoproduct induces the formation of additional photoproduct in surrounding sites.

In order to develop an improved description of the photomechanical response of 9MA microcrystals, here we undertake a more complete study of their photochemical reaction kinetics. Although the Johnson–Mehl–Avrami–Kolmogorov (JMAK) model[19] is often used to analyze solid-state photochemical reaction kinetics,[20–23] in this chapter we will utilize the alternative Finke–Watzky (FW) model that was originally developed to describe metal nanoparticle growth[24–27] but has since been applied to a variety of phenomena involving nucleation and growth, including catalyst formation,[28] protein aggregation,[29–32] and solid-state reactions.[33] When applied to solid-state reaction processes, its balanced reactions and associated rate constants enable transparent physical interpretations and easy connection to experimental observables. In order to apply the FW model to photochemically reactive systems, it must be extended to take excited state population dynamics into account. We will denote this extended version as the FW-Photochemical or FW-P model. We apply this model to the 9MA system and show that it can be used to analyze both the time-dependent decrease in reactant concentration and the speed-up in the fluorescence decay. Although some ambiguities remain in the comparison of theory and experiment, the results of this work demonstrate that the photodimerization kinetics of crystalline 9MA reflect autocatalytic product formation. The ability to quantitatively model these kinetics will be necessary to quantitatively model its photomechanical response, which we plan to do in the future.

4.2 Experimental part

4.2.1 Sample preparation

Tetrahydrofuran (THF, ACS, 99%+) and 9-methylanthracene (9MA, Sigma-Aldrich, 98%+) were used as received. To make polycrystalline thin films, 10 mL of concentrated THF (1.5 mg mL1) solution were placed on a glass coverslip. After evaporation of the

THF, a thin polycrystalline film of 9MA was left on the coverslip. The sample film was placed in a Janis ST100 cryostat under vacuum ($<10^{-4}$ Torr) for 3 minutes to remove residual O_2. Argon was then flowed into the cryostat to prevent the 9MA from subliming. After 5 minutes under Argon, the cryostat was again evacuated. This was repeated for 5–7 cycles to eliminate any residual O_2 that might react with the 9MA.

4.2.2 Absorption and fluorescence spectroscopy

Ultraviolet-visible (UV-Vis) absorption spectra of solution samples (4.5×10^{-5} M) were collected using a Varian Cary 50 UV/Vis spectrophotometer with background correction. UV-Vis absorption spectra of polycrystalline film of 9MA were collected in a Varian Cary 500 UV/Vis spectrophotometer. Steady-state fluorescence spectra of polycrystalline film were collected with a Spex Fluorolog Tau-3 fluorescence spectrophotometer. The sample was excited at 300 nm, and the spectra were collected from 400 to 600 nm.

4.2.3 Time-resolved fluorescence measurements

Time-resolved fluorescence lifetime data were collected using a Hamamatsu C4334 Streakscope using front-face geometry. The solid samples were kept in a Janis ST100 cryostat under Argon. The excitation source was a 200 fs pulse centered at 400 nm, derived from frequency doubling the 800 nm output of a Spectra Physics MaiTai Ti:Sapphire oscillator. The laser repetition rate was decreased to 1 MHz using a pulse picker to avoid thermal artifacts.

4.2.4 ^{1}H nuclear magnetic resonance measurements

The 9MA polycrystalline film was scraped gently from the glass substrate by spatula and the solid powder was then dissolved in $CDCl_3$ (Sigma-Aldrich, 99.9%+) to measure the 1H Nuclear Magnetic Resonance (^{1}H NMR) spectra. The NMR experiments were performed using a Varian Inova 400 spectrometer with a 5 mm p 4-nucleus probe.

4.2.5 Numerical fitting of the data

The differential equations described in the following sections were solved using Mathematica version 10.4.1.0. The values of the unknown rate constants in the different models (k_1, k_2 and k_{ex2}) were varied until the calculated [A](t) curves showed a reasonable overlap with the experimental plots. Given these starting points, Mathematica was then used to maximize the R2 values and the optimized values for the rate constants were determined and used for the displayed comparison of experiment and theory. The commented Mathematica workbooks are available in the ESI.† FAST Advanced Analysis of Fluorescence Kinetics software (Edinburgh Instruments Limited, 2010, version 3.0) was used for the global analysis of the fluorescence lifetime decays.

4.3 Derivation of the extended FW model for photochemical reactions

Before undertaking the detailed derivation of the photochemical FW model, we first briefly describe the more commonly used JMAK model. In this model, it is assumed that the reaction proceeds through growth of pure product domains via nucleation. For the reaction $A \rightarrow B$, the time-dependent growth of the product concentration $[B](t)$ has the general form

$$[B](t) = 1 - e^{-kt^n} \quad (1)$$

where n-1 gives the effective growth dimension of the product nucleus and k is related to both the nucleus density and geometric growth rate.[19] The JMAK model is a semi-empirical approach that is not derived from an underlying chemical mechanism. Given this, it is impossible to incorporate quantities like the light intensity or the photochemical quantum yield into the constant k, for example.

Finney and Finke showed that it is possible to replicate the dynamical behavior of the JMAK model using the FW model, which has the advantage of being derived using balanced chemical equations with well-defined rate constants.[33] The FW model postulates two sequential pathways to the photoproduct B, characterized by rates k_1 and k_2, as given in Equations (2):

$$A \xrightarrow{k_1} B \quad (2a)$$

$$A + B \xrightarrow{k_2} B + B \quad (2b)$$

The first unimolecular step can be used to take nucleation into account as a quasi-first order process[34], while the second step describes autocatalytic growth of the product. As pointed out by Finke and coworkers, the rate constants k_1 and k_2 should be thought of as composite quantities that average over nucleation and growth steps that occur on the microscopic scale.[33] This model has been shown to provide an adequate description of solid-state reaction dynamics in many cases, often giving fits to the data that are the same or better than the JMAK model.[33] The FW model has recently been used to analyze the photodimerization of crystalline 9-cyanoanthracene, but without a detailed derivation that permits us to dissect the roles of different photophysical parameters.[35] In this work, we derive an extended FW-P model for photochemically reacting systems, and then apply this model to 9MA.

To extend the FW-P model to photochemical reaction kinetics, the simple reaction scheme given in Equations (2) must be expanded to take into account the excited state reactant, *A**, as well as the ground state reactant *A* and product *B*. We consider 5 possible reaction pathways and their associated rates:

$$A \xrightarrow{\sigma I} A^* \tag{3a}$$

$$A^* \xrightarrow{k_{ex1}} A \tag{3b}$$

$$A^* \xrightarrow{k_1} B \tag{3c}$$

$$A^* + B \xrightarrow{k_{ex2}} A + B \tag{3d}$$

$$A^* + B \xrightarrow{k_2} B + B \tag{3e}$$

σ is the absorption cross section (cm^2), I is the light intensity (photons/cm^2/s), k_{ex1} is the rate of relaxation to the ground state in the absence of reaction (s^{-1}), and k_1 describes the reaction rate of A by itself (s^{-1}). k_2 and k_{ex2} are the nonradiative relaxation and reaction rates (in units of nm^{3}s^{-1}) of A in the presence of some concentration of photoproduct B. Note that here we make the assumption that the photoproduct B does not absorb the incident light and that the thermal back-reaction rate is negligible, making the photochemical reaction effectively irreversible. This reasonable for the photodimerization of 9MA (vide infra), where photodimerization destroys the conjugation of the anthracene ring and shifts the absorption below 300 nm. This reaction scheme leads to a system of three rate equations,

$$\frac{d[A]}{dt} = -\sigma I[A] + k_{ex1}[A^*] + k_{ex2}[A^*][B] \tag{4a}$$

$$\frac{d[A^*]}{dt} = +\sigma I[A] - k_{ex1}[A^*] - k_1[A^*] - k_{ex2}[A^*][B] - k_2[A^*][B] \tag{4b}$$

$$\frac{d[B]}{dt} = +k_1[A^*] + k_2[A^*][B] \tag{4c}$$

Under continuous excitation conditions, at any instant in time we can make the steady-state assumption and take $\frac{d[A^*]}{dt} = 0$. We then use the relation $[B]=[A]_0-[A]$, where $[A]_0$ is the initial concentration of the reactant, to find an expression for $[A^*]$:

$$\left[A^*\right] = \frac{\sigma I\left[A\right]}{k_{ex1} + k_1 + \left(k_{ex2} + k_2\right)\left[B\right]} \tag{5}$$

This then allows us to eliminate $[A^*]$ from Equations (4a-c) and derive a single nonlinear differential equation that describes the time-dependent change in $[A]$:

$$\frac{d[\tilde{A}]}{dt} = \sigma I[\tilde{A}]\left(\frac{\alpha + \gamma\left(1-[\tilde{A}]\right)}{\alpha + 1 + (\gamma + \beta)\left(1-[\tilde{A}]\right)} - 1\right) \tag{6}$$

In Equation 5, $\alpha = \frac{k_{ex1}}{k_1}$, $\beta = \frac{k_2[A]_0}{k_{ex1}}$, $\gamma = \frac{k_{ex2}[A]_0}{k_{ex1}}$ and $[\tilde{A}] = \frac{[A]}{[A]_0}$. Note that α, β and γ are unitless quantities. We denote Equation (6), which takes into account the effect of $[B]$ on both the photochemical and nonradiative relaxation rates, as the FW-P2 model. If we neglect the effect of product formation on the nonradiative relaxation, i.e. $\gamma = \frac{k_{ex2}[A]_0}{k_{ex1}} = 0$, then we obtain a simpler differential equation with only the α and β parameters, which we call the FW-P1 model:

$$\frac{d[\tilde{A}]}{dt} = \sigma I[\tilde{A}]\left(\frac{\alpha}{\alpha+1+\beta\left(1-[\tilde{A}]\right)}-1\right) \tag{7}$$

Finally, in order to make contact with the standard FW model, we consider the limiting case where $(\alpha+1) >> (\gamma+\beta)$, which is equivalent to $(k_{ex1}+k_1) >> (k_{ex2}+k_2)[A]_0$. In this case, Equation (6) can be rewritten as

$$\frac{d[\tilde{A}]}{dt} = -\frac{\sigma I}{\alpha+1}[\tilde{A}] - \frac{\sigma I\beta}{\alpha+1}[\tilde{A}]\left(1-[\tilde{A}]\right) \tag{8}$$

or

$$\frac{d[A]}{dt} = -\sigma I\varphi_1[A] - \sigma I\varphi_2[A]\left([A]_0-[A]\right)$$

(9)

where $\phi_1 = \frac{1}{\alpha+1} = \frac{k_1}{k_1+k_{ex}}$ and $\phi_2 = \frac{k_2}{k_1+k_{ex}}$ are effective quantum yields for the two photochemical reaction pathways. We then define new rate constants $k_1' = \sigma I\phi_1$ and $k_2' = \sigma I\phi_2$ and rewrite Equation (9) as

$$\frac{d[A]}{dt} = -k_1'[A] - k_2'[A]\left([A]_0-[A]\right) \tag{10}$$

Equation (10) is the standard FW equation for ground state reactions, which we call the FW-P0 model. In this limit, the excited state dynamics are subsumed into the effective rate constants k_1' and k_2'. Note that the standard FW rate constants k_1' and k_2' can be related to α and β via the equations

$$k_1' = \frac{\sigma I}{1+\alpha} \tag{11a}$$

$$k_2' = \frac{\sigma I}{[A]_0} \frac{\beta}{1+\alpha} \tag{11b}$$

Equation (10) can be solved analytically to give

$$[A](t) = \frac{\frac{k_1'}{k_2'} + [A]_0}{1 + \frac{k_1'}{k_2'[A]_0} \exp\left[\left(k_1' + k_2'[A]_0\right)t\right]} \tag{12}$$

It is straightforward to show that if $k_2' = 0$ then Equation (12) reduces to the standard single exponential decay expected for a homogeneous system. Equations (6) and (7) cannot be solved to generate analytical expressions for [A](t), but they can be solved to give single-valued functions that give t as a function of [A], which is just as useful for data fitting. For the FW-P1 model, we find

$$t([\tilde{A}]) = \frac{-\beta(1+\alpha+\beta)\log([\tilde{A}]) + \alpha\log(1+\beta(1-[\tilde{A}]))}{\sigma I(1+\beta)} \tag{13}$$

For the FW-P2 model, we find

$$t([\tilde{A}]) = \frac{-\beta(1+\alpha+\beta+\gamma)\log([\tilde{A}]) + (\alpha\beta-\gamma)\log(1+\beta(1-[\tilde{A}]))}{\sigma I\beta(1+\beta)} \tag{14}$$

Equations (12)-(14) comprise a hierarchy of successive approximations that can be used to systematically analyze the experimental data. For the FW-P2 model, we vary α, β and γ to match the data, while for the FW-P1 model we vary only α and β, and for the FW-P0 model we have k_1' and k_2' as the variable parameters. In practice, we only need to consider the FW-P1 and FW-P2 models in cases where the product-catalyzed photoreaction rate becomes competitive with *A*'s intrinsic excited state lifetime as determined by k_1+k_{ex1}. This can be tested simply by measuring the photoluminescence lifetime of the sample during the course of the photoreaction, since in the transient regime (after excitation by a short laser pulse), Equation (4b) predicts an exponential decay of the form

$$PL(t) = \exp\left[-(k_{ex1}+k_1+(k_{ex2}+k_2)[B])t\right] = \exp\left[-(k_{ex1}+k_1+(k_{ex2}+k_2)([A]_0-[A]))t\right] \qquad (15)$$

If k_2 and/or k_{ex2} are not negligible, then the PL decay rate should change as $[B]$ increases. Note that this prediction can only be derived using the FW-P model, since the JMAK model describes the growth of the ground state populations only. In the FW-P approach it is straightforward to predict how the reaction progress depends on experimental parameters like intensity I, excitation wavelength (via the absorption cross section σ) and the photochemical quantum yields ϕ_1 and ϕ_2. The FW-P approach allows us to explicitly predict how changing experimental parameters will affect the reaction while making new predictions that can be used to test the validity of the model.

4.4. 9MA photodimerization kinetics

In order to evaluate the 9MA photodimerization kinetics, we need to have a reliable way to measure the time-dependent change in reactant and/or product concentration. We tried using peak intensities in the powder x-ray diffraction (PXRD) pattern to monitor the reaction progress in a 9MA crystalline powder but had trouble obtaining reproducible results between different samples. We think the photomechanical response of the material may influence the PXRD peak intensities in an unpredictable manner. During the course of the photoreaction, the crystallites in a powder can be observed to jump and shatter, which changes the morphology of the powder. Changes in the powder texture and particle alignment can change individual diffraction peak intensities in ways that do not necessarily reflect the amount of reactant and product in the sample.[36] PXRD can be used to provide a qualitative picture of the transformation from reactant to product crystal phases, but it could not provide reproducible quantitative information on the rate of this transformation. Solid-state nuclear magnetic resonance (SSNMR) is another method that can in principle be used to follow the reaction progress[20,21,37], but we found that heating due to high magic angle spinning speeds could dissociate the photodimers[38] during the long measurement times, leading to an underestimation of the amount of product formation.

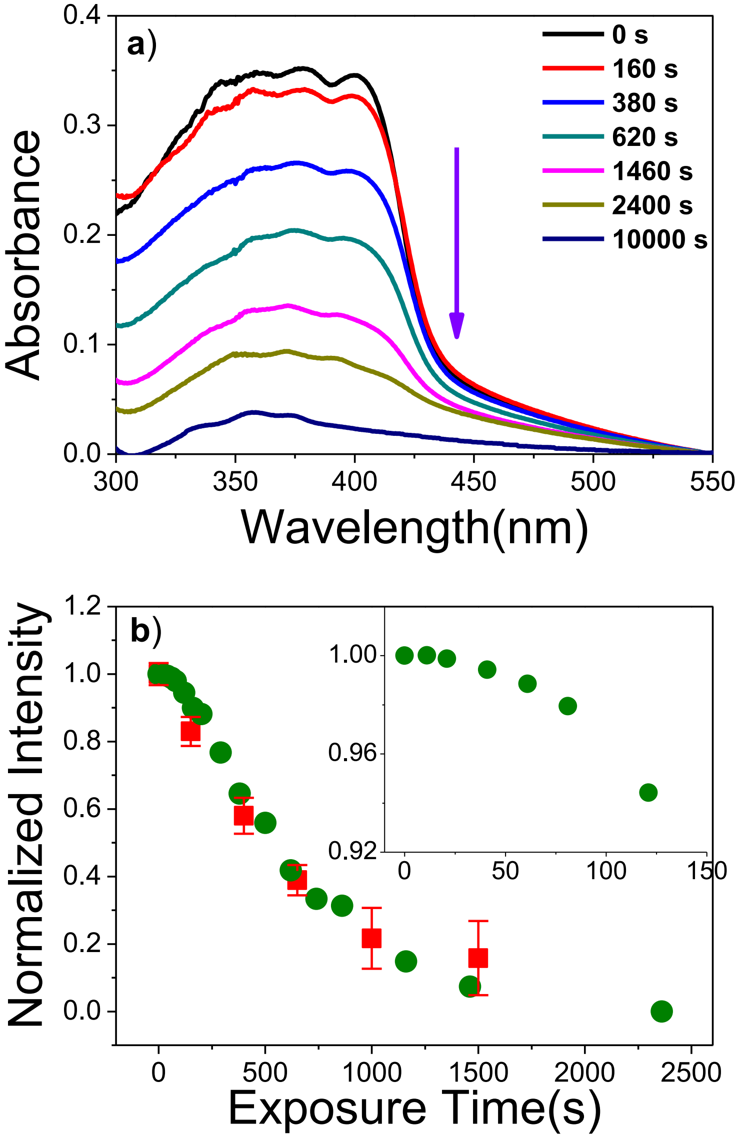

Figure 4.2 (a) Time-dependent evolution of the absorption spectrum of a 9MA polycrystalline film under 365 nm irradiation at room temperature. The irradiation times are given in the figure. After 10000 s, the residual absorption spectrum resembles that of monomeric 9MA that is trapped in the photodimer matrix. (b) Decay of the 9MA integrated absorption (green circles) and the ^{1}H NMR monomer signal (red squares) during the photoreaction. The error bars of NMR data points come from the baseline correction and phase correction of NMR spectrum.

Previous workers have shown that the UV-Vis absorption of thin crystalline films provides a more reliable estimate of reaction progress than x-ray diffraction.[39] Typically composed of randomly oriented crystal plates with an average thickness of less than 1 μm, the absorption of this sample deposited on glass substrates can be reliably measured because the scattering background is a relatively minor component. The use of optically thin films has the added benefit that the light intensity is almost constant across the sample, allowing us to assume I is a constant in Equations (4). For powders and thicker single crystals, I will vary depending on the spatial position within the sample. Figure 4.2a shows the absorption spectrum of the crystalline thin film. The 9MA absorption is shifted to lower energy, relative to the solution spectrum, as expected for the higher dielectric solid-state environment. It is also significantly broadened, but the characteristic anthracene vibronic progression can still be discerned. This absorption provides an unambiguous way to monitor the reactant phase.

Under 365 nm radiation in an oxygen-free atmosphere, the absorbance steadily decreases until only a small (<5%) residual absorption remains. We attribute this decrease to the loss of the anthracene monomer to form the less conjugated photodimers. The residual absorption probably originates from surviving anthracene monomers that are trapped within the photodimer crystal matrix (see discussion of the fluorescence spectrum below). In order to confirm that our absorption measurements provide an accurate measure of the 9MA concentration, we checked them by measuring the decrease of the monomer proton NMR signal at various points during the photoreaction. This was done by making a thin film using a fixed amount of 9MA, measuring the absorbance before and after a fixed irradiation time, and then dissolving the film in a fixed volume of $CDCl_3$ to take an NMR spectrum. Monomeric 9MA has a signature CH_3 resonance at $\delta = 3.1$ ppm (Figure 4.3).[40,41] As the reaction progresses, the area of this peak declines. Note that we did not try to quantify the photodimer NMR signal due to its very low solubility. The decay of the 9MA NMR peak areas closely tracks the decay of the UV-VIS absorption peak areas, as shown in Figure 4.2b. Therefore, we conclude that the thin film UV-Vis absorption is a reliable indicator of the 9MA concentration in the thin film.

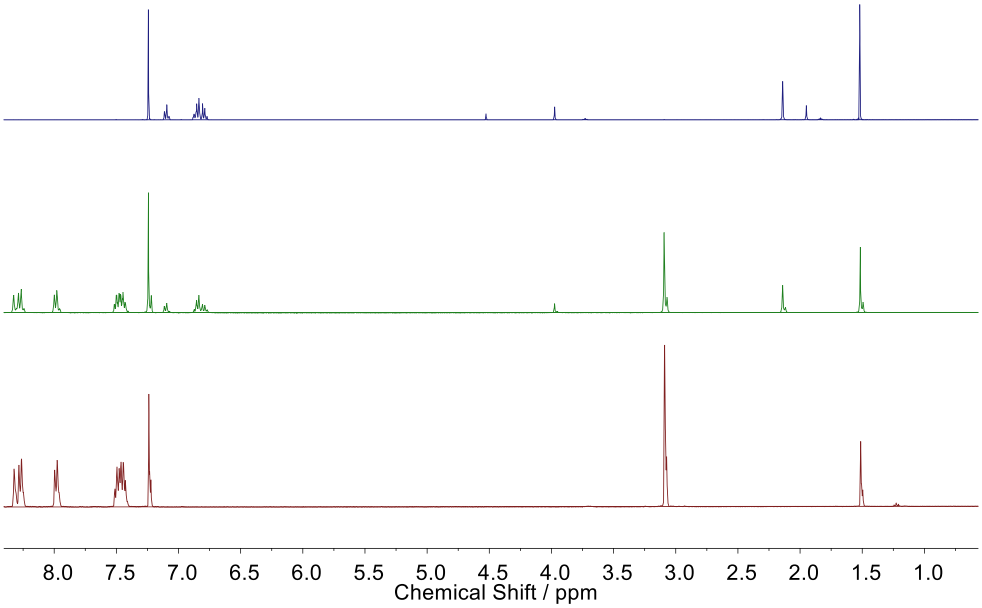

Figure 4.3 The ^{1}HNMR data of pure 9MA monomer (red), a mixture of 9MA monomer and dimer after irradiation by 365 nm light (green), and pure dimer (blue, made by long time 365 nm irradiation in THF solution of 9MA monomer). Deuterated chloroform was used as solvent and the CH_3 resonance at 3.1 ppm indicates the amount of monomeric 9MA. This peak will decrease as the irradiation time increases.

After subtracting a small scattering background and integrating the absorbance between 300 and 450 nm, we have a value for the time-dependent concentration of unreacted anthracene molecules at time *t*, which should be directly proportional to the concentration of reactive pairs [*A*](*t*). A plot of [*A*](*t*) in Figure 4.2b shows that its decay is nonexponential, with a Gaussian-like behavior that is clearly evident at early times, as shown in the inset. This decay shape is not observed when the same reaction is performed in solution (Figure 4.4). No recovery of the 9MA monomer absorbance was observed when the irradiated sample was monitored over the course of days, consistent with a high activation barrier observed for dimer dissociation.[38]

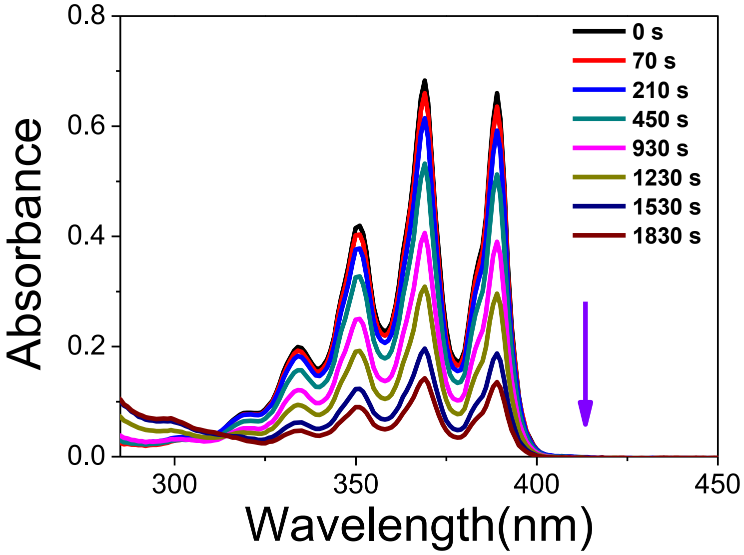

Figure 4.4 Time-dependent spectral evolution of 9MA (in THF, ~4.5×10^{-5} M) by 365 nm irradiation at ambient temperature. The black trace is the absorption spectrum of 9MA without any irradiation.

4.5. 9MA fluorescence lifetime decays

As explained in Section III, the FW-P models allow us to predict other quantities for the photochemical reaction, for example that the PL lifetime can decrease as [*A*](*t*) decays (Equation (13)). It turns out that 9MA's PL signal provides evidence that static homogeneity exists even before the reaction commences. The unreacted 9MA crystal exhibits a broad emission centered at 510 nm, characteristic of an excimer species often seen in this class of anthracene crystals. This excimer is usually assumed to be the precursor of the photodimer[42,43] and can be assigned to the excited state of the reactive monomer pair, *A**. The PL spectrum of 9MA evolves as the dimerization proceeds. After prolonged irradiation, the excimer emission disappears, replaced by a structured emission, peaked at 420 nm that resembles that of monomeric 9MA in solution. This transformation in the steady-state PL spectrum is shown in Figure 4.5. The observation of monomer emission is consistent with the presence of a residual 9MA monomer population trapped in the photodimer matrix.[15,44]

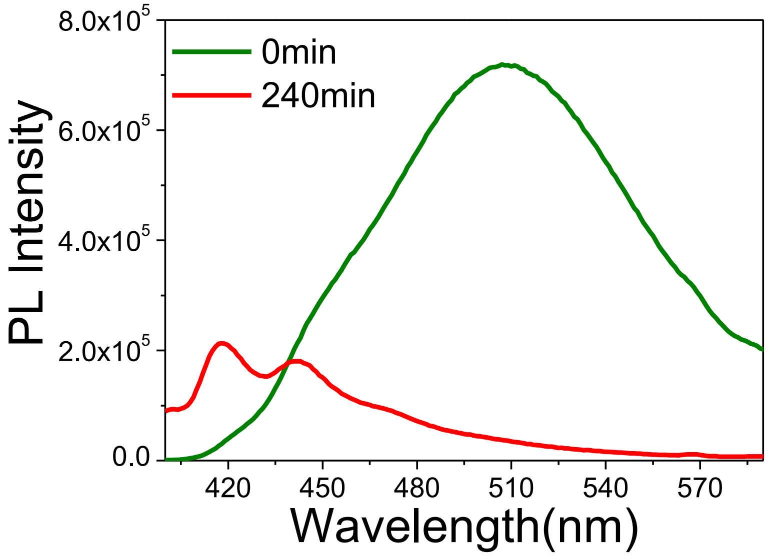

Figure 4.5 Fluorescence emission spectra of an unreacted 9MA polycrystalline film (green line) and the same sample after 4 hours by 365 nm light (red line). Samples were excited at 300 nm. The excimer luminescence centered around 515 nm disappears and is replaced by a monomer luminescence with peaks at 415 nm and 445 nm.

From the steady state spectra at the beginning and endpoints of the photoreaction, we can expect that the PL output at intermediate points will be comprised of a mixture of species. This expectation is confirmed when the fluorescence decays are measured. In general, the decays at all wavelengths are multiexponential and the PL spectrum changes over the course of its decay. We used global lifetime analysis[45,46] to fit the PL decays over 10 different wavelength intervals to a biexponential decay of the form:

$$PL(\lambda,t) = A_1(\lambda)\exp\left[-k_{fl1}t\right] + A_2(\lambda)\exp\left[-k_{fl2}t\right] \tag{16}$$

The same rate constants k_{fl1} and k_{fl2} were used for each wavelength interval, but their respective amplitudes A_1 and A_2 were allowed to vary for different spectral regions. In this way we could obtain the spectra $A_1(\lambda)$ and $A_2(\lambda)$ associated with each decay rate k_{fl1} and k_{fl2}. The results for the unreacted samples confirm that there are two different excimer species in the 9MA crystals, with decay rates of k_{fl1} = 1.2x10^8 s^{-1} (8.5 ns lifetime) and k_{fl2} = 3.7x10^7 s^{-1} (27 ns lifetime). After a 900 s irradiation, most of the emission has shifted to the blue with a decay rate k_{fl1} = 2.12x10^8 s^{-1} (4.7 ns lifetime). The remaining excimer-like emission at longer wavelengths decays with a rate k_{fl2} = 5.65x10^7 s^{-1} (17.7 ns lifetime). The $A(\lambda)$ spectra for these two irradiation times are shown in Figures 4.6a and 4.6b, respectively.

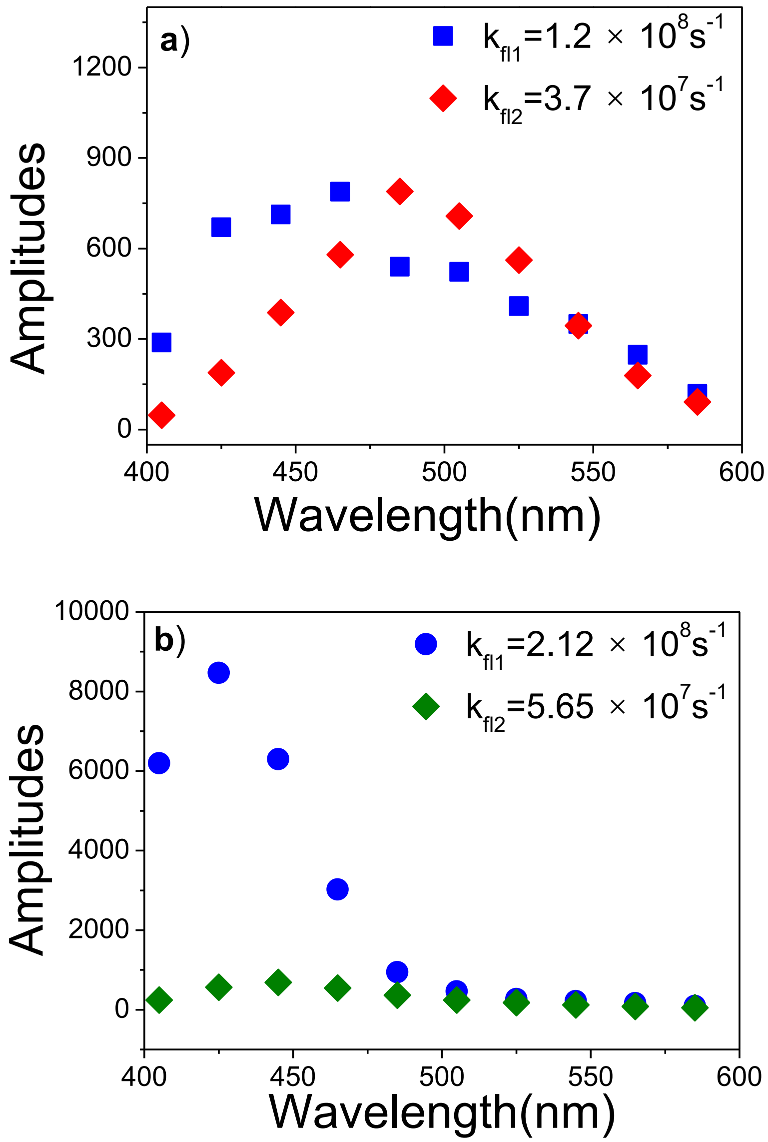

Figure 4.6 A(λ) amplitudes for the biexponential decays in a polycrystalline 9MA film (a) before irradiation with k_{fl1} =1.2×10^{8} s^{-1} and k_{fl2} = 3.7×10^{7} s^{-1}; and (b) after 900s of 365 nm irradiation with k_{fl1} =2.12 ×10^{8} s^{-1} and k_{fl2} =5.65×10^{7} s^{-1}. Each point represents a fit of the time-dependent decay integrated over a 20 nm wavelength interval using a global lifetime analysis algorithm.

The quality of the global fits can be assessed from the data in Figure 4.7, which show PL decays for irradiation times of 0, 600, and 900 s in the wavelength ranges 460-480 nm

(Figure 4.7a) and 560-580 nm (Figure 4.7b). This data also serves to illustrate the steady acceleration of the excimer decay, in qualitative agreement with the prediction of the FW-P2 model via Equation (13).

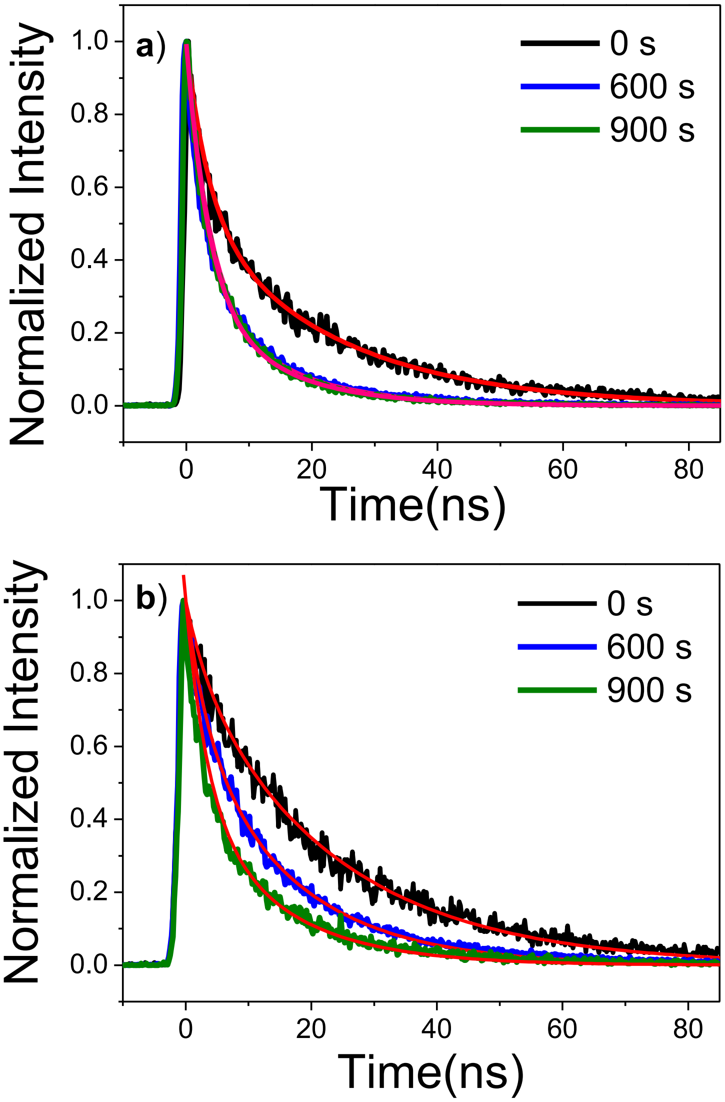

Figure 4.7 Fluorescence lifetime delay data and fits using Equation (16) in the text (red lines) for the 9MA polycrystalline film after exposure to 365 nm UV light exposures for 0 s (black), 600 s (blue) , and 900 s (green) for (a) data integrated over the wavelength range 460-480 nm and (b) data integrated over the wavelength range 560-580 nm.

4.6 Analysis

Solid-state samples can have defect sites and disorder, which give rise to a distribution of ground state structures. This type of structural heterogeneity can also give rise to a distribution of rates that reflect diverse local microenvironments. However, once a photochemical reaction starts, even a perfect crystal becomes heterogeneous due to the creation of photoproduct molecules, which can be thought of as local defects. This leads to a dynamic evolution of the reaction environment, since the distribution of photoproduct changes with time. In crystalline 9MA, both types of phenomena appear to lead to fluorescence decays that are not single exponentials. From the spectra in Figure 4a, even before the reaction starts, there exist two types of excimer sites, one with a lifetime of 8.5 ns that disappears after the first 60 s of irradiation, and one with an initial lifetime of 27 ns that reacts more slowly. These two emitting sites indicate that there is already some structural heterogeneity in the sample, since the pristine crystal structure of 9MA consists only of equivalent pairs of molecules.[17,47] The presence of such emissive defect sites may give rise to different photochemical reaction rates, which would be consistent with their different PL lifetimes. But if this structural disorder was the only factor affecting the photochemical reaction kinetics, then we would expect the fastest rate will dominate at early times, followed by slower dynamics at later times. The overall reaction would get slower as the irradiation time progressed, the opposite of what is observed in Figure 4.2b.

Experimentally, the overall reaction of 9MA as measured by absorption is characterized by an induction period (0-60 s in Figure 4.2b) during which the reaction is quite slow, followed by an acceleration period where the effective rate increases by at least a factor of 10. For completeness, we first analyze the time-dependent monomer pair concentration in the context of the JMAK model. In this case, we use the fact that the photodimer concentration $[B](t) = [A]_0\text{-}[A](t)$ and then use the Sharp-Hancock equation

$$\ln\left(-\ln\left(1-\frac{[B]_\tau}{[A]_0}\right)\right)=n\ln(t)+n\ln(k) \tag{17}$$

where n, the Avrami exponent, and k are given in Equation (1). From the fit to the data in Figure 4.8, we obtain $n = 1.65$ or a nucleation dimensionality of n-1 = 0.65. This value of n is substantially larger than the value of 0.6 obtained in an earlier PXRD study of the 9MA photodimerization in a crystalline powder.[17] We have no easy explanation for the discrepancy other than the preceding observation that we could not measure reproducible kinetics by analyzing the PXRD peak areas. The data in Figure 6 confirm that the JMAK model can do a reasonable job of reproducing the nonexponential kinetics of this solid-state reaction.

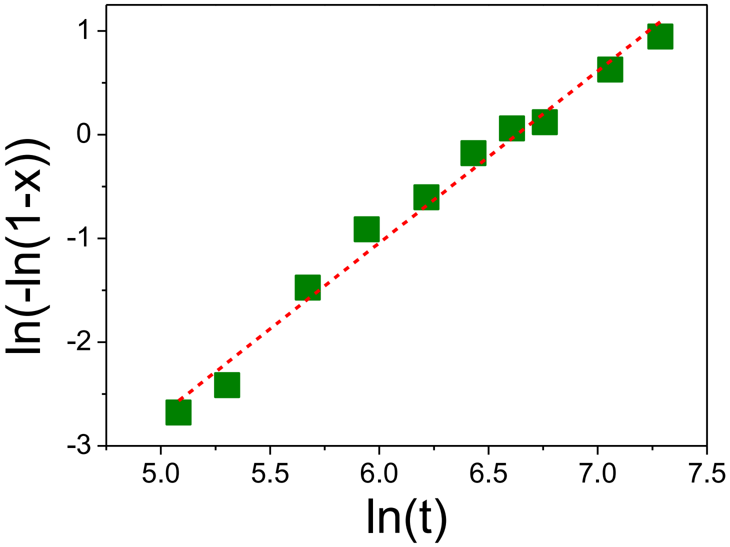

Figure 4.8 Johnson-Mehl-Avrami-Kolmogorov (JMAK) fit of the time-dependent 9MA dimer formation during irradiation. The data points are fit using the Sharp-Hancock equation $ln(-ln(1 - x)) = n\ ln(t) + n\ ln\ k$. (k is dimerization rate and n (~1.65) is Avrami exponent which indicates the dimension of the nucleation of crystalline film. x represents the fraction of dimer formed during the irradiation period.)

The simple FW-P0 model can also provide an adequate fit to the $[A](t)$ data, as shown in Figure 4.9a, using the parameters $k_1 = 2.13\text{x}10^5\ s^{-1}$ and $k_2 = 1.14\text{x}10^6\ s^{-1}nm^{-3}$ with the parameters $[A]_0 = 1.925$ pairs/nm^3 (obtained from the crystal structure), $\sigma(365\ \text{nm}) = 1.7\ \text{x}10^{-17}\ cm^2$ (estimated from the absorption spectrum in solution), $k_{ex1} = 3.7\text{x}10^7\ s^{-1}$ (obtained from the PL decay of the long-lived excimer component), and $I = 3.1\text{x}10^{15}$ photons/cm^2/s as measured using a power meter. There is some uncertainty in these values due to the fact that σ is estimated from the solution absorption coefficient and that the solid-state absorption is distorted due to the scattering background. From varying the fit parameters, we estimate a total uncertainty of ±20% in the k_1 and k_2 parameters, as judged from the point at which the calculated curves visibly deviate from the experimental points.

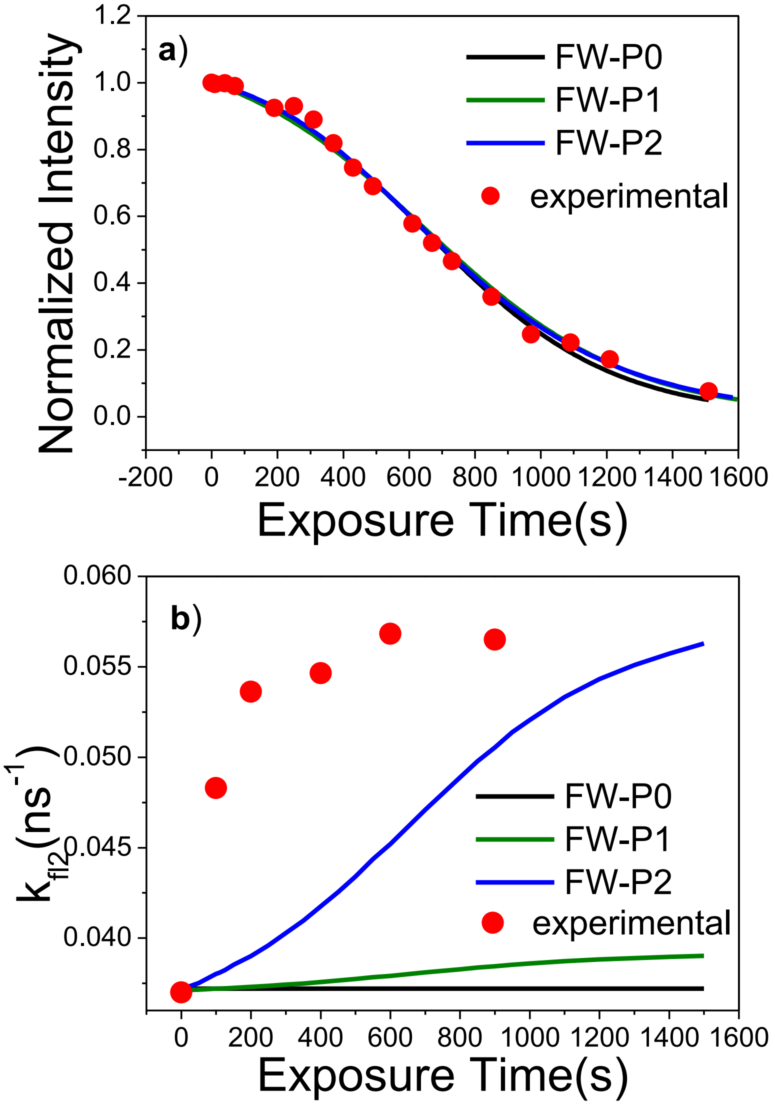

Figure 4.9 (a) Experimental data for the decay of the 9MA monomer concentration [A](t) (red circles) overlaid with fits using FW-P0 model (black), FW-P1 model (green) and FW-P2 model (blue). (b) PL decay rates k_{fl2} of the excimer peak at 515 nm as the irradiation time is increased (orange circles) overlaid with the predictions of Equation (13) for the FW-P0 model (black), the FW-P1 model (green) and the FW-P2 model (blue). There is a maximum uncertainty of ~5% in the experimental k_{fl2} points. All three models do an adequate job of describing [A](t). The FW-P2 model, taking into account the role of photoproduct in accelerating both the photoreaction and the nonradiative decay, capture the magnitude of change in k_{fl2} but does not reproduce the detailed dependence on UV exposure time.

Although our FW-P0 model provides an adequate description of $[A](t)$, it does not predict any change in the fluorescence decay rate, since it assumes $(k_{ex1}+k_1)>>(k_2+k_{ex2})[B]$ at all times. Furthermore, we see that this inequality is not fulfilled by the values of k_1 and k_2 obtained from the FW-P0 fitting. The next step in the analysis is to relax this condition by allowing k_2 to vary while setting $k_{ex2} = 0$. This is our FW-P1 model. We can then fit the data in Figure 2 using Equation (13) and the same σ, I and $[A]_0$ parameters to obtain k_1=1.21x10^5 s^{-1} and k_2=1.05×10^6 s^{-1}nm^3. As compared to the FW-P0 model, the value of k_1 decreases almost by a factor of 2, but k_2 changes less than 10%. Additionally, the FW-P1 model now predicts that the PL decay rate k_{fl2} should increase by a factor of 1.2. The FW-P1 model predicts the qualitative trend in k_{fl2} but underestimates its quantitative magnitude, since the experimental k_{fl2} increases by a factor of 1.8 (Figure 7b). To describe the full change in the observed PL lifetime, we turn to the FW-P2 model and use Equation (14). In order to reproduce the approximate magnitude of change in k_{fl2}, we set $(\beta+\gamma)/(\alpha+1)$=0.55 and then vary α, β and γ subject to this constraint. We obtain the best fit parameters α=203.5, β=15.6 and γ=96.9, leading to k_1 = 1.82x10^5 s^{-1}, k_2 = 1.47x10^6 s^{-1}nm^3, and k_{ex2} = 9.16x10^6 s^{-1}nm^3. The calculated change in PL lifetime, as deduced from Equation (15) and the $[A](t)$ data in Figure 4.2b, is shown in Figure 4.9b along with the data points. Adding the additional parameter (k_{ex2}) allows the model to reproduce the magnitude of the increase in k_{fl2}, but its calculated dependence on irradiation time is clearly very different from the data.

From the analysis of the data in Figures 4.8 and 4.9, we can make several general observations. First, both the JMAK and FW-P0 models do an acceptable job of describing the $[A](t)$ behavior. The JMAK model approximates the induction period by making the decay more Gaussian-like by setting $n=1.65$ instead of $n=1$. The FW-P0 model does this by postulating a new $A+B \rightarrow B+B$ reaction pathway. It should be emphasized that both models lead to photochemical reaction rates in the crystal are changing with time. However, the more transparent nature of the FW-P model allows us to systematically improve it and make additional predictions about independently measured quantities like the PL lifetime. The data and fits in Figure 4.9b show that the FW-P1 and FW-P2 models enable the presence of the photodimer (B) to accelerate both the photochemical reaction rate and the nonradiative relaxation through the k_2 and k_{ex2} terms, respectively. It is remarkable that these autocatalytic rate processes can by accelerated by up to a factor of 10 in the presence of the photoproduct. The acceleration of the PL decay cannot be predicted by the basic FW-P0 model. The interplay between the reaction progress and the photophysics must be explicitly taken into account in order to correctly describe this photoreactive crystal system.

Although the FW-P2 model can describe magnitude and direction of the experimental PL decay change, it cannot reproduce the detailed time dependence. Equation (15) predicts that the change in the overall fluorescence decay rate should track $[B](t)=[A]_0-[A](t)$ which has a sigmoidal shape similar to the decay shown in Figure4.2b. Experimentally, k_{fl2} grows very rapidly at the start, then saturates after about 600 s of irradiation. The calculated change grows much more slowly and begins to saturate only after 1200 s of irradiation. Varying the k_2 and/or k_{ex2} rates in the FW-P1 and FW-P2 models cannot change the overall shape of their predicted k_{fl2} curve. The fact that the time-dependent changes in $[B](t)=[A]_0-[A](t)$ and k_{fl2} are not linearly correlated, as predicted by Equation (15), suggests that either 1) our analysis of the photophysics is incomplete or 2) the FW-P2 model does not take all possible pathways into account. We think possibility 1) is most likely. As discussed earlier, the fluorescence decay involves contributions from multiple species, and our assumption that the red-shifted component corresponding to k_{fl2} accurately reports on $[A](t)$ may not be correct. For example, during the course of the reaction low energy defect sites with shorter lifetimes may be introduced into the crystal lattice. Exciton diffusion to these shorter lifetime sites could artificially reduce the fluorescence lifetime and result in a premature increase in k_{fl2}. Considering possibility 2), we can further extend the reaction scheme in Equations (3) to take additional pathways into account. For example, we could consider a catalyzed reverse reaction, e.g. $A^*+B \rightarrow A+A$. However, since we have no clear evidence for such a process, we did not develop a more complex kinetic model at this point. Clearly, additional work is needed to fully connect the spectroscopy and reaction rate measurements. But we should emphasize that fundamental advantage of the FW-P approach is that it provides a systematic way to test assumptions about chemical reaction pathways and photophysical behavior, as well as a clear route for stepwise improvement of the model.

Finally, we note that the FW-P model is designed to describe ensemble kinetics, and rate constants k_2 and k_{ex2} each probably reflect multiple processes that are occurring on the molecular level.[33] For example, the presence of defects, both structural and light-induced, provide both quenching centers (as reflected by k_{ex2}) and nucleation sites for the growth of photoproduct domains (as reflected by k_2). Both rates are likely to be mediated by exciton diffusion through the monomer domains. If we could map out quantities like the PL lifetime and reactant concentration with high spatial and temporal resolution in a single reacting crystal, a more sophisticated model that explicitly take spatial variations and exciton dynamics into account would be required. Given the ensemble measurements reported here, the FW-P2 model represents a good starting point to describe both the photophysical and photochemical data. It should be noted that this model is more sophisticated than any that have previously been applied to solid-state photochemical systems.

4.7 Conclusion

This project had several goals. First, we presented a rigorous derivation of a generalized FW-P model for photochemically reactive systems. Second, we have shown that monitoring the UV-Vis absorption spectrum of an optically thin film provides a reliable way to follow the reaction progress, which enables us to measure the reaction kinetics in photomechanically active 9MA crystals. Third, although both the FW and JMAK models can describe the time-dependent change in reactant/product concentrations, our extended FW-P2 model furthermore correctly predicts the observed trend in PL lifetime. This prediction can only be derived using the FW-P model. Furthermore, using the FW-P approach it is straightforward to predict how experimental parameters like intensity, absorption cross section and quantum yields will affect the reaction progress. Because it can be formulated in terms of chemical reaction steps and well-defined rate constants, the FW-P approach has a predictive power that makes it a useful tool for the quantitative analysis of photochemical reaction kinetics in solid-state molecular systems. Understanding the reaction kinetics will in turn provide a framework for quantitatively analyzing the dynamics of mechanical deformations in molecular crystals. We will address how non-first-order reaction kinetics will influence the photoinduced bending of 9MA crystalline microneedles in our future work.

4.8 References

(1). Schmidt, G. M. J. Photodimerization in the Solid State. *Pure Appl. Chem.*, **1971**, 27, 647–678.

(2). Schmidt, G. M. J.; Cohen, M. D.; Donitz, J. D.; Hammond, C. S. Solid-State Photochemistry; *Verlag Chemie: Germany*, **1976**.

(3). MacGillivray, L. R.; Papaefstathiou, G. S.; Friscic, T.; Hamilton, T. D.; Bucar, D. K.; Chu, Q.; Varshney, D. B.; Georgiev, I. G. Supramolecular Control of Reactivity in the Solid State: From Templates to Ladderanes to Metal-Organic Frameworks. *Acc. Chem. Res.*, **2008**, 41, 280–291.

(4). Biradha, K.; Santra, R. Crystal Engineering of Topochemical Solid State Reactions. *Chem. Soc. Rev.*, **2013**, 42, 950–967.

(5). Lauher, J. W.; Fowler, F. W.; Goroff, N. S. Single-Crystal-to-Single-Crystal Topochemical Polymerizations by Design. *Acc. Chem. Res.*, **2008**, 41, 1215–1229.

(6). Luty, T.; Eckhardt, C. J. General Theoretical Concepts for Solid State Reactions: Quantitative Formulation of the Reaction Cavity, Steric Compression, and Reaction-Induced Stress Using an Elastic Multipole Representation of Chemical Pressure. *J. Am. Chem. Soc.*, **1995**, 117, 2441–2452.

(7). McBride, J. M.; Segmuller, B. E.; Hollingsworth, M. D.; Mills, D. E.; Weber, B. A. Mechanical Stress and Reactivity in Organic Solids. *Science.*, **1986**, 234, 830–835.

(8). Peachey, N. M.; Eckhardt, C. J. Energetics of Organic Solid-State Reactions: Lattice Dynamics in the 2,5-Distyrlpyrazine Photoreaction. *J. Phys. Chem.*, **1993**, 97, 10849–10856.

(9). Kaupp, G.; Herrmann, A.; Schmeyers, J. Waste-Free Chemistry of Diazonium Salts and Benign Separation of Coupling Products in Solid-State Reactions. *Chem. Eur. J.*, **2002**, 8, 1395–1406.

(10). Verman, M.; Resendiz, M. J. E.; Garcia-Garibay, M. A. Large-Scale Photochemical Reactions of Nanocrystalline Suspensions: A Promising Green Chemistry Method. *Org. Lett.*, **2006**, 8, 2615–2617.

(11). Kim, T.; Zhu, L.; Al-Kaysi, R. O.; Bardeen, C. J. Organic Photomechanical Materials. *ChemPhysChem.*, **2014**, 15, 400–414.

(12). Naumov, P.; Chizhik, S.; Panda, M. K.; Nath, N. K.; Boldyreva, E. Mechanically Responsive Molecular Crystals. *Chem. Rev.*, **2015**, 115, 12440–12490.

(13). Nath, N. K.; Pejov, L.; Nichols, S. M.; Hu, C.; Saleh, N.; Kahr, B.; Naumov, P. Model for Photoinduced Bending of Slender Molecular Crystals. *J. Am. Chem. Soc.*, **2014**, 136, 2757–2766.

(14). Warner, M. Photoinduced Deformations of Beams, Plates, and Films. *Phys. Rev. Lett.*, **2004**, 92, 134302/1–134302/4.

(15). Kim, T.; Zhu, L.; Mueller, L. J.; Bardeen, C. J. Mechanism of Photo-Induced Bending and Twisting in Crystalline Microneedles and Microribbons Composed of 9-Methylanthracene. *J. Am. Chem. Soc.*, **2014**, 136, 6617–6625.

(16). Kaupp, G. Photodimerization of Anthracenes in the Solid State: New Results from Atomic Force Microscopy. *Angew. Chem. Int. Ed.*, **1992**, 31, 595–598.

(17). Mabied, A. F.; Muller, M.; Dinnebier, R. E.; Nozawa, S.; Hoshino, M.; Tomita, A.; Sato, T.; Adachi, S. A Time-Resolved Powder Diffraction Study of In-Situ Photodimerization Kinetics of 9-Methylanthracene Using a CCD Area Detector and Parametric Rietveld Refinement. *Acta Cryst. B.*, **2012**, 68, 424–430.

(18). Heller, E.; Schmidt, G. M. J. Topochemistry. Part XXXIII. The Solid-State Photochemistry of Some Anthracene Derivatives. *Isr. J. Chem.*, **1971**, 9, 449–462.

(19). Christian, J. W. The Theory of Transformations in Metals and Alloys; *Pergamon: Oxford, UK*, **1981**.

(20). Bertmer, M.; Nieuwendaal, R. C.; Barnes, A. B.; Hayes, S. E. Solid-State Photodimerization Kinetics of a-Trans-Cinnamic Acid to a-Truxillic Acid Studied Via Solid-State NMR. *J. Phys. Chem. B.*, **2006**, 110, 6270–6273.

(21). Fonseca, I.; Hayes, S. E.; Blumich, B.; Bertmer, M. Temperature Stability and Photodimerization Kinetics of B-Cinnamic Acid and Comparison to Its a-Polymorph as Studied by Solid-State NMR Spectroscopy Techniques and DFT Calculations. *Phys. Chem. Chem. Phys.*, **2008**, 10, 5898–5907.

(22). Benedict, J. B.; Coppens, P. Kinetics of the Single-Crystal to Single-Crystal Two-Photon Photodimerization of a-Trans-Cinnamic Acid to a-Truxillic Acid. *J. Phys. Chem. A.*, **2009**, 113, 3116–3120.

(23). More, R.; Busse, G.; Hallmann, J.; Paulmann, C.; Scholz, M.; Techert, S. Photodimerization of Crystalline 9-Anthracenecarboxylic Acid: A Nontopotactic Autocatalytic Transformation. *J. Phys. Chem. C.*, **2010**, 114, 4142–4148.

(24). Watzky, M. A.; Finke, R. G. Transition Metal Nanocluster Formation Kinetic and Mechanistic Studies. A New Mechanism When Hydrogen Is the Reductant: Slow, Continuous Nucleation and Fast Autocatalytic Surface Growth. *J. Am. Chem. Soc.*, **1997**, 119, 10382–10400.

(25). Finney, E. E.; Finke, R. G. Fitting and Interpreting Transition-Metal Nanocluster Formationa Nd Other Sigmoidal-Appearing Kinetic Data: A More Thorough Testing of Dispersive Kinetics vs Chemical-Mechanism-Based Equations and Treatments for 4-Step Type Kinetic Data. *Chem. Mater.*, **2009**, 21, 4468–4479.

(26). Finney, E. E.; Finke, R. G. Nanocluster Nucleation and Growth Kinetic and Mechanistic Studies: A Review Emphasizing Transition-Metal Nanoclusters. *J. Colloid. Interfac. Sci.*, **2008**, 317, 351–374.

(27). Kent, P. D.; Mondloch, J. E.; Finke, R. G. A Four-Step Mechanism for the Formation of Supported-Nanoparticle Heterogeneous Catalysts in Contact with Solution: The Conversion of Ir(1,5-COD)Cl/g-Al_2O_3 to Ir(0)~170/g-Al_2O_3. *J. Am. Chem. Soc.*, **2014**, 136, 1930–1941.

(28). Sonnenberg, J. F.; Morris, R. H. Distinguishing Homogeneous from Nanoparticle Asymmetric Iron Catalysis. *Catal. Sci. Tech.*, **2014**, 4, 3426–3438.

(29). Borgia, M. B.; Nickson, A. A.; Clarke, J.; Hounslow, M. J. A Mechanistic Model for Amorphous Protein Aggregation of Immunoglobulin-like Domains. *J. Am. Chem. Soc.*, **2013**, 135, 6456–6464.

(30). Morris, A. M.; Watzky, M. A.; Finke, R. G. Protein Aggregation Kinetics, Mechanism, and Curve-Fitting: A Review of the Literature. *Biochim. Biophys. Acta.*, **2009**, 1794, 375–397.

(31). Morris, A. M.; Watzky, M. A.; Agar, J. N.; Finke, R. G. Fitting Neurological Protein Aggregation Kinetic Data via a 2-Step, Minimal/"Ockham's Razor" Model: The Finke-Watzky Mechanism of Nucleation Followed by Autocatalytic Surface Growth. *Biochemistry.*, **2008**, 47, 2413–2427.

(32). Sievers, S. A.; Karanicolas, J.; Chang, H. W.; Zhao, A.; Jiang, L.; Zirafi, O.; Stevens, J. T.; Munch, J.; Baker, D.; Eisenberg, D. Structure-Based Design of Non-Natural Amino-Acid Inhibitors of Amyloid Fibril Formation. *Nature.*, 2011, 475, 96–100.

(33). Finney, E. E.; Finke, R. G. Is There a Minimal Chemical Mechanism Underlying Classical Avrami-Erofe'ev Treatments of Phase-Transformation Kinetic Data? *Chem. Mater.*, **2009**, 21, 4692–4705.

(34). Laxson, W. W.; Finke, R. G. Nucleation Is Second Order: An Apparent Kinetically Effective Nucleus of Two for Ir(0)n Nanoparticle Formation from [(1,5-COD)IrI.$P_2W_{15}Nb_3O_{62}]^{8-}$ Plus Hydrogen. *J. Am. Chem. Soc.*, **2014**, 136, 17601–17615.

(35). Salzillo, T.; Zaccheroni, S.; Valle, R. G. Della; Venuti, E.; Brillante, A. Micro Raman Investigation of the Photodimerization Reaction of 9-Cyanoanthracene in the Solid State. *J. Phys. Chem. C.*, **2014**, 118, 9628–9635.

(36). Dinnebier, R. E.; Billinge, S. J. L. Powder Diffraction: Theory and Practics; *Royal Soc. Chem.: Cambridge*, **2008**.

(37). Takegoshi, K.; Nakamura, S.; Terao, T. Solid-State Photodimerization of 9-Methylanthracene as Studied by Solid-State 13C NMR. *Solid State Nucl. Magn. Reson.*, **1998**, 11, 189–196.

(38). Ebeid, E. M.; Habib, A. M.; Azim, S. A. Phase Transformation and Thermal Monomerization of 9-Methylanthracene Photodimer. *React. Solids.*, **1988**, 6, 39–44.

(39). Davaasambuu, J.; Busse, G.; Techert, S. Aspects of the Photodimerization Mechanism of 2,4-Dichlorocinnamic Acid Studied by Kinetic Photocrystallography. *J. Phys. Chem. A.*, **2006**, 110, 3261–3265.

(40). Bringmann, S.; Brodbeck, R.; Hartmann, R.; Schafer, C.; Mattay, J. Anthracene-resourci[4]arene-Based Capsules: Synthesis and Photoswitchable Features. *Org. Biomol. Chem.*, **2011**, 9, 7491–7499.

(41). Pfeffer, M. G.; Pehlken, C.; Staehle, R.; Sorsche, D.; Streb, C.; Rau, S. Supramolecular Activation of a Molecular Photocatalyst. *Dalt. Trans.*, **2014**, 43, 13307–13315.

(42). Birks, J. B.; Aladekomo, J. B. The Photo-Dimerization and Excimer Fluorescence of 9-Methyl Anthracene. *Photochem. Photobio.*, **1963**, 2, 415–418.

(43). Ferguson, J.; Miller, S. E. H. Effects of Molecular Structure and Environment on the Photodimerization of Substituted Anthracenes. *Chem. Phys. Lett.*, **1975**, 36, 635–638.

(44). MacFarlane, R. M.; Philpott, M. R. Excimer and Photochemically Induced Fluorescence of 9-Cyanoanthracene Crystals. *Chem. Phys. Lett.*, **1976**, 41, 33–36.

(45). Knutson, J. R.; Beechem, J. M.; Brand, L. Simultaneous Analysis of Multiple Fluorescence Decay Curves: A Global Approach. *Chem. Phys. Lett.*, **1983**, 102, 501–507.

(46). Burdett, J. J.; Gosztola, D.; Bardeen, C. J. The Dependence of Singlet Exciton Relaxation on Excitation Density and Temperature in Polycrystalline Tetracene Thin Films: Kinetic Evidence for a Dark Intermediate State and Implications for Singlet Fission. *J. Chem. Phys.*, **2001**, 135, 214508.

(47). Turowska-Tyrk, I.; Trzop, E. Monitoring Structural Transformations in Crystals. 6. The [4+4] Photodimerization of 9-Methyl-Anthracene. *Acta Cryst. B*., **2003**, 59, 779–786.

Chapter 5 Surfactant-enhanced photoisomerization and photomechanical response in molecular crystal nanowires

5.1 Introduction

Light actuated mechanical elements have potential applications in medicine, biology, engineering or as integral parts in micromachines. Organic photomechanical materials are the subject of increasing research efforts since they could form the active element in such actuators.[1] These materials rely on photochemical reactions to transform absorbed photon energy into mechanical motion at the molecular scale. In order to coordinate multiple molecular-level reactions so they can generate larger scale motion, the photoreactive molecules are usually organized in a polymer matrix[2-3] or as a crystal.[4] Photomechanical molecular crystals may have some advantages relative to polymer-based materials, including faster response time, higher Young's modulus, and a highly ordered structure that can be precisely characterized using x-ray diffraction techniques.[5-8] They have demonstrated a variety of macroscopic motions such as bending[9-19], twisting[20-21], expansion[22], ratchet-like spinning[23], photosalient jumping[24-25] and surface restructuring.[26-27] Almost all of these motions rely on the formation of a reactant-product mixed phase crystal where interfacial strain between the two phases causes the crystal to deform.[10, 15, 28] This bimorph or bimetal model depends on the reaction kinetics and spatial distribution of reactant and product molecules within the crystal. While the reactant phase is crystalline, the product phase can be either crystalline or amorphous.

We recently observed that crystalline nanowires composed of either *Z* or *E* isomers of a conjugated anthracene derivative, dimethyl-2- (3-anthracen-9-yl)allylidene)malonate (DMAAM) could undergo a novel photoinduced coiling when exposed to a pulse of visible (450-550 nm) light.[29] These large shape changes that continued even after the light source was turned off and were qualitatively different from what had been typically observed in molecular crystals. Nuclear magnetic resonance (NMR) studies confirmed that the presence of both *Z* and *E* isomers are necessary for a nanowire to collapse into its coiled form, suggesting a mixed phase was formed. X-ray diffraction and electron microscopy experiments, however, suggested that the crystalline nanowires became amorphous after illumination, rather than forming two different crystalline phases, as usually observed for other photomechanical crystals. The underlying mechanism of the photoinduced coiling remained unclear.

Here, we investigate the mechanism of the photoinduced coiling of DMAAM nanowires using a variety of experimental techniques, including powder X-ray diffraction, polarized light microscopy, ^{1}H-NMR and UV-Vis spectroscopy. We have used surfactants to help disperse the nanowires in aqueous media and minimize their agglomeration. Up to now, we have assumed that this external coating did not affect the solid-state reaction occurring within the crystalline nanowires. However, the data in this work clearly show that the presence of a surfactant accelerates the photochemical reaction rate by at least a factor of 10 within the nanowire and is required to observe the photoinduced coiling. The accelerated reaction facilitates the transition to an amorphous phase composed of reactant and photoproduct and eventually leads to the dissolution of the mixed-phase nanowire into the aqueous solution. The interplay of photochemistry and surfactant-catalyzed crystal amorphization results in the rapid, largescale shape changes that we observe. To the best of our knowledge, the effect of surfactants on solid-state photochemical reactivity has not been considered before. Our study of DMAAM nanowires suggests that the reaction dynamics of nanoscale molecular crystals can be extremely sensitive to surface species, and this in turn can affect the photomechanical motion.

5.2 Experimental part

Both (*E*)-DMAAM and (*Z*)-DMAAM were synthesized following the procedures described in our previous paper.[29] All solvents and reagents, including cetyltrimethylammonium bromide (CTAB), were of reagent grade (Sigma-Aldrich) and were used as received. Commercial Anodic Aluminum Oxide (AAO) templates (Whatman Anodisc inorganic filter membrane, diameter 13 mm, pore diameter 0.2 μm) were purchased from Whatman-Inc. and used as received.

5.2.1 Preparation of DMAAM nanowires

A concentrated solutions of either (*E*)-DMAAM or (*Z*)-DMAAM was prepared by dissolving roughly 4 mg of either isomer in warm N,N-DMF (55 μL). The solution was deposited on an AAO template. The solution-soaked AAO template was suspended on top of a hollow Teflon holder (2 cm in height) resting inside a small beaker. The entire setup was covered with a glass bell jar and placed inside a convection oven set at 65 °C for a period of 24 h. This gives the DMF solvent enough time to slowly evaporate from the jar, leaving behind crystallized DMAAM inside and on the surface of the AAO template. The loaded AAO template was then carefully polished with 2000 grit sandpaper to remove surface crystals before dissolving the alumina template in a 20% phosphoric acid aqueous solution. It requires on average 48 h for the whole template to dissolve at room temperature, releasing the organic nanowires.

5.2.2 Powder X-Ray diffraction (PXRD)

Two carefully polished AAO templates containing (*E*)-DMAAM nanowires were dissolved in a 10 mL aqueous solution (~20 % H_3PO_4 by mass). CTAB was dissolved in the suspension containing the (*E*)-DMAAM nanowires to a typical concentration of 2 mM, and the mixture was irradiated by a 462 nm diode laser with an intensity of 44 mW/cm^2 for various periods. To avoid precipitation of CTAB crystals, the CTAB concentration was kept below 3 mM (the critical micelle concentration is approximately 0.9 mM[30-31]) throughout the entire set of experiments. A magnetic stir bar (1/2 × 1/8 inch) was used to stir the suspension of nanowires at 400 rpm providing uniform illumination for the entire sample. The irradiated nanowires were filtered through AAO template and rinsed with copious amounts of Milli-Q purified water in order to remove any residual H_3PO_4 and CTAB. The nanowire residue, deposited on top of the AAO template, was air dried at 50 ^{o}C. All PXRD data were collected on a Bruker D8 Advance X-ray powder diffractometer (CuK radiation, λ=1.5418 Å, 45 kV/40 mA power) at room temperature.

5.2.3 ^{1}H Nuclear magnetic resonance (^{1}HNMR) measurements

A similar procedure to the one described in the previous PXRD section was used to prepare photoreacted DMAAM nanowires. The dry nanowires were dissolved in $CDCl_3$ (Sigma-Aldrich, 99.9 % +). ^{1}HNMR data were collected using a Varian Inova 300 spectrometer with a 5 mm p 4-nucleus probe.

5.2.4 Optical spectroscopy measurements

The DMAAM nanowires were prepared and reacted as a suspension as described in the PXRD section. After each period of illumination, a 0.50 mL of suspension was deposited in a standard 1 cm path length cuvette and diluted with 2.5 mL Milli-Q purified water to give a total volume of 3.0 mL. UV-Vis absorption spectra of the suspensions were obtained using a Varian CARY 50 spectrometer.

5.2.5 Optical microscopy measurements

A drop of the (*E*)-DMAAM nanowire suspension was deposited on top of a microscope glass slide and covered with a microscope coverslip. To monitor the photomechanical motion, an Olympus IX70 microscope was used with a 20× 0.4 numerical aperture objective: Videos and images were taken using an AMScope MU900 digital camera. The nanowires were irradiated using 450 nm light from a microscope Hg lamp filtered through a dichroic mirror with an intensity of 175 mW/cm^2. For polarized optical microscopy measurements, the sample was placed between two square (2 cm × 2 cm) polarizers aligned at a 90^o angle for measurements.

5.3 Results and discussion

Figure 5.1 shows the photoisomerization of DMAAM between its (*E*) and (*Z*) conformations. In solution, irradiation with visible light (462 nm) induces an *E* → *Z* isomerization that changes the UV-Vis absorption as shown in Figure5.2. If the resulting mixture is then photolyzed with UV light (365 nm), where the *Z* isomer absorbs more strongly, the E isomer is partially recovered. The *E* and *Z* absorption bands overlap in the visible region, and the presence of multiple isosbestic points (most prominent at 330 nm) provides evidence that the photochemical reaction is unimolecular in nature. A strong absorption peak at 253 nm, due to the $S_0 \rightarrow S_2$ absorption feature of anthracene chromophore is also present in both chromophores, and is more prominent for the (*Z*) isomer (Figure 5.3, $\varepsilon_{253nm}(E) = 9.5\times10^4$ cm/M, $\varepsilon_{253nm}(Z) = 1.2\times10^5$ cm/M in cyclohexane). This feature of the absorption spectrum provides a convenient measure of the total amount of DMAAM present, while the lower energy S_0-S_1 transition, polarized along the short axis of the anthracene ring, is a sensitive indicator of the isomerization reaction.

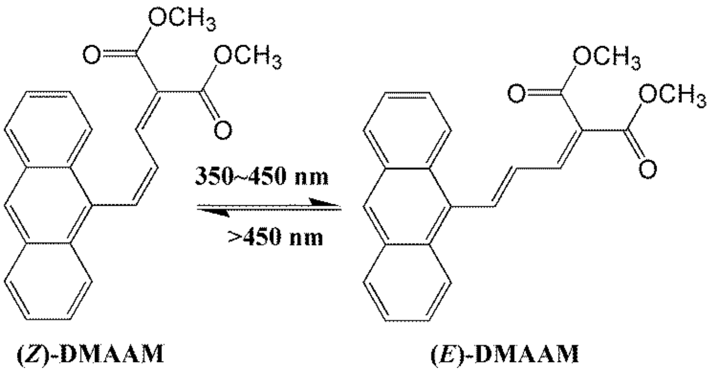

Figure 5.1 Photoisomerization of the DMAAM molecule between *E* and *Z* conformations.

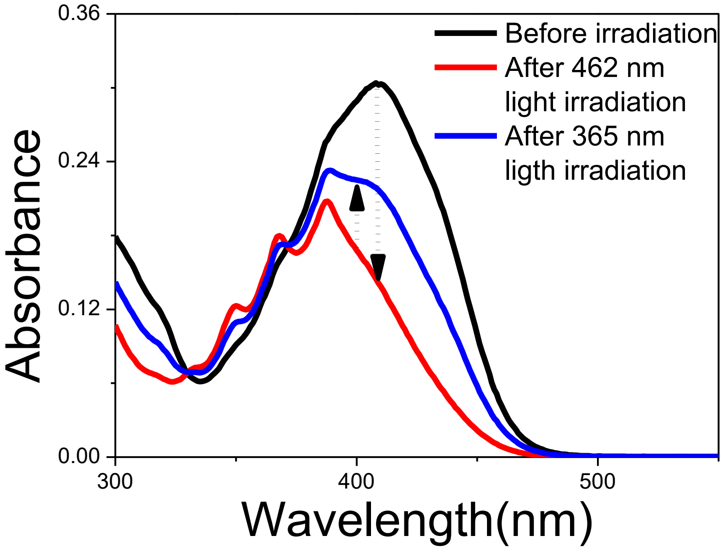

Figure 5.2 The UV-Vis absorption spectrum of irradiation of (*E*)-DMAAM in cyclohexane (~ 2.1 ×10^{-5} M). Pure (*E*)-DMAAM (black) was irradiated at 462 nm for 2 hours to partially convert the sample to (*Z*)-DMAAM (red). The solution wan then exposed to 365 nm light for 2 hours. The resulting spectrum (blue) shows partial recovery of the (*E*)-DMAAM

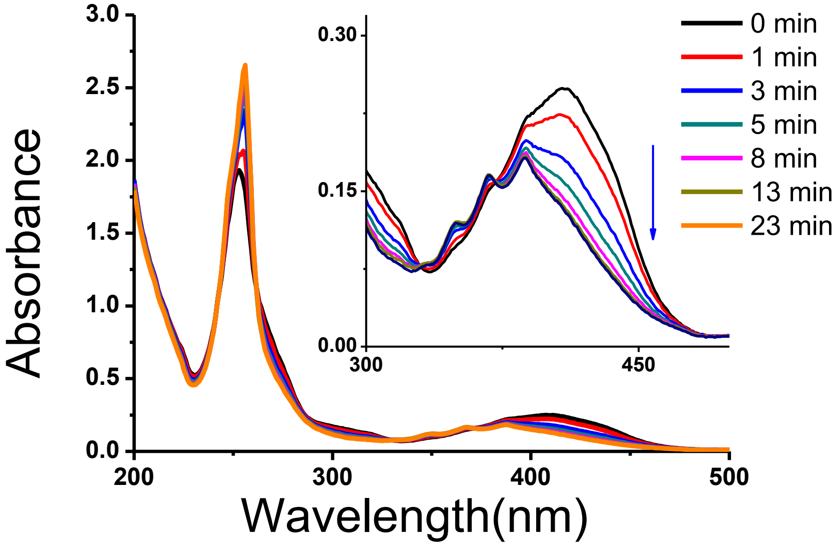

Figure 5.3 UV-Vis absorption spectra of (*E*)-DMAAM in liquid phase (cyclohexane as solvent, 2 × 10^{-5}M) illuminated by visible light (mixture wavelength, I_{average} = 20 mW/cm^2)

Both (E)- and (Z)-DMAAM crystalline nanowires can be prepared using solvent-annealed crystallization inside the channels of AAO templates, as reported in our previous papers.[29, 32] Here we focus on the (E)-DMAAM nanowire behavior. Previously, we performed our experiments in a 2 mM SDS/20% H_3PO_4 mixture. We confirmed that nanowires in this mixture could undergo photoinduced coiling. After careful experimentation with various surfactant/acid concentrations, we found that varying the pH did not affect the coiling, as long as it was kept at 7.0 or below. Basic pH solutions tend to hydrolyze the ester and dissolve the nanowires. Removal of the surfactant, however, could prevent the photoinduced coiling entirely. Changing the nature of the surfactant from anionic (SDS) to cationic (CTAB) did not affect the coiling behavior

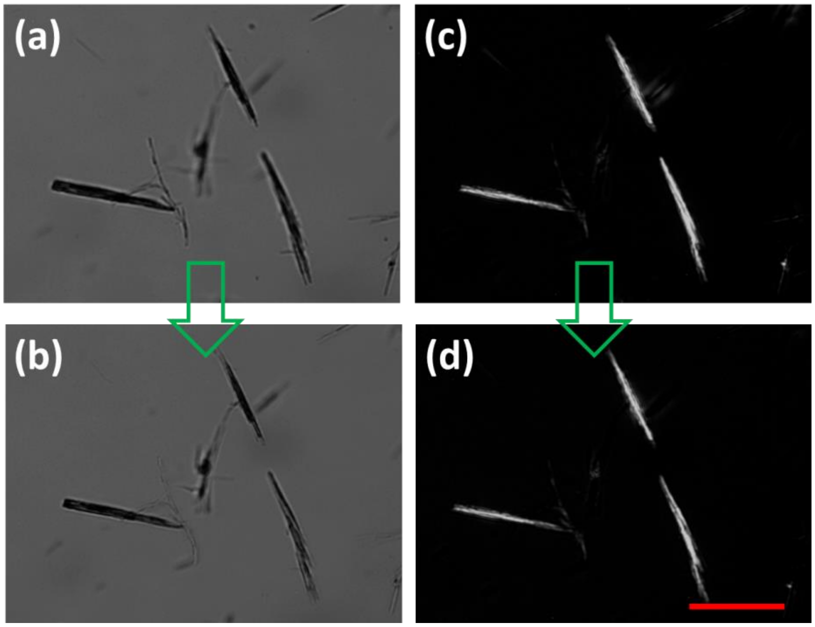

Figure 5.4 Optical microscopy images of (E)-DMAAM nanowires in pure water (a) before light exposure and (b) after 1 min light irradiation. Cross polarized optical microscope images of (E)-DMAAM nanowires (c) before light exposure and (d) after 1 min light irradiation. No significant changes are observed. Scale bar: 50 μm

The role of the surfactant is illustrated by imaging the dynamics of small bundles of nanowires using brightfield and polarized light microscopy. Nanowires in pure aqueous solution barely showed any photomechanical response under 450 nm light irradiation (Figure 5.4a and b). We occasionally observed some slight bending during a 1 min exposure that stopped even while the excitation light was still on. Nanowires in aqueous CTAB, on the other hand, showed a strong photomechanical response after only 5 s of light exposure (Figure 5.5a and b). This result is consistent with our previous observations and is also confirmed by SEM images of the nanowires before and after irradiation (Figure 5.6).

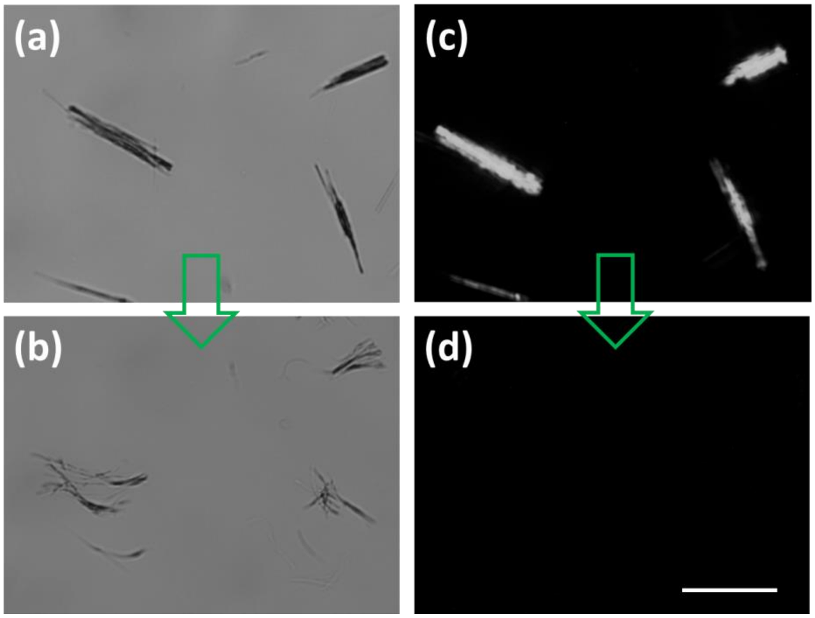

Figure 5.5 Optical microscopy images of (*E*)-DMAAM nanwires in 2 mM CTAB before (a) light exposure and (b) after 5s light irradiation. Cross polarized optical microscope images of (*E*)-DMAAM nanowires with CTAB before (c) light exposure and after (d) 5s light irradiation. Bending and loss of birefringence are observed. Scale bar: 50 µm

In a CTAB solution, nanowire motion continued even after the light was switched off. Interestingly, the duration of these post-irradiation motions depended on the CTAB concentration (Figure 5.7). Higher CTAB concentrations led to longer persistence of the motion, suggesting that slow structural changes were still occurring up to 1 minute after the photochemistry stopped. The motion of the nanowires could act to separate bundles or initiate drifting across the microscope slide. With prolonged light exposure (>5 min), the coiled nanowires gradually dissolved in the CTAB solution. None of these effects was observed in the absence of CTAB.

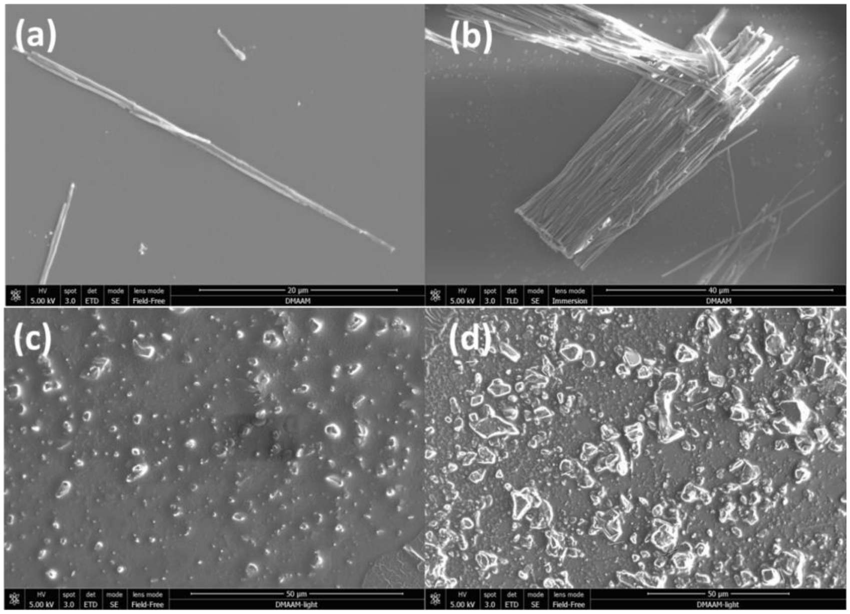

Figure 5.6 SEM images of (*E*)-DMAAM nanowires with CTAB ((a) and (b)) before irradiation and after irradiation ((c) and (d))

(*E*)-DMAAM nanowires in both solutions (with and without CTAB) are birefrigent and appear bright when imaged between crossed polarizers due to their crystalline nature (Figure 5.4c and 5.5c). The sample in pure water retained its crystallinity after even 1 min of light irradiation (Figure 5.4d). The nanowires suspended in CTAB solution started losing crystallinity as soon as the excitation light (450 nm) was turned on. All birefrigence was lost after 5 s of irradiation (Figure 5.5d). The sample without CTAB eventually lost crystallinity after a long (~ 5 min) period of irradiation, but this rate was at least 10 times slower than that in CTAB solution.

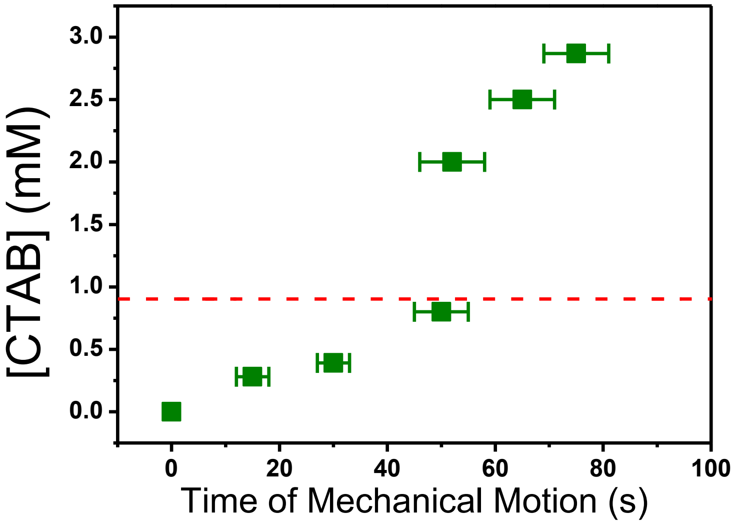

Figure 5.7 The CTAB concentration dependence of mechanical motion of (*E*)-DMAAM nanowires after light was switched off. The concentrations of CTAB are 0 mM, 0.3 mM, 0.4 mM, 0.8 mM, 2 mM, 2.5 mM, 2.9 mM, respectively. The red dashed line indicates the critical micelle concentration of CTAB in water (CMC = 0.92 mM)

We confirmed these results by using PXRD to track the intensity of the DMAAM diffraction peaks. Before irradiation, (*E*)-nanowires suspended in both pure water and CTAB solution showed crystal peaks (Figure 5.8b) that correspond well with those calculated from the single crystal structure (Figure 5.8a), with significant peaks at $2\theta = 13^{o}, 16^{o}, 22^{o}$ and 23^{o}. The peak intensities of the nanowires in pure water decreased but still retained recognizable crystal peaks even after 10 hours of irradiation (Figure 5.8c).

In contrast, the sample in the CTAB suspension lost all crystallinity after 2 hours of irradiation, with no distinct peaks observed (Figure 5.8d). Note that the irradiation times for this experiment were longer than for the microscopy experiments due to the larger sample and lower light intensity.

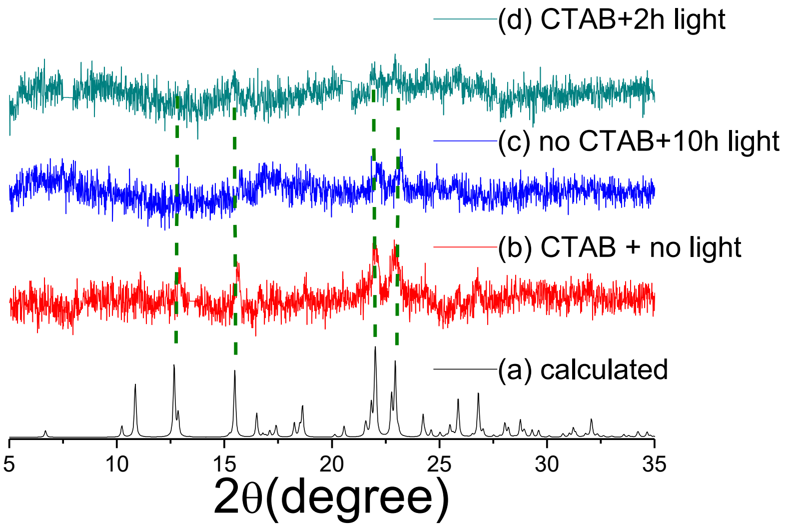

Figure 5.8 Powder x-ray diffraction patterns (a) calculated from the (*E*)-DMAAM crystal structure; (b) (*E*)-DMAAM nanowires from aqueous CTAB solution without light illumination; (c) E-DAAM nanowires in pure water after 10 h light irradiation (462 nm laser, 44 mW/cm^2); (d) (*E*)-DMAAM nanowires in aqueous CTAB solution after 2 h light irradiation, showing loss of diffraction intensity.

From the results described above, the presence of a surfactant is necessary to observe the rapid coiling and crystal-to-amorphous transition in the nanowires. One possible explanation is that the surfactant catalyzes the photochemical reaction, perhaps by facilitating structural rearrangements at the surface. To test this hypothesis, we followed the photochemical reaction kinetics using ^{1}HNMR measurements. A suspension of (*E*)-DMAAM nanowires was irradiated for various periods of time. The nanowires were later filtered over AAO template, washed with water, air dried and dissolved in $CDCl_3$. We tracked the feature peaks of methyl groups of the DMAAM molecule at 3.81 ppm and 3.89 ppm for (*E*)-isomer and 3.56 ppm and 3.95 ppm for (*Z*)-isomer (Figure 5.9). By integrating the *E* and *Z* peaks as I_E and I_Z respectively, we could calculate the fractional conversion to *Z* by taking the ratio $I_Z/ (I_E+I_Z)$. In the CTAB suspension, the (*Z*)-isomer peaks grew much faster than in the water suspension.

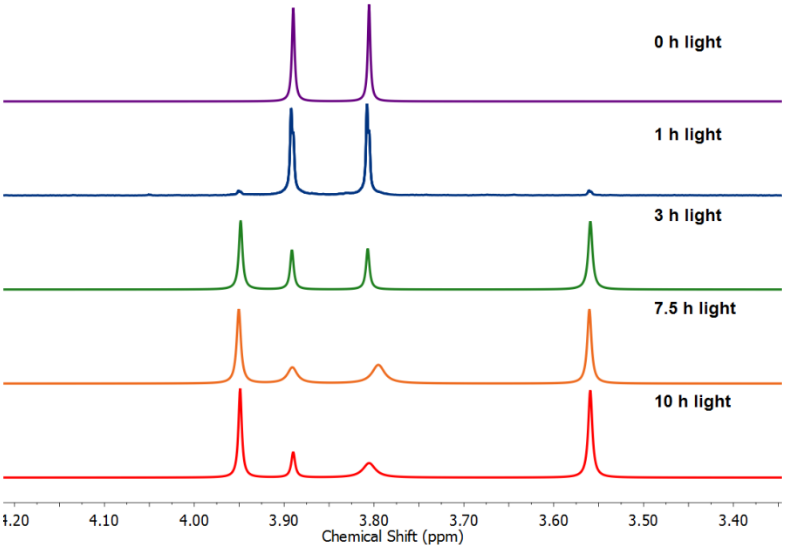

Figure 5.9 The ^{1}H NMR spectra of (*E*)-DMAAM nanowires in CTAB aqueous solution under light irradiation with various times. Purple: no light exposure, blue: 1 hour, green: 3 hours, orange: 7.5 hours, red: 10 h

Figure 5.10 shows the conversion fraction of Z-isomer formed in nanowires as a function of irradiation time. In the CTAB sample, one can covert more than 50 % of the (*E*)-nanowires into *cis*-isomers within 3 hours and more than 80 % after 7.5 hours of irradiation. On the other hand, in pure water less than 20% of the (*E*)-DMAAM was converted after more than 10 hours of irradiation. It should be noted that the irradiation wavelength of 462 nm cannot achieve 100 % conversion due to the overlapping absorption spectra of the *E* and *Z*-isomers that lead to a photostationary state.

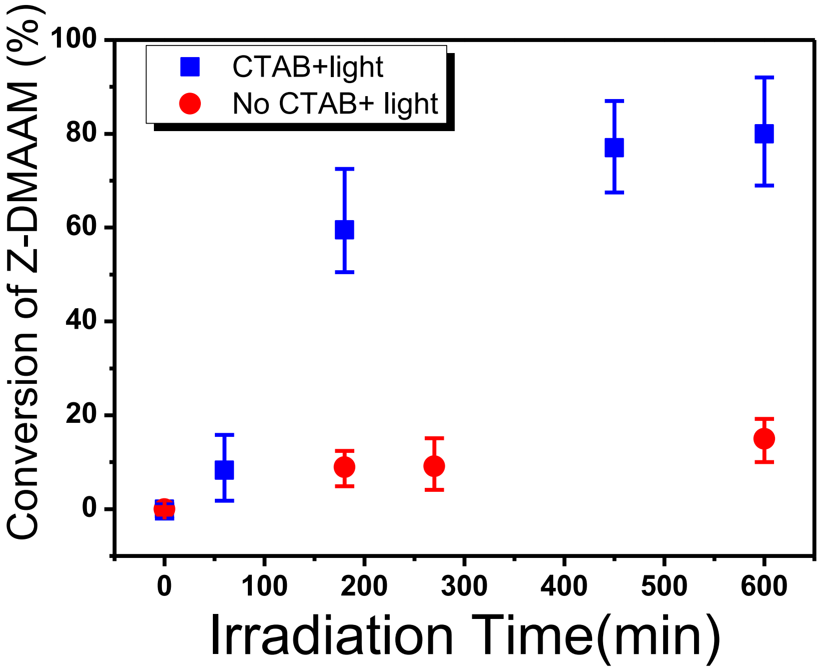

Figure 5.10 The formation of (*Z*)-DMAAM with [CTAB] = 2 mM (blue squares) and without CTAB (red circles) under illumination (462 nm light, 44 mW/cm^2). The error bars are due to baseline correction, phase correction, and peak integrations

Our original motivation to use surfactants was to make a stable suspension of nanowires in H_2O. On the timescale of days, the nanowires appear completely stable in 2 mM CTAB. However, we found that crystalline DMAAM nanowires could partially dissolve in 2 mM CTAB after 2 months (Figure 5.11). If the composition and crystallinity of the wires changed during irradiation, it is reasonable to expect that the dissolution rate could be affected as well. In order to study the dissolution of the DMAAM nanowires, we measured the UV-Vis absorption of the suspensions, operating under the assumption that the absorption signal is dominated by dissolved molecules. A stirred suspension of nanowires was irradiated for a fixed period of time. Then a 0.5 mL aliquot of the suspension was diluted with 2.5 mL Milli-Q purified water and transferred to a quartz cuvette for UV-Vis absorption measurements. Before irradiation, no visible absorbance could be observed in any of the samples, indicating negligible dissolution of DMAAM.

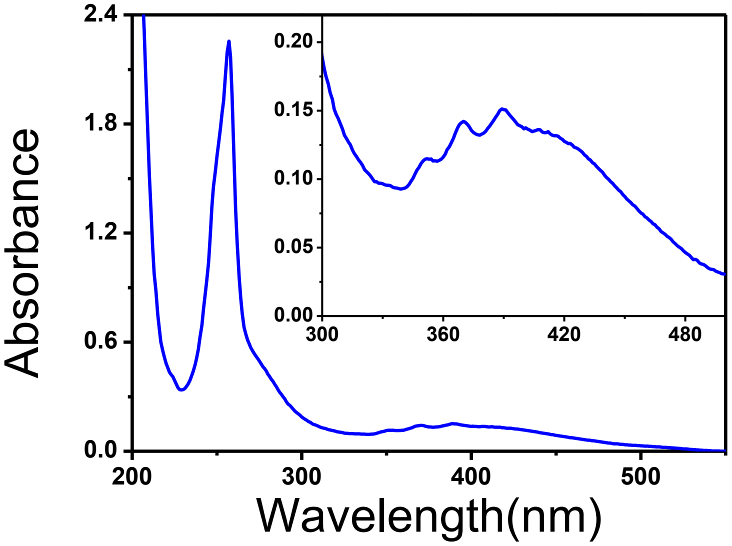

Figure 5.11 UV-Vis absorption spectrum of suspension of (*E*)-DMAAM nanowires suspended in a 2 mM CTAB solution at ambient environment without UV light exposure for 60 days.

In order to track the total DMAAM concentration, both *E* and *Z* forms, we measured the growth of the absorbance at 253 nm (Figure 5.12c). For both the *E* and *Z* nanowires, a peak at 253 nm started to appear after about 5 min of light irradiation (Figures 5.12a, c). The peak at 253 nm increased and the DMAAM absorption spectra also appeared in the visible region with increasing irradiation time (Figures 5.12b, d). For both the *E* and *Z* starting crystals, the solution absorption spectra are a mixture of isomers. This confirms that the photoisomerization is proceeding in parallel with the dissolution. Only small absorbance changes (<0.06) at 253 nm were observed in the pure water samples (Figure 5.13a) or in samples with surfactant but without light exposure (Figure 5.13b). Finally, we note that the nanowires do not completely dissolve during irradiation, but afterward they continue to slowly dissolve over the course of weeks, until the absorption at 253 nm reached a maximum of about 2.3 (Figure 5.11). The effect of the photoisomerization reaction on crystal dissolution is not simply the result of higher solubility of one isomer versus the other, since the effect is independent of the starting isomer.

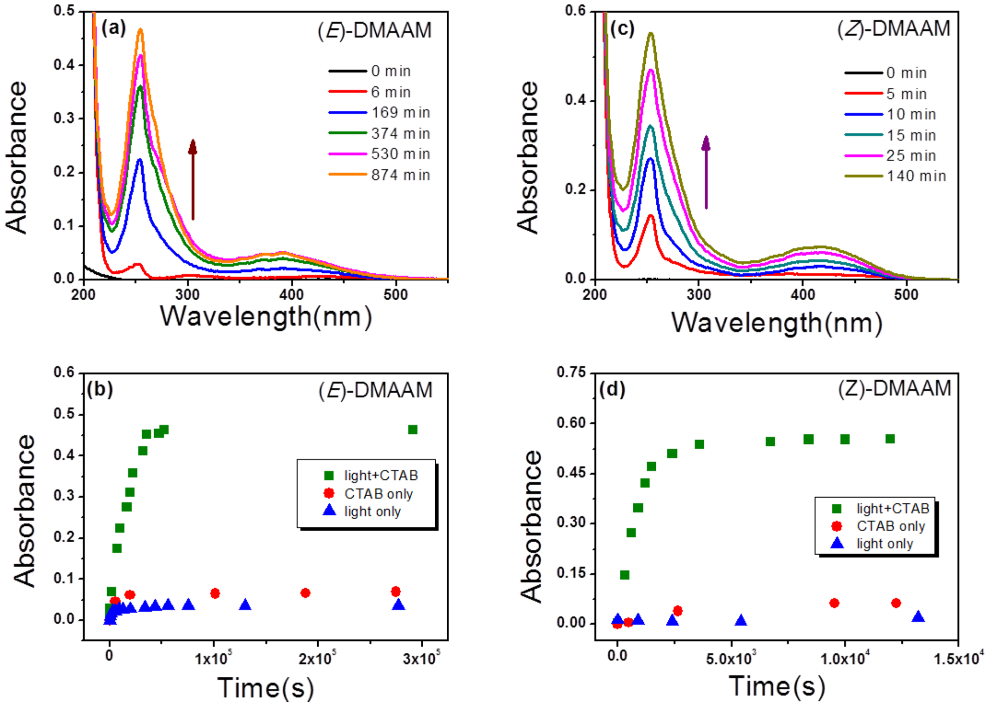

Figure 5.12 (a) Time-dependent evolution of solution absorption after (*E*)-DMAAM nanowires are irradiated at 462 nm in CTAB (1.3mM). (b) Absorbance increase at 253 nm: green squares = CTAB with light, red circles = CTAB without light, blue triangles = light without CTAB. (c) Time-dependent evolution of solution absorption after (*Z*)-DMAAM nanowires are irradiated at 365 nm in CTAB (1.3mM). (d) Absorbance increase at 253: green squares = CTAB with light, red circles = CTAB without light, blue triangles = light without CTAB.

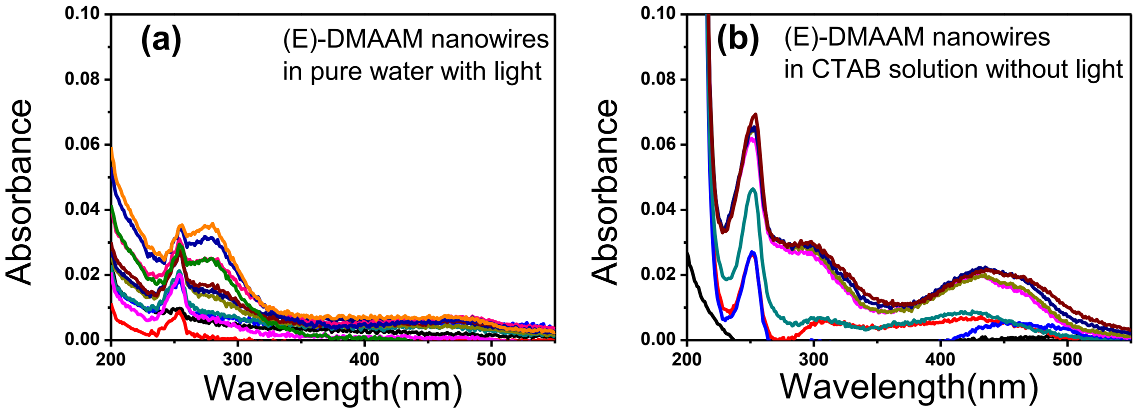

Figure 5.13 UV-Vis absorption spectra of suspension of (a) (*E*)-DMAAM nanowires in pure water with light exposure and (b) (*E*)-DMAAM nanowires in CTAB solution without light exposure.

The data in Figure 5.2-13 allow us to conclude that the surfactant gives rise to four interrelated effects: 1) accelerated E↔Z photoisomerization; 2) amorphization; 3) large deformations that continue even in the absence of light; and 4) accelerated dissolution. A possible mechanism that could give rise to these effects is outlined in Figure 5.14. Acting as a traditional surfactant, CTAB stabilizes the nanowire in solution by adsorbing to its exterior. But it also provides a surface environment that facilitates molecular motion on the surface, even if this motion does not immediately lead to molecules dissolving into the liquid. Because the light intensity is highest at the surface, and the surface molecules are presumably less constrained by crystal packing on all sides, it is expected that the photoisomerization will begin preferentially at the surface. In the case of nanowires with surfactant, the CTAB molecules can help rearrange the crystal packing structure and facilitate the mechanical motion as the steric barrier of *E*↔*Z* isomerization has been lowered. This process will also result in the initial formation of amorphous structure at the surface of the crystals.[33] Photochemical reactions can lead to packing rearrangements and disrupt the surface, exposing new regions to the surfactant molecules that further catalyze the photochemical reaction. In this way, the photons and the surfactant act synergistically to propagate the photoisomerization throughout the crystal, destroying its crystallinity. Note that the reaction does not have to proceed to completion: a conversion of 5-10% is sufficient to initiate these morphology changes.[29]

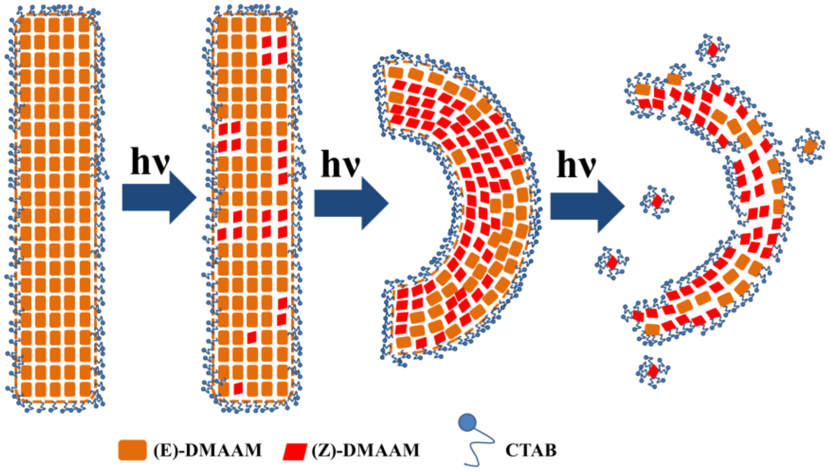

Figure 5.14 The proposed sequence of photoinduced isomerization, deformation, and dissolution for DMAAM nanowires in the presence of CTAB and light.

Once the nanowire has become amorphous due to the surfactant-enhanced photoisomerization, two effects are observed. The slower one, dissolution, is straightforward to understand. If the surface of a DMAAM nanowire is highly crystalline, dissolution of DMAAM molecules inside the CTAB micelle is an energy demanding process, since the surface molecules are leaving the low-energy state (crystalline) to go inside a high energy micelle. On the other hand, when the nanowire is irradiated with a suitable light source, a non-crystalline phase of mixed isomers is generated at the surface of the nanowire. When this non-crystalline surface is surrounded by micelle forming CTAB, it becomes less energy demanding to encapsulate the photoisomer in the CTAB micelle. The ability of disordered or amorphous solids to dissolve more rapidly is well-established, especially in the pharmaceutical community.[34-35]

What is more difficult to understand is why the nanowires undergo such drastic deformations before they dissolve. We do not think that the CTAB penetrates into the crystal to form a mixed phase at the molecular level. First, it is hard to see how such a process would not also lead directly to dissolution. Second, we could find no evidence for CTAB incorporated into the solid phase in our NMR measurements on the reacted nanowires. Instead, we think that the coiling is due to the relatively slow loss of crystallinity within the nanowire. This loss is caused initially by the creation of the photoisomer by light exposure. But it may be accelerated by the action of the surfactant as it solubilizes the DMAAM molecules. The process of dissolution can initiate dynamic changes in crystal structure even before the bulk of the molecules detach and migrate into the liquid. Crystal-to-amorphous transitions[36], polymorphic transitions[37], and even amorphous-to-crystal transitions[38] have been observed to occur during dissolution, as well as dislocation propagation within the crystal.[39] The structural rearrangements involved in this process may be relatively slow and can continue after the light is removed. Physical deformations like twisting have been observed for crystals being grown from solution and ascribed to spatial heterogeneity of impurities or defects during growth.[40] Similarly, in our nanowires the coiling results from heterogeneous concentrations of photoisomers and crystal packing, which also gives rise to internal strain. The ultimate limit of amorphization would be a solid→liquid melting transition, which would cause a mechanical transformation of the wire into a spherical droplet. We suspect that the coiling we observe is analogous to a melting type of phase transition, facilitated by the presence of surfactant.

5.4 Conclusion

We have demonstrated that both the photomechanical response and the photoisomerization rate of DMAAM nanowires can be accelerated by at least an order of magnitude by using ionic surfactants such as CTAB. We hypothesize that these changes are caused by surfactant molecules that adsorb at the surface of the nanowires, lowering the barrier to isomerization and facilitating the crystal-to-amorphous phase transition. Disruption of the highly packed crystal structure by photoisomerization in turn enhances both the mechanical deformation and the dissolution rate by more than one order of magnitude. The fact that these nanowires have a nominal diameter of 200 nm suggests that the presence of surface species, like CTAB, can influence the dynamics of much deeper layers in the crystal. We were not able to find a previous example in which the transition from crystalline to amorphous solid can be significantly accelerated by the presence of a surface species. The results in this work suggest that a better understanding of the interplay between surface chemistry and solid-state photochemistry may be helpful for understanding the photomechanical motions of crystalline nanostructures in solution.

5.5 Reference

(1) White, T. J., *Photomechanical Materials, Composites, and Systems*. 1 ed.; Wiley: Hoboken, New Jersey, 2017.

(2) Yamada, M.; Kondo, M.; Mamiya, J.; Yu, Y.; Kinoshita, M.; Barrett, C. J.; Ikeda, T., Photomobile polymer materials: towards light-driven plastic motors. *Angew. Chem. Int. Ed.* **2008,** *47*, 4986-4988.

(3) Ionov, L., Polymeric Actuators. *Langmuir* **2015,** *31*, 5015-5024.

(4) Kim, T.; Zhu, L.; Al-Kaysi, R. O.; Bardeen, C. J., Organic photomechanical materials. *ChemPhysChem* **2014,** *15*, 400-414.

(5) Garcia-Garibay, M. A., Molecular crystals on the move: From single-crystal-to-single-crystal photoreactions to molecular machinery. *Angew. Chem. Int. Ed.* **2007,** *46*, 2-5.

(6) Irie, M.; Yokoyama, Y.; Seki, T., *New Frontiers in Photochromism*. Springer: Japan, 2013.

(7) Naumov, P.; Chizhik, S.; Panda, M. K.; Nath, N. K.; Boldyreva, E., Mechanically Responsive Molecular Crystals. *Chem. Rev.* **2015,** *115*, 12440-12490.

(8) Sato, O., Dynamic Molecular Crystals with Switchable Physical Properties. *Nat. Chem.* **2016,** *8*, 644–656.

(9) Al-Kaysi, R. O.; Bardeen, C. J., Reversible photoinduced shape changes of crystalline organic nanorods. *Adv. Mater.* **2007,** *19*, 1276-1280.

(10) Kim, T.; Zhu, L.; Mueller, L. J.; Bardeen, C. J., Mechanism of photo-induced bending and twisting in crystalline microneedles and microribbons composed of 9-methylanthracene. *J. Am. Chem. Soc.* **2014,** *136*, 6617-6625.

(11) Kobatake, S.; Takami, S.; Muto, H.; Ishikawa, T.; Irie, M., Rapid and reversible shape changes of molecular crystals on photoirradiation. *Nature* **2007,** *446*, 778-781.

(12) Morimoto, M.; Irie, M., A diarylethene cocrystal that converts light into mechanical work. *J. Am. Chem. Soc.* **2010,** *132*, 14172-14178.

(13) Kobatake, S.; Hasegawa, H.; Miyamura, K., High-Convertible Photochromism of a Diarylethene Single Crystal Accompanying the Crystal Shape Deformation. *Cryst. Growth Des.* **2011,** *11*, 1223-1229.

(14) Naumov, P.; Kowalik, J.; Solntsev, K. M.; Baldridge, A.; Moon, J.-S.; Kranz, C.; Tolbert, L. M., Topochemistry and photomechanical effects in crystals of green fluorescent protein-like chromophores: effects of hydrogen bonding and crystal packing. *J. Am. Chem. Soc.* **2010,** *132*, 5845-5857.

(15) Nath, N. K.; Pejov, L.; Nichols, S. M.; Hu, C.; Saleh, N.; Kahr, B.; Naumov, P., Model for photoinduced bending of slender molecular crystals. *J. Am. Chem. Soc.* **2014,** *136*, 2757-2766.

(16) Bushuyev, O. S.; Singleton, T. A.; Barrett, C. J., Reversible, and General Photomechanical Motion in Single Crystals of Various Azo Compounds Using Visible Light. *Adv. Mater.* **2013,** *25*, 1796-1800.

(17) Bushuyev, O. S.; Tomberg, A.; Friscic, T.; Barrett, C. J., Shaping Cyrstals with Light: Crystal-to-Crystal Isomerization and Photomechanical Effect in Fluorinated Azobenzenes. *J. Am. Chem. Soc.* **2013,** *135*, 12556-12559.

(18) Koshima, H.; Ojima, N.; Uchimoto, H., Mechanical motion of azobenzene crystals upon photoirradiation. *J. Am. Chem. Soc.* **2009,** *131*, 6890-6891.
(19) Koshima, H.; Takechi, K.; Uchimoto, H.; Shiro, M.; Hashizume, D., Photmechanical bending of salicylideneaniline crystals. *Chem. Commun.* **2011,** *47*, 11423-11425.
(20) Zhu, L.; Al-Kaysi, R. O.; Bardeen, C. J., Reversible photoinduced twisting of molecular crystal microribbons. *J. Am. Chem. Soc.* **2011,** *133*, 12569-12575.
(21) Kitagawa, D.; Nishi, H.; Kobatake, S., Photoinduced twisting of a photochromic diarylethene crystal. *Angew. Chem. Int. Ed.* **2013,** *52*, 9320-9322.
(22) Al-Kaysi, R. O.; Muller, A. M.; Bardeen, C. J., Photochemically driven shape changes of crystalline organic nanorods. *J. Am. Chem. Soc.* **2006,** *128*, 15938-15939.
(23) Zhu, L.; Al-Kaysi, R. O.; Bardeen, C. J., Photoinduced Ratchet-Like Rotational Motion of Branched Molecular Crystals. *Angew. Chem. Int. Ed.* **2016,** *55*, 7073-7076.
(24) Medishetty, R.; Husain, A.; Bai, Z.; Runceviski, T.; Dinnebier, R. E.; Naumov, P.; Vittal, J. J., Single crystals popping under UV light: a photosalient effect triggered by a [2+2] cycloaddition reaction. *Angew. Chem. Int. Ed.* **2014,** *53*, 5907-5911.
(25) Naumov, P.; Sahoo, S. C.; Zakharov, B. Z.; Boldyreva, E. V., Dynamic single crystals: kinematic analysis of photoinduced crystal jumping (the photosalient effect). *Angew. Chem. Int. Ed.* **2013,** *52*, 9990-9995.
(26) Uchida, K.; Izumi, N.; Sukata, S.; Kojima, Y.; Nakamura, S.; Irie, M., Photoinduced reversible formation of microfibrils on a photochromic diarylethene microcrystalline surface. *Angew. Chem. Int. Ed.* **2006,** *45*, 6470-6473.
(27) Oropesa-Nunez, R.; Fragouli, D.; Pignatelli, F.; Scarpellini, A.; Gigliotti, E.; Samoylova, E.; Athanassiou, A., Spontaneous Formation of Photochromic Coatings Made of Reversible Microfibrils and Nanofibrils on an Elastomer Substrate. *Langmuir* **2014,** *30*, 13058-13064.
(28) Kitagawa, D.; Kobatake, S., Crystal Thickness Dependence of Photoinduced Crystal Bending of 1,2-Bis(2-methyl-5-(4-(1-naphthoyloxymethyl)phenyl)-3-thienyl)perfluorocyclopentene. *J. Phys. Chem. C* **2013,** *117*, 20887–20892.
(29) Kim, T.; Al-Muhanna, M. K.; Al-Suwaidan, S. D.; Al-Kaysi, R. O.; Bardeen, C. J., Photo-induced Curling of Organic Molecular Crystal Nanowires. *Angew. Chem. Int. Ed.* **2013,** *52*, 6889-6893.
(30) Li, N.; Liu, S.; Luo, H., A New Method for the Determination of the First and Second CMC in CTAB Solution by Resonance Rayleigh Scattering Technology. *Analyt. Lett.* **2002,** *35*, 1229-1238.
(31) Modaressi, A.; Sifaoui, H.; Grzesiak, B.; Solimando, R.; Domanska, U.; Rogalski, M., CTAB Aggregation in Aqueous Solutions of Ammonium Based Ionic Liquids; Conductimetric Studies. *Coll. Surf. A* **2007,** *296*, 104-108.
(32) Al-Kaysi, R. O.; Bardeen, C. J., General method for the synthesis of crystalline organic nanorods using porous alumina templates. *Chem. Comm.* **2006**, 1224-1226.
(33) Paik, M. Y.; Krishnan, S.; You, F.; Li, X.; Hexemer, A.; Ando, Y.; Kang, S. H.; Fischer, D. A.; Kramer, E. J.; Ober, C. K., Surface Organization, Light-Driven Surface Changes, and Stability of Semifluorinated Azobenzene Polymers. *Langmuir* **2007,** *23*, 5110-5119.

(34) Hancock, B. C.; Parks, M., What is the True Solubility Advantage for Amorphous Pharmaceuticals. *Pharmaceut. Res.* **2000,** *17*, 397-404.
(35) Murdande, S. B.; Pikal, M. J.; Shanker, R. M.; Bogner, R. H., Solubility Advantage of Amorphous Pharmaceuticals: I. A Thermodynamic Analysis. *J. Pharm. Sci.* **2010,** *99*, 1254-1265.
(36) Jiang, G.; Huang, W.; Wang, B.; Zhang, Y.; Wang, H., The Changes of Crystalline Structure of Cellulose During Dissolution in 1-Butyl-3-methylimidazolium Chloride. *Cellulose* **2012,** *19*, 679-685.
(37) Panchagnula, R.; Bedi, S.; Yasvanth, A., Rifampicin Dissolution: Polymorphism or Crystal Defects. *Clin. Res. Reg. Affairs* **2006,** *23*, 71-83.
(38) Tres, F.; Patient, J. D.; Williams, P. M.; Treacher, K.; Booth, J.; Hughes, L. P.; Wren, S. A. C.; Aylott, J. W.; Burley, J. C., Monitoring the Dissolution Mechanisms of Amorphous Bicalutamide Solid Dispersions via Reat-Time Raman Mapping. *Molec. Pharm.* **2015,** *12*, 1512-1522.
(39) Clark, J. N.; Ihli, J.; Schenk, A. S.; Kim, Y.-Y.; Kulak, A. N.; Campbell, J. M.; Nisbet, G.; Meldrum, F. C.; Robinson, I. K., Three-Dimensional Imaging of Dislocation Propagation During Crystal Growth and Dissolution. *Nat. Mater.* **2015,** *14*, 780-784.
(40) Shtukenberg, A. G.; Freudenthal, J.; Kahr, B., Reversible Twisting during Helical Hippuric Acid Crystal Growth. *J. Am. Chem. Soc.* **2010,** *132*, 9341-9349.

Chapter 6 Summary and outlook

6.1 Summary of my research work

This PhD thesis focused on solid-state photomechanical molecular crystals based on anthracene derivatives. The ultimate goal is to make novel photomechanical materials that can show more interesting motions. The research can basically be divided into three parts which have been discussed in previous chapters in this thesis. The project of 9TBA was initially started with the aim of making photoresponsive 9TBA crystals through a large molecular structure change leading to a large change of crystal packing and eventually cause shape and morphology changes. However, none of these results were observed as the 9TBA crystal itself cannot exhibit any photomechanical response under light irradiation. Instead, the reverse reaction of D-9TBA to 9TBA showed significant pressure dependence when 9TBA molecules were put into a polymer film. These results proved that the photochemical reaction of molecular crystals might not lead to photomechanical behaviors. Also, although the pressure sensitivity was not as high as in bis-anthracene (BA) and its photo-isomer (PI) [1], our results showed it is possible to engineer molecular structures to be pressure sensitive.

The investigation of photochemical process in solid-state of 9MA crystal system can give some idea of how to study the kinetics in molecular crystal systems and predict photoluminescence changes. The rigorous equations we have derived and the model we obtained from computational work can fit our experimental results to some degree. However, since they did not fully match with each other, we cannot claim that our extended Finke – Watzky (F–W) model is the perfect model to describe the photochemical process of molecular crystal. One reason, we may have not considered is the polycrystalline film of 9MA itself has different crystal faces or packing structures. These various crystal faces may undergo different photochemical process which can lead to a premature increase of fluorescence decay rates, such as k_2 in our case. Therefore, more experimental and theoretical work needed to be done in the future.

The 9MA experiments showed that the existence of photoproducts can contribute to speed up both the photochemical reaction rates and fluorescence decay rates, as leading to an autocatalytic process. In addition to this intrinsic mechanism, we are also quite interested in extrinsic effects on the molecular crystal reactions. The observation of DMAAM crystals that only showed big photomechanical motions like curling and coiling with the existence of ionic surfactants under light irradiation motivated us to study external environmental effects upon molecular crystal. Even though our previous research provided some hints, this was the first time we studied systematically. We found 10 fold increase in photochemical reaction rates and 30 fold increase in crystal dissolution rates. Our results suggest that a better understanding of the interplay between surface chemistry and solid-state photochemistry may be helpful for understanding the photomechanical motions of crystalline nanostructures in solution.

6.2 Current and future research work

6.2.1 Novel photomechanical behavior of 9MA hexagon microplates

My current work is to making various shapes of molecular crystals in order to obtain more interesting photomechanical motions. One way we can do is to find new methods to prepare new shapes of materials based on old compounds. Recently, we have successfully prepared 9MA microplates with hexagonal shapes. These 9MA microplates can show rolling and unrolling motions under UV light irradiation. Such motion is different from what we have observed in 9MA crystals with other shapes such as microneedles and microribbons. However, the molecular orientation inside these microplates was found to be similar with the rod-like crystals (Figure 6.1).

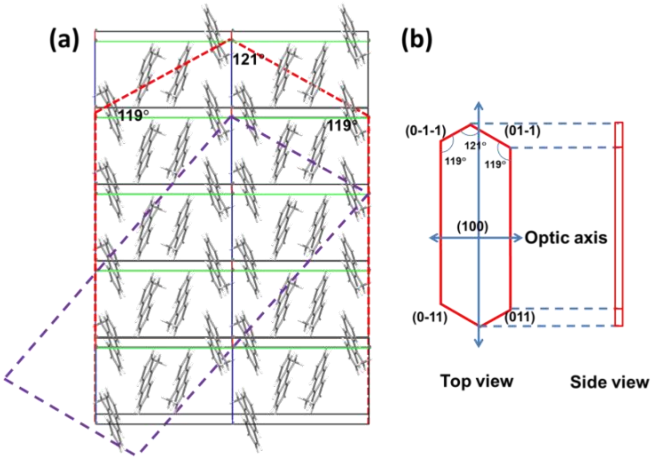

Figure 6.1. (a) Orientation of 9MA molecules in two different types of crystals. Red dash line: hexagon microplate, and purple dash line: rectangle microribbon. (b) Scheme of 9MA hexagon microplate with proposed crystal indices and optic axis, left: top view and side view.

The red dashed line in Figure 6.1a illustrates the general outline and shape of 9MA microplates with measured angles at the corner. The purple dashed line depicts the outline of 9MA rectangular ribbons. Their photomechanical behaviors are quite different. As we already know, 9MA rectangular microplates exhibit twisting and untwisting motions under light irradiation (Figure 6.2 a ~ c). On the other hand, the rolling and unrolling of 9MA hexagonal microplates demonstrated that it is possible to prepare crystals with a different function even with the same molecule and crystal packing.

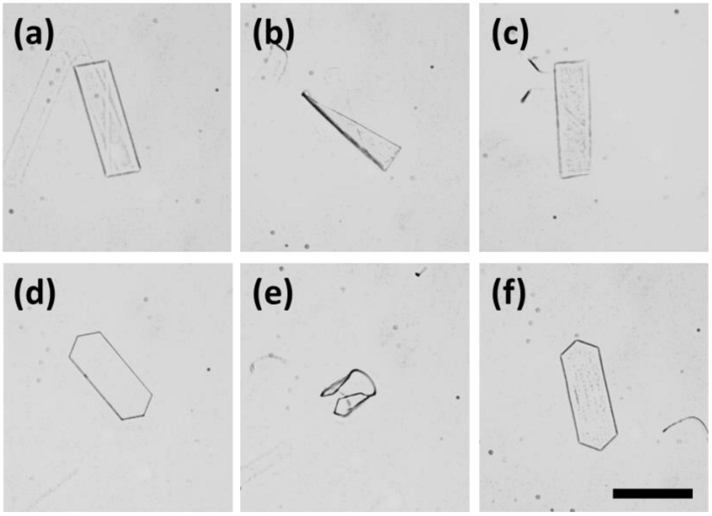

Figure 6.2 (a) 9MA rectangle microribbon before UV illumination (405 nm light, I = 29.4mW/cm^2). (b) 9MA microribbon twists during UV illumination. (c) 9MA microribbon untwists after UV illumination. (d) 9MA hexagonal microplate before UV illumination. (e) 9MA microplate rolls up during UV illumination. (f) 9MA microplate unrolls after UV illumination. Scale bar: 50 μm.

As shown in Figure 6.2 d ~ f, the rolling motion will lead to a full circle during the light irradiation period. This full circle can retain its shape for more than 10 min without external perturbation. The circle will eventually unroll back to a flat plate if the excitation light kept on. The whole process of rolling and unrolling usually takes no more than 1 s, and the rate depends on the intensity of light.

Such circle or ring formation by photomechanical rolling of 9MA microplates has guided us to think about potential applications in drug delivery, in which we may be able to utilize this structure to hold small particles inside and transport them with external forces.

As a proof of principle, we added superparamagnetic nanoparticles, and showed that a 9MA microplate can wrap them up under light irradiation. Afterwards, an external magnetic field was introduced to drive the loaded crystals in a desired direction (Figure 6.3).

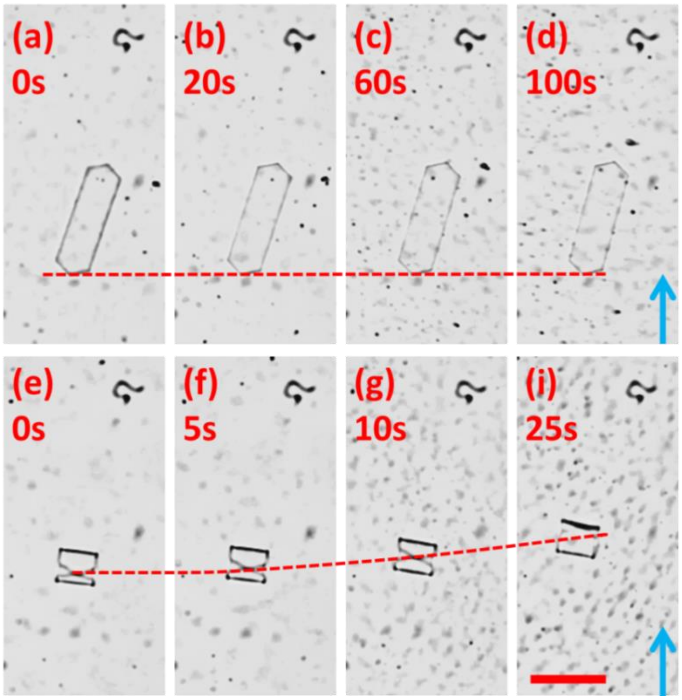

Figure 6.3. (a) ~ (d) 9MA hexagon microplate before UV light irradiation, the dark dots in the images are corresponding to superparamagnetic nanoparticles alignment due to applied external magnetic field. The intensive degree of these dots related to gradually increase of magnetic field. The strength of external magnetic is around 15~20 Gs. The cyan arrow shows the direction of magnetic field. Scale bar: 50 µm

One should notice that the microplate was not able to move by itself before light exposure, even with nanoparticle on its surface and external magnetic field applied for almost for 2 min (Figure 6.3 a ~ d). This is because when the microplate is flat, the nanoparticles on its surface do not interact strongly with the microplate. However, when the microplate rolls up, the nanoparticles are trapped and can push or drag the circle (Figure 6.4).

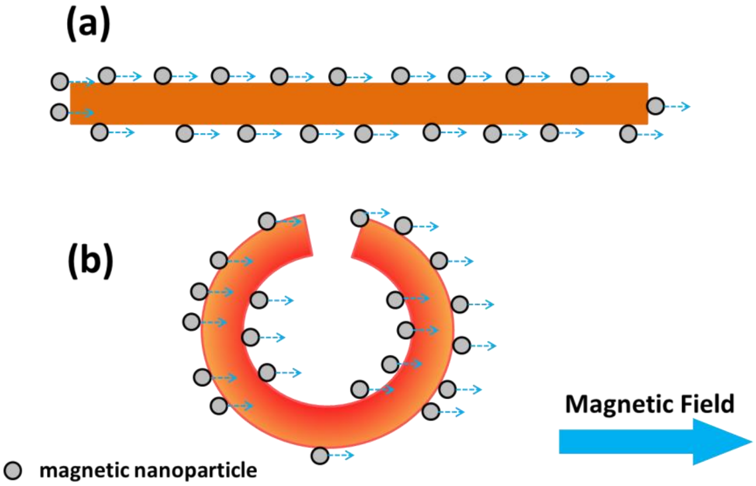

Figure 6.4 (a) Side view of 9MA microplate when it is flat before light irradiation. The transportation of superparamagnetic nanoparticles is parallel with the long axis. (b) Side view of 9MA microplate when it is wrapped up after light irradiation. Nanoparticles can push or drag microplate to move under magnetic field. The blue arrows indict the direction of magnetic field.

6.2.2 Preparing diarylethene nanowires

Diarylethene crystals can show varieties of photomechanical behaviors which involve bending[2-5], twisting[6], expansion[7], and fragmentation[8]. Moreover, the good thermal stability and excellent reversibility in photochromic reactions make diarylethene crystals promising candidates for photo-actuators in the future. However, these mechanical motions are usually shown in bulk crystals or micro-sized crystals, limiting further applications. Such large crystals are fragile and sometimes tend to disintegrate even with small deformations. One way to circumvent this issue, as we mentioned in Chapter 2, is to shrink the dimension of materials, such as by making nanocrystals. We are currently trying to use AAO templates to grow diarylethene nanowires that show photomechanical motions.

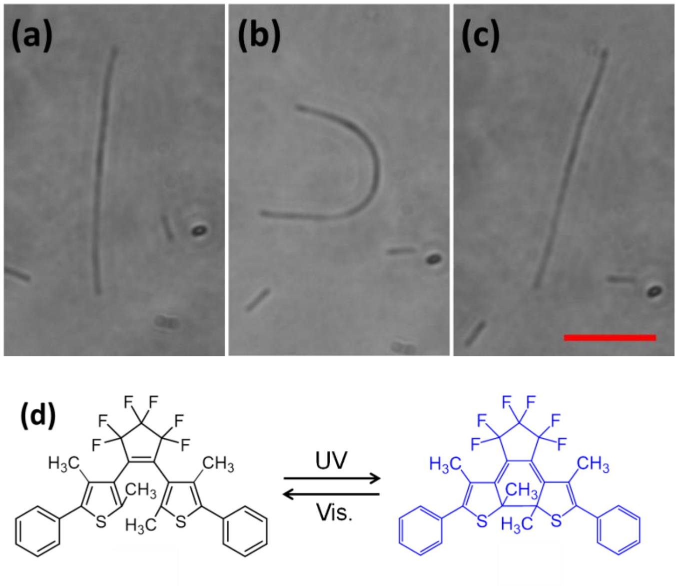

Figure 6.5 (a) diarylethene nanowire before UV light irradiation (b) diarylethene nanowire shows bending motion after UV light irradiation (365 nm, I=10mW/cm^2). (c) Diarylethene nanowire reverts to straight shape after visible light irradiation (462 nm, I=44 mW/cm^2). (d) The molecular structure of diarylethene we used in our work. Scale bar: 20 μm

We have recently successfully made nanowires of 1,2-bis(2,4-dimethyl-5-phenyl-3-thienyl)perfluorocyclopentene. These nanowires can show reversible bending with a large curvature (κ =100mm^{-1}) under 365 nm light irradiation (Figure 6.5). The whole process of bending is very rapid, occurring in less than 1s. We have checked that the nanowires can show at least 10 cycles of such reversible bending motion by alternating UV and visible light exposure. In 2001, Irie at el firstly reported that the fast reversible photochromic reaction of this compound could lead to morphology changes on the surface of bulk crystals (Figure 6.6), but no other photomechanical behaviors were reported after then[9]. One reason may be due to the difficulty for people in fabricating rod-like or needle shaped crystals of this compound using normal solvent annealing or sublimation growth methods.

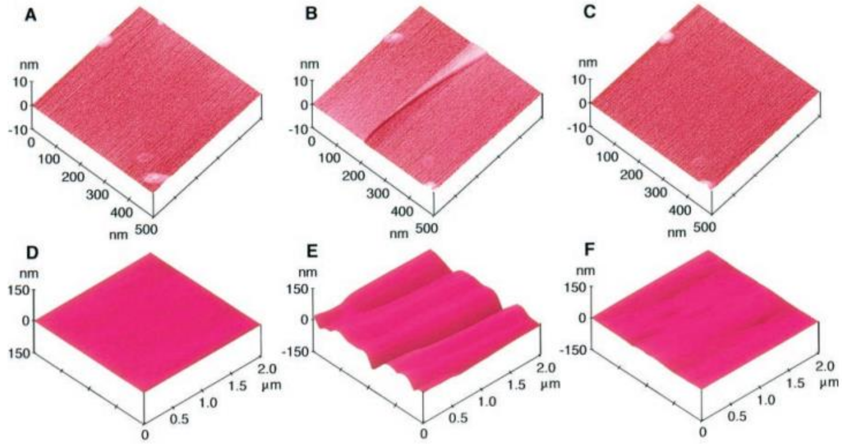

Figure 6.6 Atomic Force Microscope (AFM) images of (A to C) the (100) crystal surface and (D to F) the (010) surface: before photoirradiation, (A) and (D); after irradiation with 366 nm light for (B) 10s and (E) 15 s; and after irradiation with visible light (λ > 500 nm), (C) and (F). (Reproduced with the permission of Science.)

In order to investigate the crystal packing inside the nanowires, we measured the powder x-ray diffraction of these nanowires (Figure 6.7). Before dissolving the template with acid, the nanowires inside the channels are perpendicular to the AAO surface polishing. After dissolving the template, we filtered out nanowires onto a blank AAO template to get x-ray diffraction information of horizontal nanowires. Our results showed that diarylethene nanowires grow along b-axis inside the AAO template, which is consistent with what we have expected.

Our work in diarylethene nanowires demonstrated that the photomechanical behavior is more pronounced for small-scale materials, and that the AAO template method is a general method to produce nanosized organic crystal with well-defined sizes and shape. We hope our work can make some contributions in new materials fabrication.

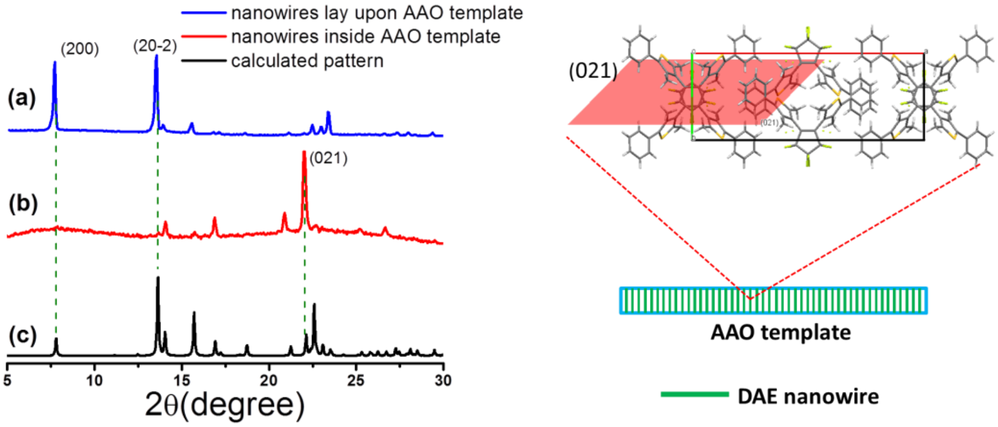

Figure 6.7 Powder x-ray diffraction data of diarylethene nanowires. (a) Nanowires lay upon AAO template. (b) Nanowires inside in AAO template. (c) Calculated pattern. The right image showed the crystal packing structure before dissolving template.

6.3 Outlook for photomechanical molecular crystals

6.3.1 New materials with new structures and shapes

The field of photomechanical molecular crystals can exploit a variety of photochemical reactions to drive mechanical motions in the solid state. Nevertheless, there is still room for people to improve both photomechanical and photochemical properties. One way is to find chemical reactions with high reaction rates and high quantum yields which translate photon energy into mechanical energy with higher efficiency.

A second strategy is to make composite materials that can generate significant force. People can take advantages of hybrid materials, such as combing metallic materials with molecular crystals. Tsujioka et al. coated diarylethene crystals with various metals and demonstrated that they could still retain their photochromism.[10] Also people can think of embedding molecular crystals into polymer matrix to get crystal-polymer composites. Koshima et al used a magnetic field to align plate-like salicylidene crystals in a silicone polymer.[11]This composite showed slight reversible bending under alternating UV and visible light irradiation. Sahoo et al. prepared a photoactive composite by putting the azobenzene adduct phenylazophenylpalladium hexafluoroacetylacetonate into a protein polymer and showed photosalient behavior.[12] Therefore; people may incorporate molecular crystals with different materials to make such composites in order to improve properties.

The third way is to find or make materials that exhibit self-propagating chemical reactions. An example of such a reaction in the solid state is the molecular decomposition of diphenyl-cyclopropane derivatives to yield CO and diphenyl-acetylene, which was found to have a photochemical quantum yield of decomposition >4.[13] In this case, the photochemical reaction releases gas, which leads to total collapse of the crystal structure, but this idea may be also generalizable to other reactions and materials.

Besides the three aspects we mentioned above, people also need to consider the stability of solid-state molecular crystals as most crystals are fragile and easy to damage. One way is to design molecules that can exhibit large shape or geometry changes upon photoexcitation but are robust enough to survive after many cycles such as diarylethene[14] and fulgides[15].

Last but not the least, we also need to think about going beyond the molecular level since the ultimate goal is make photomechanical materials functions as photoactuators. As we know, the overall photomechanical responses are usually decided by different crystals shapes. I have been focusing on making nano-/micro-sized crystals for a few of years. One reason of doing this is that we are trying to avoid the disintegration that often happens in bulk crystals. The other reason is that we believed that the advantages of photomechanical molecular crystals can be more pronounced for small-scale materials. The key is how we can approach to these small-scale materials with well-defined sizes and shapes by using different crystal growth methods. As we discussed above, we have used solvent annealing method in AAO templates[16] to obtain molecular crystal nanorods and nanowires and controlled growth on flat substrates to prepare microneedles and microribbons[17]. However, the latter method will also result in wide size distributions. We have also developed pH driven reprecipitation method to make branched structure crystals[18, 19] and used surfactants such as SDS and CTAB to generate uniform crystals of photoactive molecules that could undergo photoinduced rolling, coiling and bending.[20,21] Another strategy is to develop other methods to control the crystal sizes and shapes such as micro-printing method using soft templates like Polydimethylsiloxane (PDMS).[22]

6.4 Possible potential applications in the future

It is too early to envision solid-state photomechanical molecular crystals in practical applications, as most of the research in this field currently take place in scientific laboratories. One should still have some confidence in this field as the excellent properties of photomechanical molecular crystals have already resulted in some laboratory demonstrations that provide direction for potential applications.

6.4.1 Wireless photoswitch

One possible application of photomechanical molecular crystals is the wireless photoswitch. As a proof of principle, Kitagawa et al. demonstrated a smart photoswitch of composed a diarylethene crystal (Figure 6.8).[23]A long and rod-like photoresponsive diarylethene crystal was deposited by a gold thin film via vapor disposition. The diarylethene can bend toward to UV light irradiation, leading the switch to be off, and the crystal can turn the current on via straightening under visible light illumination. The smart photo-switch could perform at least 10 cycles with alternating light illumination.

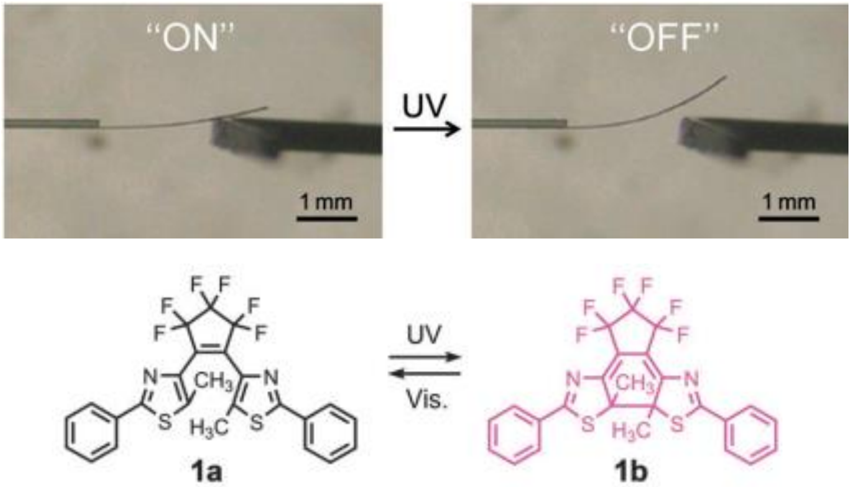

Figure 6.8 Photoreversible current switching upon alternating irradiation with UV and visible light and the molecular structure used in this work. The crystal thickness is 6.2 mm. The gold thickness is 21 nm. (Reproduced with the permission of Royal Society of Chemistry.)

One advantage of the device is that it does not need hard wires to control the switch. The thin gold film coated onto the crystal surface has increased electric conductivity and also prevented the crystal from breaking during the deformation due to the excellent metallic ductility. Moreover, the gold film is thin enough (< 30 nm) to retain light transparency, allowing enough photons to be absorbed by crystal and generate photomechanical deformation. Their work brought about not only a new strategy to design photomechanical actuators but also illustrated that the ability to combine photomechanical deformation with metallic conductivity can lead to novel functionalities.

6.4.2 Microtweezer

Another interesting application of photomechanical molecular crystals was demonstrated by Lee et al., who fabricated nanowires made from an azobenzene-containing 1,3,5-

tricarboxamide derivate using the meniscus-guided solidification method.[24] These azobenzene nanowires were observed to exhibit reversible bending and unbending with large actuating displacements (≤1.7μm) when they are alternately irradiated with UV and visible light. In addition, the bending of the photomechanical nanowires displayed high thermal stability.

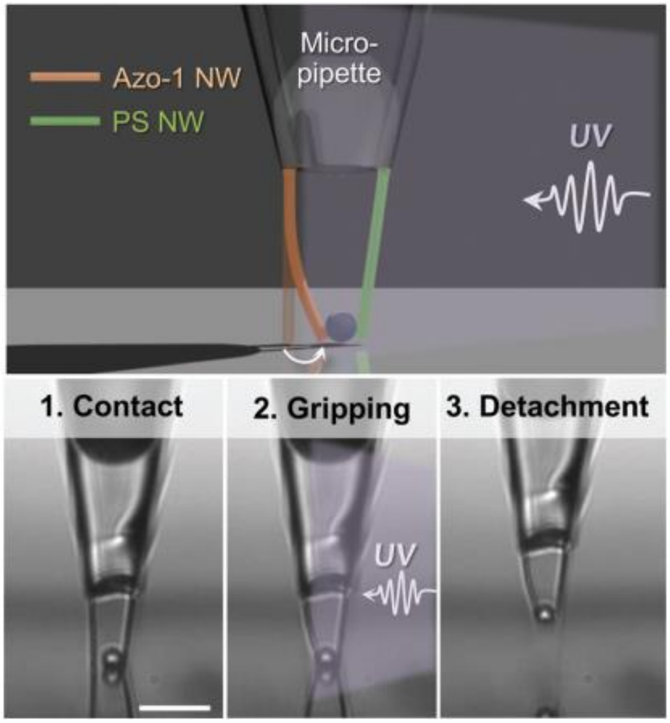

Figure 6.9 A nanowire composed of an azobenzene derivative (left side) and a polystyrene nanowire (right side) are both attached to the tip of a glass microcapillary tube. UV irradiation of the azobenzene nanowire causes it to bend toward the polystyrene nanowire, clamping a microsphere between them. Scale bar, 20μm. (Reproduced with the permission of Royal Society of Chemistry)

These nanowires were anchored vertically on a surface of a glass microcapillary tube to function as a tweezer. A polystyrene strip was attached to the same microcapillary tip, providing a hard surface which the photomechanical nanowire could press against. By irradiating the nanowire from one side, it could bend toward the polystyrene strip and grip the polymer microspheres (Figure 6.9). These photoresponsive micro-tweezers could be opened and closed by sequential UV and visible light irradiation. They might serve as nanorobotic devices for manipulation of nano/micro-objects that have general utility in engineering and nanotechnology.

6.4.3 Micro/nano wheel gear

Another proposed application of photomechanical molecular crystals is to drive wheel gears or ratchets which usually need unidirectional rotation. One issue people may confront is how to improve fatigue resistance as crystal actuators must have enough durability and substantial mechanical properties for such practical applications. Irie et al., used a platelike two-component photomechanical cocrystal composed of 1,2-bis(2-methyl-5-(1-naphthyl)-3-thienyl) perfluorocyclopentene and perfluoronaphthalene which could exhibit reversible bending for at least 1000 cycles without any crystal damage over a broad temperature range (4.6 K to 370 K). They then attached the crystal onto the tip of a metallic needle to operate a gear. The crystal bended and hit the gear, resulting in rotation of the gear under sequential UV and visible light irradiation (Figure 6.10).[14]

The maximum stress (56 MPa) generated by this crystal was found to be comparable to that of piezoelectric crystals (PZT, ca. 50 MPa). Such robust light-driven molecular crystal can be potentially used in various micro- and nanomechanical applications.

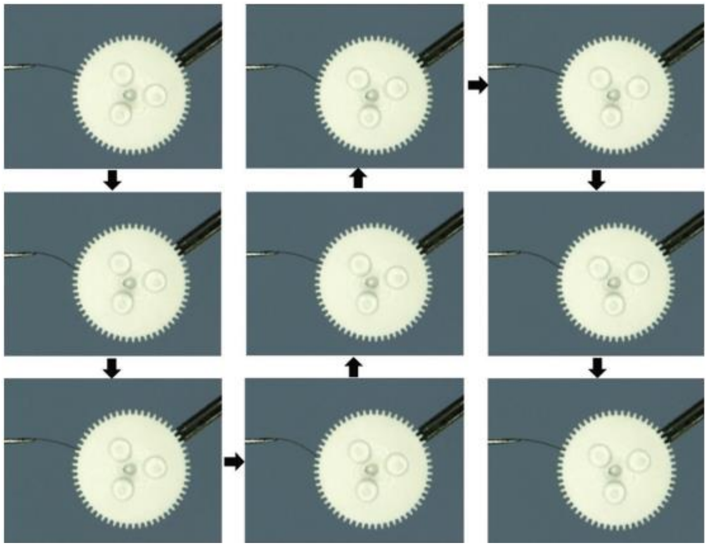

Figure 6.10 Gearwheel rotation operated by a light-driven molecular crystal actouator. The crystal containing two mixed diarylethene compounds was anchored on the tip a metal needle. The gear was rotated by the crystal, which showed reversible bending upon alternate irradiation with UV (365 nm) and visible (> 500 nm) light. (Reproduced with the permission of John Wiley and Sons.)

There is also encouraging progress in the creation of molecular crystals array in which people controlled the crystal size and orientation and tried to incorporate these arrays with small sized electronic devices with the aim of fabricating portable electronics devices with novel functionalities[25, 26].

6.5 Conclusion

This thesis reports the main research work during my five-year PhD period. Firstly, the 9TBA pressure dependence work indicated how people might engineer molecular structures to make pressure sensitive materials. Secondly, the extended F-W model of 9MA dimerization work demonstrated that the intrinsic properties of molecular crystals might lead to autocatalytic photochemical reactions. And the surfactant investigation of CTAB and DMAAM showed how external environmental effects could influence both the photochemical reaction and photomechanical behavior. Finally, this thesis discussed how different shapes of molecular crystals would lead to different photomechanical motions and also proposed some potential application of photomechanical molecular crystals in the future.

Despite of a slow beginning, the study of photomechanical molecular crystals is expanding rapidly and attracting increasing interest. This field also relies on the intersection of materials engineering, physical chemistry, synthetic chemistry and optical physics. While it is too early to determine its future potential, there is no doubt that this field of research will generate new scientific advances and technological applications for solid-state materials.

6.6 Reference

(1). Jezowski SR, Zhu L, Wang Y, Rice AP, Scott GW, Bardeen CJ, Chronister EL. Pressure catalyzed bond dissociation in an anthracene cyclophane photodimer. *J. Am. Chem. Soc.*, **2012**, 134, 17, 7459-7466.

(2) Kitagawa D, Tanaka R, Kobatake S. Photoinduced stepwise bending behavior of photochromic diarylethene crystals. *CrystEngComm*. **2016**, 18, 7236-7240.

(3) Kitagawa D, Tanaka R, Kobatake S. Dependence of photoinduced bending behavior of diarylethene crystals on irradiation wavelength of ultraviolet light. P*hys. Chem. Chem. Phys*. **2015**, 17, 27300-27305.

(4) Kitagawa D, Iwaihara C, Nishi H, Kobatake S. Quantitative Evaluation of Photoinduced Bending Speed of Diarylethene Crystals. *Crystals*. **2015**, 5, 551-561.

(5) Kitagawa D, Kawasaki K, Tanaka R, Kobatake S. Mechanical Behavior of Molecular Crystals Induced by Combination of Photochromic Reaction and Reversible Single-Crystal-to-Single-Crystal Phase Transition. *Chem. Mater.* **2017**, 29, 7524-7532.

(6) Kitagawa, D.; Nishi, H.; Kobatake, S., Photoinduced twisting of a photochromic diarylethene crystal. *Angew. Chem. Int. Ed.* **2013**, 52, 9320-9322.

(7) Kobatake S, Takami S, Muto H, Ishikawa T, Irie M. Rapid and reversible shape changes of molecular crystals on photoirradiation. *Nature.* **2007**, 446, 7137, 778-781.

(8) Kitagawa D, Okuyama T, Tanaka R, Kobatake S. Photoinduced Rapid and Explosive Fragmentation of Diarylethene Crystals Having Urethane Bonding. *Chem. Mater*. **2016**, 28, 4889-4892.

(9). Irie, M., Kobatake, S., and Horichi, M. Reversible surface morphology changes of a photochromic diarylethene single crystal by photoirradiation. *Science.*, **2001**, 291, 1769–1772.

(10). Tsujioka T, Sesumi Y, Takagi R, Masui K, Yokojima S, Uchida K, Nakamura S. Selective metal deposition on photoswitchable molecular surfaces. *J. Am. Chem. Soc.*, **2008**,130, 32, 10740-10747.

(11). Koshima H, Matsudomi M, Uemura Y, Kimura F, Kimura T. Light-driven Bending of Polymer Films in Which Salicylidenephenylethylamine Crystals are Aligned Magnetically. *Chem. Lett.*, **2013**, 42, 12, 1517-1519.

(12). Sahoo SC, Nath NK, Zhang L, Semreen MH, Al-Tel TH, Naumov P. Actuation based on thermo/photosalient effect: a biogenic smart hybrid driven by light and heat. *RSC Adv.*, **2014**, 4, 15, 7640-7647.

(13). Kuzmanich G, Natarajan A, Chin KK, Veerman M, Mortko CJ, Garcia-Garibay MA. Solid-state photodecarbonylation of diphenylcyclopropenone: a quantum chain process made possible by ultrafast energy transfer. *J. Am. Chem. Soc.*, **2008**, 130, 4, 1140-1141.

(14). Terao F, Morimoto M, Irie M. Light - Driven Molecular - Crystal Actuators: Rapid and Reversible Bending of Rodlike Mixed Crystals of Diarylethene Derivatives. *Angew. Chem. Int. Ed.*, **2012**, 23, 124, 925-928.

(15). Koshima H, Nakaya H, Uchimoto H, Ojima N. Photomechanical motion of furylfulgide crystals. *Chem. Lett.*, **2011**, 41, 107-109.

(16). Al-Kaysi RO, Bardeen CJ. General method for the synthesis of crystalline organic nanorods using porous alumina templates. *Chemi. Comm.*, **2006**, 11,1224-1226.

(17). Al-Kaysi RO, Zhu L, Al-Haidar M, Al-Muhannah MK, El-Boubbou K, Hamdan TM, Bardeen CJ. Chemical reaction method for growing photomechanical organic microcrystals. *CrystEngComm.*, **2015**, 17, 46,8835-8842.

(18). Zhu, L., Al‐Kaysi, R.O. and Bardeen, C.J., Photoinduced Ratchet‐Like Rotational Motion of Branched Molecular Crystals. *Angew. Chem. Int. Ed.*, **2016**, 55, 7073-7076.

(19). Al-Kaysi, R.O., Tong, F., Al-Haidar, M., Zhu, L. and Bardeen, C.J., 2017. Highly branched photomechanical crystals. *Chem. Comm.*, **2017**, 53, 2622-2625.

(20). Good JT, Burdett JJ, Bardeen CJ. Using Two‐Photon Excitation to Control Bending Motions in Molecular‐Crystal Nanorods. *Small.*, **2009**, 18, 5, 24,2902-2909.

(21). Kim T, Al‐Muhanna MK, Al‐Suwaidan SD, Al‐Kaysi RO, Bardeen CJ. Photoinduced curling of organic molecular crystal nanowires. *Angew. Chem. Int. Ed.*, **2013**, 52, 27, 6889-6893.

(22). Odom TW, Thalladi VR, Love JC, Whitesides GM. Generation of 30– 50 nm structures using easily fabricated, composite PDMS masks. *J. Am. Chem. Soc.*, **2002**, 124, 41, 12112-12113.

(23). Kitagawa D, Kobatake S. Photoreversible current ON/OFF switching by the photoinduced bending of gold-coated diarylethene crystals. *Chem. Comm.*, **2015**, 51, 21, 4421-4424.

(24). Lee J, Oh S, Pyo J, Kim JM, Je JH. A light-driven supramolecular nanowire actuator. *Nanoscale.*, **2015**, 7, 15, 6457-6461.

(25). Briseno AL, Mannsfeld SC, Ling MM, Liu S, Tseng RJ, Reese C, Roberts ME, Yang Y, Wudl F, Bao Z. Patterning organic single-crystal transistor arrays. *Nature.*, **2006**, 444, 7121, 913-917.

(26). Liu S, Mannsfeld SC, Wang WM, Sun YS, Stoltenberg RM, Bao Z. Patterning of α-Sexithiophene Single Crystals with Precisely Controlled Sizes and Shapes. *Chem. Mater.*, **2008**, 21, 1, 15-17.